

# **Solar variability and solar irradiance reconstructions on time scales of decades to centuries**

Von der Fakultät für Elektrotechnik, Informationstechnik, Physik  
der Technischen Universität Carolo-Wilhelmina  
zu Braunschweig  
zur Erlangung des Grades einer  
Doktorin der Naturwissenschaften  
(Dr.rer.nat.)  
genehmigte  
Dissertation

von Laura Antonia Balmaceda  
aus Rosario / Argentinien

## **Bibliografische Information Der Deutschen Bibliothek**

Die Deutsche Bibliothek verzeichnet diese Publikation in der Deutschen Nationalbibliografie; detaillierte bibliografische Daten sind im Internet über <http://dnb.ddb.de> abrufbar.

1. Referentin oder Referent: Dr. Prof. Sami K. Solanki

2. Referentin oder Referent: Prof. Dr. Karl-Heinz Glassmeier

eingereicht am: 22 Januar 2007

mündliche Prüfung (Disputation) am: 11 April 2007

Copyright © Copernicus GmbH 2007

ISBN 978-3-936586-68-8

Copernicus GmbH, Katlenburg-Lindau

Druck: Schaltungsdienst Lange, Berlin

Printed in Germany

# Vorveröffentlichungen der Dissertation

Teilergebnisse aus dieser Arbeit wurden mit Genehmigung der Fakultät für Physik, vertreten durch den Mentor oder den Betreuer der Arbeit, in folgenden Beiträgen vorab veröffentlicht:

## Publikationen

- Balmaceda, L.; Krivova, N.; Solanki, S. K. "Reconstruction of solar irradiance using the Group sunspot number", *Adv. Space Res.*, accepted
- Krivova, N.; Balmaceda, L.; Solanki, S. K. "Reconstruction of solar total irradiance since 1700 from the surface magnetic flux", *A&A*, 467, 335-346, 2007
- Balmaceda, L.; Solanki, S. K.; Krivova, N. "A cross-calibrated sunspot areas time series since 1874", *Memorie della Societa Astronomica Italiana*, 76, 929, 2005

## Tagungsbeiträge

- Balmaceda, L.; Solanki, S. K.; Krivova, N. *Reconstruction of solar irradiance variations since the Maunder Minimum* (Talk). Oberseminar, Technical University Braunschweig, Germany, November 20, 2006.
- Balmaceda, L.; Solanki, S. K.; Krivova, N. *Reconstruction of total solar irradiance variations since the Maunder Minimum* (Talk). ISCC-2: Long-term Changes in the Sun and their Effects in the Heliosphere and Planet Earth, Sinaia, Romania, September 13-16, 2006.
- Balmaceda, L. *Solar variability and a possible impact on climate* (Talk). 1st Interdisciplinary Max Planck PhDnet workshop: Global Changes - Environment, Society & Science, Cologne, Germany, August 17 - 19, 2006.
- Balmaceda, L. *Solar variability and climate changes* (Talk). 3rd El Leoncito School of Solar Physics, El Leoncito, San Juan, Argentina, November 28 - December 05, 2005
- Balmaceda, L.; Solanki, S. K.; Krivova, N. *A Homogeneous Sunspot Areas time series since 1874* (Poster). Solar Variability and Earth Climate, Villa Mondragone, Monte Porzio Catone (Rome), Italy, 27 June - 1st July, 2005.



*Aim at the sun, and you may not reach it; but your arrow will fly far higher than if aimed at an object on a level with yourself.*

Joel Hawes (1789 - 1867)



*Dedicada a quienes siempre estuvieron a mi lado:*

*Oscar, Inés y Virginia*





# Contents

<b>Summary</b>	<b>11</b>
<b>1 Introduction</b>	<b>13</b>
1.1 Why study solar variability?	13
1.2 Our magnetic Sun	14
1.3 Solar irradiance variations	15
1.3.1 Total solar irradiance variations	15
1.3.2 Spectral irradiance variations	19
1.4 Sun-climate: is there a link?	20
1.5 Outline of the thesis	22
<b>2 A homogeneous sunspot areas database covering more than 130 years</b>	<b>25</b>
2.1 Abstract	25
2.2 Introduction	25
2.3 Observational data	26
2.4 Analysis	27
2.4.1 On the effect of including offset to calculate cross-calibration factors	29
2.4.2 An alternative method to calculate cross-calibration factors	30
2.4.3 Error estimates	32
2.5 Results and discussion	33
2.5.1 Comparison between sunspot areas	33
2.5.2 Comparison with sunspot number	35
2.5.3 Cross-calibrated sunspot area records	37
2.6 The Photometric Sunspot Index	37
2.7 Summary and conclusions	39
<b>3 Reconstruction of solar total and UV irradiance from the sunspot and plage areas</b>	<b>41</b>
3.1 Abstract	41
3.2 Introduction	41
3.3 Quantifying the active-region contribution to the solar irradiance variations	42
3.3.1 Sunspot darkening	42
3.3.2 Facular brightening	43
3.4 Reconstruction of irradiance from plage and sunspot areas	45
3.5 Comparison with climate records	47

3.6	Discussion . . . . .	47
3.7	Concluding remarks . . . . .	49
<b>4</b>	<b>Reconstruction of solar total irradiance from the surface magnetic flux</b>	<b>51</b>
4.1	Abstract . . . . .	51
4.2	Introduction . . . . .	51
4.3	Approach . . . . .	53
4.3.1	Photospheric magnetic flux . . . . .	53
4.3.2	Solar irradiance . . . . .	55
4.3.3	Parameters and optimization . . . . .	59
4.4	Results . . . . .	60
4.4.1	Standard model . . . . .	60
4.4.2	A possible shift between the ER and AR evolution . . . . .	65
4.4.3	Constant ER flux . . . . .	67
4.4.4	Reconstruction based on the Group sunspot number . . . . .	69
4.5	Conclusions . . . . .	73
<b>5</b>	<b>Outlook: First steps towards a millennial reconstruction of solar irradiance</b>	<b>75</b>
5.1	Abstract . . . . .	75
5.2	Introduction . . . . .	75
5.3	Description of the data . . . . .	76
5.4	Searching for relations . . . . .	78
5.4.1	Total solar irradiance and sunspot number . . . . .	78
5.4.2	Total solar irradiance and total magnetic flux . . . . .	80
5.4.3	Total solar irradiance and open magnetic flux . . . . .	81
5.4.4	Open magnetic flux and total magnetic flux . . . . .	85
5.5	Discussion . . . . .	87
5.6	Summary and conclusions . . . . .	93
<b>6</b>	<b>Concluding remarks</b>	<b>95</b>
	<b>Bibliography</b>	<b>97</b>
	<b>Acknowledgements</b>	<b>109</b>
	<b>Lebenslauf</b>	<b>111</b>

# Summary

One principal record of solar variability is the time series of "Total Solar Irradiance" which is the total amount of energy per second per unit angle normalized to 1 AU. This quantity is available since November 1978 and the most striking result is that it varies by about 0.1% on time scales of the solar cycle (~ 11 years). Dark (sunspots) and bright (faculae and the network) features continuously appear and disappear on the solar surface and traverse the visible solar disc as the Sun rotates, thus modulating the solar irradiance. Both, sunspot darkening and facular brightening are magnetic phenomena. The observations do not provide any information on longer-term secular trends in the irradiance, however, and models are required to set tighter constraints on this quantity. The aim of this research is to understand the physical mechanisms responsible for solar brightness variations on time scales from the solar cycle to centuries and millennia. The main goal of the thesis is to carry out quantitative modelling of total and spectral irradiance variations based on a model of the surface magnetic flux. In a first step the magnetic flux and irradiance since the Maunder minimum (a time of extended lack of sunspots which coincided with the Little Ice Age) are reconstructed using a simple but consistent physical model. By using all available data on total and open magnetic flux and total irradiance to constrain the model parameters the increase in total solar irradiance since the Maunder minimum could be estimated to be about 0.1%. Necessary for the study of the possible role of the Sun's variability on Earth's climate are reconstructions covering time scales of thousands of years. In this thesis we also present the first steps towards such a reconstruction of solar irradiance. Using the results obtained here, it will be possible in a next step to reconstruct the total solar irradiance for a period of approximately 8000 years based on sunspot records derived from isotope data.



# 1 Introduction

## 1.1 Why study solar variability?

The Sun is a typical middle-aged dwarf star on the main sequence (Tayler 1997), with a radius  $R_{\odot} = 7 \times 10^5$  km, a mass  $M_{\odot} = 2 \times 10^{30}$  kg and a luminosity  $L_{\odot} = 4 \times 10^{26}$  W. Energy is generated by thermonuclear processes (the p-p reaction) in a central core with a radius of  $0.2R_{\odot}$  and is carried outwards by photons through the radiative zone which extends to  $0.7R_{\odot}$ . The outer 30% by radius is the convection zone, where energy transport is by turbulent convective motions, which are visible at the solar surface (the photosphere). The central temperature is  $1.5 \times 10^7$  K, falling to  $2 \times 10^6$  K at the base of the convection zone and  $6 \times 10^3$  K at the photosphere. The temperature drops off slightly in the upper photosphere, before increasing somewhat in the chromosphere, before it rises abruptly to values of  $1-3 \times 10^6$  K in the tenuous corona, which extends outward for several solar radii and merges into the solar wind. The corona's structure is dominated by magnetic fields which emerge from the interior of the Sun and cause solar activity. Solar activity occurs on a large range of time scales, from minutes to decades, and has been monitored and recorded over multiple centuries.

The first indication of solar variability came from the observation of sunspots appearing on the solar disc by Galileo in the 17th century. However, it was only in the mid-19th century when the  $\sim 11$ -year variation of the sunspot number was first recognized by the German astronomer Heinrich Schwabe. Apart from this cyclic variation, the Sun was observed to undergo extended periods of low activity. One of these periods is the so-called Maunder Minimum, extending roughly from 1645 to 1715 A.D., when sunspots became exceedingly rare, as noted by solar observers of that time. The Maunder minimum coincides with the so-called "Little Ice Age", a period of extremely low temperature in North of Europe. Whether this period could have been directly related to lack of activity of the Sun is not yet clear, but this coincidence called the attention of the scientific community to the study of the influence of solar activity on the Earth's climate (Eddy 1976).

In addition, there are also intense transient events, such as flares, prominence eruptions and coronal mass ejections occurring at very short time scales (from minutes to hours). Such phenomena also affect the Earth's environment, injecting particles and energy into the magnetosphere, ionosphere and upper atmosphere. There they produce aurorae, substorms and other phenomena that are known as space weather. Thus, the study of solar variability is important in the context of Sun-Earth relationships, on time scales ranging from hours to days (space weather) and from centuries to millennia (climate system).

On the other hand, the study of solar variability on evolutionary time scales is also relevant in the stellar context. Photometric observations of solar-type stars clearly show

that year-to-year brightness variations connected to magnetic activity are a widespread phenomenon among such stars (Radick et al. 1998, Schrijver and Zwaan 2000). As our nearest star, the Sun is the only object where we can observe and identify a variety of structures and processes which lead to variations in the energy output. Moreover, the Sun and its variability provide unique constraints on models of stellar evolution, which in turn provide scenarios for stellar variability on exceedingly long time scales.

To investigate solar variability on time scales of days to centuries and longer, different indices or proxies of solar activity have been employed. The number of sunspots appearing on the solar disc has been recorded since 1610 (Hoyt and Schatten 1998). The continuous record of the sunspot number provides the longest time series of direct indices describing the changes in solar activity. Other available proxies are sunspot areas (since 1874) and facular areas (available during the period 1874–1976), Mg II core-to-wing ratio (available since 1978), the total photospheric magnetic flux (regularly measured since 1974). Indirect proxies of solar activity are geomagnetic indices such as aa-index (since 1868). Continuous direct records of solar variability are limited to the telescopic era covering approximately the past four centuries. For longer records one has to rely on indirect indices such as cosmogenic isotopes (for instance  $^{14}\text{C}$  and  $^{10}\text{Be}$ ; Beer 2000). Some of these records are available for the whole Holocene (period that extends from the present day back to approximately between 9560 and 9300 BC). Analysis of appropriate well-dated natural archives such as ice cores or tree-rings offers the possibility to reconstruct past solar activity over many millennia. The presently available data show cyclic variability ranging from 11-year to millennial timescale with changing amplitudes, as well as irregularly distributed intervals of very low solar activity (so called minima) lasting typically 100 years (Wagner et al. 2001, Peristykh and Damon 2003).

Despite the importance of these historic records of solar activity for a long period, of more direct relevance for climate is the Sun's energy output, i.e. irradiance. Unfortunately, regular and accurate measurements of solar irradiance are available for less than 30 years. If we want to understand the mechanisms and the magnitude of the solar influence on climate, we need much longer records. It is therefore necessary to reconstruct solar irradiance variability back in time for the pre-satellite period, for which we first need to understand the physical processes leading to the variations in this quantity.

## 1.2 Our magnetic Sun

The activity of the Sun is driven by the evolution of the magnetic field which is generated in the solar interior by electric currents flowing in the plasma in accordance with Ampere's law. Although the exact mechanism that generates the magnetic field is not yet understood, it is proposed that it is caused by a hydromagnetic dynamo located at the interface of the convection zone and the radiative core (see reviews by Weiss 1994, Schmitt 1993, Schüssler et al. 1997). The magnetic field emerges at the solar surface by buoyancy (Parker 1955, 1975), forming bipolar regions of high intensity at different spatial and temporal scales as observed in magnetograms (Zwaan and Harvey 1994). The largest among these regions are known as active regions and they consist of sunspots surrounded by bright faculae and the overlying chromospheric plages. Smaller bipolar regions are referred to as ephemeral (active) regions. They have shorter lifetimes, lasting

only some hours (Harvey 1992, 1993, Hagenaar 2001). Active regions erupt and decay with lifetimes of weeks to a few months. As an active region evolves, its spots decay. Its faculae disperse, merging with the surrounding network and also gradually disappear. A large part of the emerged flux is quickly removed from the solar surface by cancellation with opposite polarity flux within days. The remaining flux is redistributed over the solar surface through different processes such as turbulent diffusion, differential rotation and meridional flow at timescales from months to years.

Most part of the magnetic flux spreading through the solar photosphere is filamented into a range of flux tubes with field strength of  $\sim 100$  mT and oriented mainly in the vertical direction. The largest photospheric magnetic flux tubes are sunspots with diameters between a few Mm and 50 Mm. They represent the biggest accumulations of magnetic flux in the photosphere. The relative darkness of sunspots is caused by the suppression of convective energy transport due to their strong magnetic field. On the other hand, small flux tubes (e.g., faculae) appear brighter than the surrounding average solar surface because their partially evacuated interior is efficiently heated by radiation from their surroundings in the deeper layers and, presumably, also by dissipation of mechanical energy in their higher atmospheric layers. Averaged over the whole Sun, the enhanced brightness of the magnetic elements dominates over the reduced energy flux in the sunspots, so that the total radiation output increases with growing magnetic flux in the photosphere. As a consequence, the brightness of the Sun increases by about 0.1% from minimum to maximum during the solar activity cycle (Spruit 1982, Krivova et al. 2003, Wenzler et al. 2004, 2005, 2006).

## 1.3 Solar irradiance variations

### 1.3.1 Total solar irradiance variations

The total solar irradiance (TSI) is the total energy of the Sun integrated over the whole spectrum and normalized at 1 astronomical unit. Total solar irradiance monitoring from space started with the launch of the NIMBUS 7 spacecraft in November 1978 (Hickey et al. 1980). Since then, different experiments onboard satellites (HF on Nimbus-7, ACRIM I on SMM, ACRIM II on UARS, VIRGO on SOHO and TIM on SORCE) have been monitoring the so-called "solar constant" (Fröhlich 2006). In Fig. 1.1 the daily irradiance measurements from different instruments are plotted vs time. A composite of data collected by those instruments had to be created. Due to instrument degradation, the original measurements need to be corrected for sensitivity changes. This is not trivial, and there are three different composites currently available (see lower panels of Fig. 1.1): PMOD (Fröhlich 2006), ACRIM (Willson and Mordvinov 2003) and IRMB (Dewitte et al. 2004). One major disagreement among them is the different levels of solar irradiance at solar minima (years 1986 and 1996). The trends differ because of the different cross-calibrations and drift adjustments applied to the radiometric sensitivities (see details in Fröhlich 2006).

The most evident feature in the record of irradiance measurements is the solar cycle variation. Apart from this variation, large downward spikes due to the passage of dark sunspots across the visible disc are also observed. At sunspot maximum, however, TSI

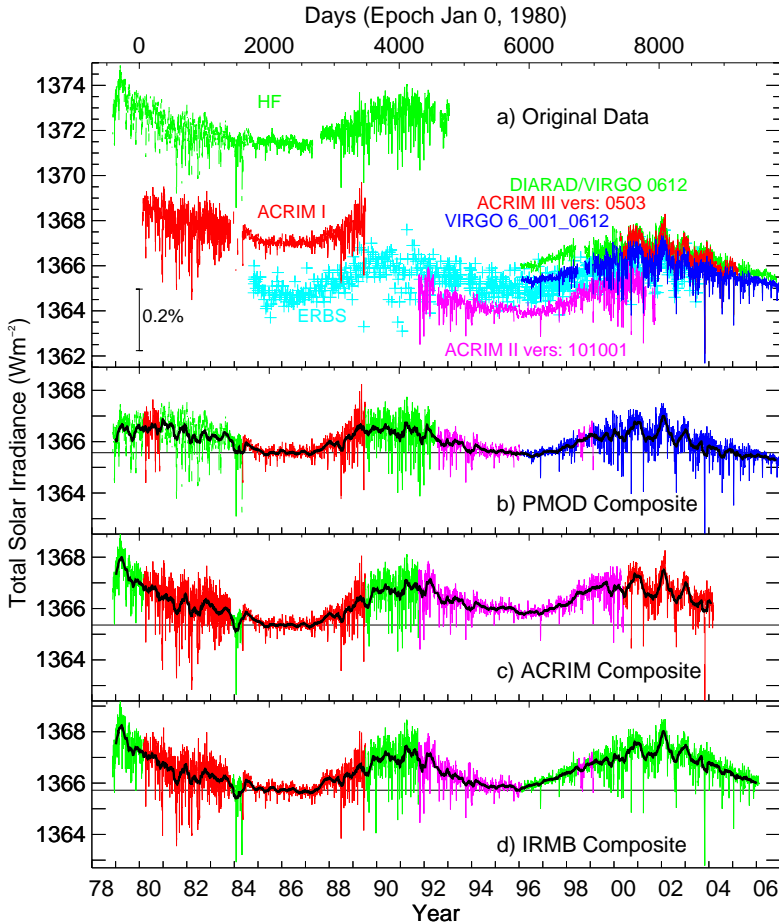


Figure 1.1: Upper panel: Compared are daily averaged values of the total solar irradiance from radiometers on different spacecrafts since November 1978: HF on Nimbus7, ACRIM I on SMM, ERBE on ERBS, ACRIM II on UARS, VIRGO on SOHO, and ACRIM III on ACRIM-Sat. The data are plotted as published by the corresponding instrument teams. Lower Panels: The PMOD, ACRIM and IRMB composite TSI as daily values plotted in different colors to indicate where the data are coming from. Courtesy: PMOD/WRC.



increases and this is due to the presence of bright areas called faculae. This record shows a day-to-day variation of about 0.3% peak-to-peak amplitude more evident near maxima of solar activity while the variation on time scales of a solar cycle is less than 0.1%. On time scales of days and longer changes in irradiance are caused by the changing photospheric magnetic field (Krivova et al. 2003, Ermolli et al. 2003, Wenzler et al. 2004, 2005, 2006). Some other mechanisms of irradiance variations have been also proposed. However, there is no evidence for them. Some of these are: fields deep inside the convection zone (Kuhn et al. 1988, Kuhn and Libbrecht 1991, Kuhn and Stein 1996, Sofia and Li 2000), temporal variations of the radius of the Sun, effective temperature and solar oscillations frequencies (Wolff and Hickey 1987) and changes in the radiative sources of the Sun.

Since the time series of measured irradiance is relatively short, covering only less than 3 solar cycles, different approaches were employed in order to model its variations on time scales much longer than a solar cycle. The construction of such models requires an understanding of the physical mechanisms of irradiance changes, and of course must reproduce the direct measurements.

The most successful models are those attributing the irradiance variations to the evolution of the solar surface magnetic field (Foukal and Lean 1986, 1988, Chapman et al. 1996, Fligge and Solanki 1998, Fligge et al. 2000, Krivova et al. 2003, Ermolli et al. 2003, Wenzler et al. 2004, 2005, 2006). They could reproduce observed irradiance changes (on scales from days to solar rotation) with high accuracy. This indicates that a good understanding of these mechanisms has been gained in the last decades.

In particular, the SATIRE model (Spectral And Total Irradiance REconstructions - Krivova et al. 2003, Solanki and Krivova 2004) explained more than 90 % of the variations in total solar irradiance on time scales of days up to the solar cycle. An extension of this model to earlier times (e.g., end of the Maunder Minimum), is of crucial importance for evaluating the solar influence on climate.

Short-term reconstructions of solar irradiance generally make use of detailed maps of the solar surface (e.g.: magnetograms, Ca II K or continuum images). On longer time scales (from solar cycle to centuries), instead, the accuracy of the models decreases considerably due to the noticeable degradation of the amount and quality of the available proxies of solar magnetic activity.

In general, long-term reconstructions of solar irradiance consist of modelling both, a cyclic and a secular component. While the cyclic component can be successfully reconstructed from diverse solar proxies, the slowly varying (secular) component is more tricky to calculate.

A variety of historic solar observations provide information about sunspots and faculae (associated with plages and active network). The only direct solar index available all the time since 1610 is the sunspot number. Ground-based white light images made from 1874 to 1976 by the Greenwich Observatory, and most recently by the US Air Force operational SOON sites, provide the basic time-dependent information about sunspot areas and locations. These sunspot observations are also reasonable (although not ideal) proxies for the cyclic evolution of the bright magnetic features (faculae), which usually accompany the eruption of sunspots. The use of such proxies, permitted a number of quite detailed reconstructions for the cyclic component of the variations, some going back to the end or beginning of the Maunder Minimum (Lean et al. 1995, Solanki and Fligge 1998, 1999, Fligge et al. 2000). But apart from this cyclic component, there is also evidence

for a longer-term component that leads to a secular variation of the solar irradiance and is more difficult to estimate. This could, however, be of greater importance for climate studies.

Evidence for this longer-term variation came first from the stellar observations. Emission in the cores of the Ca II H and K lines of Sun-like stars is a good proxy to estimate the magnetic activity. Baliunas and Jastrow (1990) found a bimodal distribution of the Ca II brightness of Sun-like stars, with a broader peak corresponding to high emission levels and a narrower peak at very low emission levels. This was interpreted as distinguishing between cycling and non-cycling stars. Using a relationship between solar Ca II brightness and irradiance, and assuming that this relationship does not change with time, an increase in the solar irradiance since the end of the Maunder minimum ranging from 2 to  $8 \text{ Wm}^{-2}$  was found (White et al. 1992, Hoyt and Schatten 1993, Zhang et al. 1994, Lean et al. 1995, Lean 2000a, Solanki and Fligge 1998, 1999, Fligge et al. 2000). However, a reassessment of the stellar data did not confirm the original bimodal separation of lower Ca emission in non-cycling stars compared with the higher emission of cycling stars (Hall and Lockwood 2004, Wright et al. 2004, Giampapa 2005), so that the stellar evidence for a secular change was no longer supported.

A second indication for such a trend came from the reconstruction of the coronal source flux from the geomagnetic *aa*-index made by (Lockwood et al. 1999). The coronal source flux is where the solar magnetic field becomes approximately radial and lies at heliocentric distance of about 2.5 solar radii (Wang and Sheeley 1995). Lockwood et al. (1999) showed that this quantity has doubled during the last century, indicating the presence of a slowly varying component. However the presence of a secular trend in the coronal source flux (or open flux) does not necessarily imply a significant secular trend in the total magnetic flux. For instance, the amount of open flux can change due to the rearrangement of magnetic polarities on the solar surface without any change in the amount of total magnetic flux. Nevertheless, a secular change in the irradiance requires a change in the amount of the latter at the solar surface. A possible mechanism to explain such a secular variation of the total magnetic flux was proposed by Solanki et al. (2002) based on the overlap of consecutive solar activity cycles. Observations indicated that the network, which decays within hours if not replenished (Hagenaar 2001), is maintained by the flux emergence in ephemeral active regions (Harvey 1993). These ephemeral regions emerge not only in times of high solar activity, but rather over an extended solar cycle, so that flux appearing in one cycle is still present when flux of the next cycle starts to appear. This overlap of consecutive cycles produces then a background level of flux still present in times of activity minima. The model by Solanki et al. (2002) reproduces not only the available photospheric flux measurements since 1974 but also the doubling of the open magnetic flux over the last century (Lockwood et al. 1999).

There have been several attempts to estimate the magnitude of the secular change in the solar irradiance, but it remains highly uncertain. Alternative approaches, other than the comparison with stellar activity, have been developed in the recent years.

For instance, assuming that faculae are located near sunspots, Foster (2004), cf. Lockwood (2005), reconstructed the butterfly diagram for faculae using the historical record of sunspot areas and positions. Averaged functions for the centre-to-limb variations of the facular contrasts derived by Ortiz et al. (2002), were employed in order to model facular brightening. Analysing the distribution of the magnetic field in the recent period and as-

suming that the Sun was magnetically quiet during the Maunder minimum he set an upper limit of  $\approx 1.7 \text{ Wm}^{-2}$  on the secular variation since that time. This limit increases to approx  $2.1 \text{ Wm}^{-2}$  if the weak magnetic flux escaping registration in the Michelson Doppler Imager (MDI) magnetograms due to insufficient spatial resolution (Krivova and Solanki 2004) is taken into account. Additional uncertainty in this model is introduced by the fact that the contrasts derived at a single wavelength are used instead of more realistic facular models. A lower value of about  $1 \text{ Wm}^{-2}$  for the increase in the cycle-averaged total solar irradiance (TSI) since the beginning of the 18th century was published by Wang et al. (2005). They used a flux transport model to simulate the evolution of the solar magnetic flux and then the TSI could be reconstructed by following the basic porcedure of Lean (2000a). In Table 1.1, a summary of some of the recent approaches is presented.

Table 1.1: Estimates of the increase in TSI since the Maunder Minimum

Reference	Assumption / technique	Estimated increase of TSI since Maunder Minimum ( $\text{Wm}^{-2}$ )
Hoyt and Schatten (1993)*	convective restructuring implied by changes in sunspot umbra/penumbra ratios	3.7
Lean et al. (1995)	comparison with non-cycling stars	2.6
Fligge and Solanki (2000)*	use of model flux spectra of solar magnetic features - comparison with stellar data	4.3
Lean (2000b)	comparison with non-cycling stars	2.2
Foster (2004)	(revised solar stellar calibration) non-magnetic Sun estimates by removing bright features from MDI images	0.5–2.2
Wang et al. (2005)*	flux transport model of total magnetic flux evolution	$\sim 1$

The references identified with \* extend to the end of the Maunder Minimum.

### 1.3.2 Spectral irradiance variations

Space-based observations of solar spectral irradiance have concentrated primarily on measurements at UV wavelengths. Reliable measurements of solar UV irradiance are available only since 1991, after the launch of UARS. Two instruments measure irradiance at around 120–400 nm: SUSIM (Brueckner et al. 1993) and SOLSTICE (Rottman

et al. 1993). Previous measurements made by SME (Rottman 1988) are unfortunately of very low accuracy. Solar UV irradiance shows a much larger variation than the change of about 0.1 % observed in the total irradiance over one solar cycle. In the wavelength interval 200–300 nm, the UV irradiance varies only by a few percent. At 150–200 nm the variation is of 10–20% while around the Ly- $\alpha$  emission line (121.6 nm) and shorter wavelengths this variation is of more than 50 % (Floyd et al. 2003). At 300–400 nm, the amplitude of variation is uncertain. According to Krivova et al. (2006b), up to 60 % of total solar irradiance variations over a solar cycle might be produced at wavelengths below 400 nm.

The variation at different wavelengths intervals may have an important impact on the terrestrial climate system. However, the time series of spectral solar irradiance is still too short to allow a reliable estimate of the solar influence on the Earth's climate. In the same way as for total solar irradiance, this can be only assessed with the help of models.

Variations of the total solar irradiance at wavelengths longer than 300 nm have been successfully reproduced (see, e.g., Unruh et al. 1999, Ermolli et al. 2003, Krivova et al. 2003, Wenzler et al. 2004, 2005, 2006). However, at shorter wavelengths the LTE assumption taken in the calculations of brightness of the different photospheric components fails and the non-LTE nature of the radiative transfer must be taken into account (Fontenla et al. 1999, Haberreiter et al. 2005). A recent approach consists of the empirical extrapolation of SATIRE models down to 115 nm using available data (Krivova and Solanki 2005, Krivova et al. 2006b).

### 1.4 Sun-climate: is there a link?

The Earth's climate is changing. A number of observations support this conclusion and provides insight about the rapidity of these changes. The most evident manifestation of these changes is the increase of the global surface temperatures by about 0.6°C since the late 19th century and about 0.46°C in the last 25 years (IPCC 2001). The present debate is about which amount of these changes are due to the variation of natural forcing agents (e.g., solar variation) and how much can be attributed to the anthropogenic influence (e.g., greenhouse gases).

Unfortunately, this is not a straightforward task. The Earth's climate system is influenced by a complex combination of diverse factors. Temperature, motions and composition of the atmosphere and their variations are determined by many complex interactions between the atmosphere itself and the oceans, cryosphere and biosphere. The main energy source into this system is the solar irradiance.

The Sun's influence on the Earth's climate cannot be measured directly. However, there exist a variety of ways to approach this problem. One approach consists of empirical comparisons between solar proxies and climate records.

In the past decades good correlations have been found between different proxies of solar activity and climate records. Statistical evidence for solar influence on various meteorological parameters, such as temperature (global, Northern and Southern hemispheres, oceanic records), on all timescales was found. Evidence for this are relations found between: cosmic rays (which are modulated by solar activity) and ocean sediments (Bond et al. 2001), sunspot number and cosmic rays with reconstructed Northern Hemisphere

mean surface temperatures (Usoskin et al. 2005), total and spectral solar irradiance and cosmic rays with global and Northern hemisphere temperatures (Solanki and Krivova 2003), the 10.7 cm solar flux and the geopotential height of the 30 hPa pressure surface (as a measure of the mean temperature of the atmosphere below 24 km of altitude), or the mean summer temperature of the upper atmosphere (Labitzke and van Loon 1995, van Loon and Labitzke 2000), as well as the cosmic ray intensity and the change in low cloud fraction (Marsh and Svensmark 2000). However, such correlation studies are based only on statistics and not on the understanding of how the presumed solar influence takes place. How the Sun influences the climate and which are the mechanisms playing the main role is matter of research.

So far, three possible mechanisms of the Sun-climate relationship have been proposed. First of all, variations in total solar irradiance may affect climate since Sun's radiative output is ultimately responsible for driving the climate system (Haigh et al. 2005, Reid 2000). Even small variations in this quantity have the potential to influence Earth's climate (see, Cubasch and Voss 2000, Haigh 2003, Lean 2001). For another point of view see Foukal et al. (2006).

The Sun's total irradiance is about  $1365 \text{ Wm}^{-2}$  in space. Since the incoming radiation is distributed over the surface of the Earth, the average solar radiation at the top of the atmosphere is one quarter of this, or about  $340 \text{ Wm}^{-2}$ , and a variation of 0.1% corresponds to  $0.34 \text{ Wm}^{-2}$ . Planetary albedo reduces this further to about  $0.24 \text{ Wm}^{-2}$ . This is small but not totally insignificant, compared with the current estimates of the radiative forcing by anthropogenic greenhouse gases of 2 to  $2.5 \text{ Wm}^{-2}$  (Schimel et al. 1996) and comparable with the current estimates of the forcing by other anthropogenic sources such as sulfate aerosols or tropospheric ozone. The cyclical nature of the solar forcing, however, substantially reduces its climatic impact, since the thermal inertia of the ocean is large enough to be able to dampen an 11-year cycle considerably (Reid 2000).

A second possible mechanism is caused by the influence of solar ultraviolet irradiance variations. The UV radiation affects the temperature structure of the stratosphere through photochemical reactions, e.g. involving ozone production and destruction (Larkin et al. 2000). Finally, there is also an indirect effect through changes in the fluxes of energetic charged particles impinging on the Earth's atmosphere that may affect the cloud cover (Belov 2000, Marsh and Svensmark 2000). This link, however, remains controversial and is also difficult to verify.

In order to understand the role of the anthropogenic factors on the Earth's climate, we also need a reliable estimate of the Sun's contribution. Several attempts have been made to estimate the change in the Sun's radiative output since the time of the Maunder Minimum and the impact of the change on global climate (see, Lean et al. 1992, 1995, Nesme-Ribes et al. 1993, Hoyt and Schatten 1993, Reid 1997, Lean and Rind 1998, 1999, Cubasch and Voss 2000, Rind et al. 1999, Shindell 2001, Solanki and Krivova 2003). The general conclusion is that the predicted Sun's total irradiance variation over the last 300 years would not be sufficient to be responsible for the significant warming of the Earth in the last 30 – 40 years (Solanki and Krivova 2003).

However, the reconstructions employed in such simulations (Hoyt and Schatten 1993, Lean et al. 1995, Lean 2000a) were based mainly in statistical correlations between different proxies of solar activity and adopted a speculative long-term component in the variation. The development of physics-based models of past irradiance variations is then

crucial for the understanding of the terrestrial climate evolution. In addition climate simulations also require models of the spectral solar irradiance as an input. In particular, the UV irradiance effects in both the radiative heating and in the stratospheric ozone photochemistry are needed in more realistic simulations.

### 1.5 Outline of the thesis

In recent years, the study of the variation of total solar irradiance on time scales of days to a solar cycle has undergone significant progress. The good agreement between observed and modelled irradiance variations (Krivova et al. 2003, Wenzler et al. 2004, 2005, 2006) indicates that a good understanding of the processes leading to such variations has been reached. The extension of these models to longer time scales (from solar cycle to centuries and millennia) is essential in order to study the influence of the Sun on the Earth's climate.

The goal of this thesis is to study the variability of the solar irradiance at timescales of decades to centuries and millennia. For this purpose, quantitative modelling is carried out in order to get an estimate of the variation of this quantity during the last centuries. In addition, diverse sources of historical solar proxies commonly used in such reconstruction are revised and appropriately combined.

In particular, one of the most commonly used indices of solar variability are the sunspot areas. They represent valuable data necessary in models of irradiance variations. Sunspot areas have been systematically recorded since 1874 by a number of observatories. In order to employ this data set in irradiance reconstructions it is necessary in the first place to cross-calibrate the observations before combining them in a uniform final time series, as already pointed out by diverse authors (Fligge and Solanki 1997, Hathaway et al. 2002, Foster 2004). The analysis and comparison between different data sets in order to get the cross-calibration factors are described in Chapter 2.

Both, total and spectral solar irradiance estimates for periods extending for several centuries are necessary in order to investigate their influence on the evolution of the climate system. Recently, Foukal (2002) presented a reconstruction of total and UV solar irradiance back to 1915 from sunspot and plage area records. However, the time series of sunspot areas employed are combined without a proper calibration. This leads to an erroneous estimate of the secular change in these two quantities. In Chapter 3 we redo this reconstruction but employing the composite of cross-calibrated sunspot areas obtained in Chapter 2.

In previous attempts, long-term reconstructions of solar irradiance have been mainly based on relationship between different proxies of solar activity. Assuming that these relationships remain valid at earlier times, the cyclic behaviour of the irradiance variations could be successfully reproduced. However, the secular trend is more difficult to assess and is usually based on speculative assumptions. Solanki et al. (2000, 2002) proposed a mechanism to explain the secular change in the total magnetic flux and solar irradiance consisting of the overlap of consecutive activity cycles. The model employs sunspot number as an input data and it allows to estimate the contribution of active regions, ephemeral regions and open flux to the total magnetic flux. In Chapter 4, we use this model to reconstruct the evolution of the Sun's total magnetic flux and its components since the Maunder Minimum. In a second step, we use these estimated fluxes to reconstruct the total solar

irradiance by extending SATIRE models (Krivova and Solanki 2005, Solanki et al. 2005) for the same period.

In order to study how the Sun affects the Earth's climate, it is necessary to use an irradiance time series longer than the one available at the moment. Recently a sunspot number time series has been reconstructed for the whole Holocene epoch using isotope data (Solanki et al. 2004). It is then possible to reconstruct solar irradiance for the same period of time from this sunspot number record. This is the main topic of Chapter 5.

Finally, in Chapter 6 we summarize results presented in the previous chapters and identify promising areas for future research in this field.





# **2 A homogeneous sunspot areas database covering more than 130 years**

## **2.1 Abstract**

The historical record of sunspot areas is a valuable and widely used proxy of solar activity and variability. The Royal Greenwich Observatory (RGO) regularly measured this and other parameters between 1874 and 1976. After that time records from a number of different observatories are available. These, however, show systematic differences and often have significant gaps. Our goal is to obtain a uniform and complete sunspot area time series, by combining different data sets. Data recorded simultaneously at different observatories are statistically compared in order to determine the intercalibration factors. Using these data we compile a complete and cross-calibrated time series. The Greenwich data set is used as a basis until 1976, the Russian data (a compilation of observations made at stations in the former USSR) between 1977 and 1985 and data compiled by the USAF network since 1986. Other data sets (Rome, Yunnan, Catania) are used to fill in the remaining gaps.

## **2.2 Introduction**

The total area of all sunspots visible on the solar hemisphere is one of the fundamental indicators of solar magnetic activity. Measured since 1874, it provides a proxy of solar activity over more than 130 years that is regularly used, e.g., to study the solar cycle or to reconstruct total and spectral irradiance at earlier times ( e.g., Brandt et al. 1994, Solanki and Fligge 1998, Li 1999, Li et al. 2005, Preminger and Walton 2005). Consequently, a reliable and complete time series of sunspot areas is essential. Since no single observatory made such records over this whole interval of time, different data sets must be combined after an appropriate intercalibration. In this sense, several comparative studies have been carried out in order to get an appropriately cross-calibrated sunspot area data set (see, for instance: Sivaraman et al. 1993, Fligge and Solanki 1997, Baranyi et al. 2001, Foster 2004, and references therein). They pointed out that differences between data sets can arise due to random errors introduced by the personal bias of the observer, limited seeing conditions at the observation site, different amounts of scattered light, or the difference in the time when the observations were made. Systematic errors also account for a disparity in the

area measurements. They are related to the observing and measurement techniques and different data reduction methods. For example, areas measured from sunspot drawings are on average smaller than the ones measured from photographic plates (Baranyi et al. 2001).

In this work, we compare data from Russian stations in addition to the data from the USAF (US Air Force) network and from other sources (Rome, Yunnan, Catania) with Royal Greenwich Observatory (RGO) data. This combination provides a good set of observations almost free of gaps after 1976. Combining them appropriately improves the sunspot area time series available at present. In Section 2 we describe the data provided by the different observatories analyzed here. The method to calculate the appropriate cross-calibration factors is explained in Section 3. The results are discussed in Section 4 and in Section 5 we discuss one central application of sunspot areas: the Photometric Sunspot Index. Finally Section 5 presents the summary and conclusions.

## 2.3 Observational data

Data from RGO provide the longest and most complete record of sunspot areas. The data were recorded at a small network of observatories (Cape of Good Hope, Kodaikanal and Mauritius) between 1874 and 1976, thus covering nine solar cycles. Heliographic positions and distance from the center of the solar disk of sunspot groups are also available.

The second data set is completely independent and is known as the Russian books — Solar Data from stations belonging to the former USSR. These stations provided sunspot areas corrected for foreshortening, together with the heliographic position (latitude, longitude) and radial distance to Sun center for each sunspot group. These data were published by the "Solnechnye Dannye" Bulletin issued by the Pulkovo Astronomical Observatory.

After RGO ceased its programme, the US Air Force (USAF) started compiling data from its own Solar Optical Observing Network (SOON). This network consists of solar observatories located in such a way that 24-hour synoptic solar monitoring can be maintained. The basic observatories are Boulder and the members of the network of the US Air Force (Holloman, Learmonth, Palehua, Ramey and San Vito). Also data from Mt. Wilson Observatory are included. This programme has continued through to the present with the help of the US National Oceanic and Atmospheric Administration (NOAA). This data set is referred to by different names in the literature, e.g., SOON, USAF, USAF/NOAA, USAF/Mt. Wilson. In the following, we will refer to it as SOON.

One feature of the SOON data is that for a given sunspot group  $n$  on a particular day  $d$  multiple measurements are provided by the different stations. In order to get a unique value for this group, averages of sunspot areas recorded on this day  $d$  ( $A_{n,d}$ ) are calculated, including only those values which fulfill the following condition:

$$\overline{A_{n,d}} - 2 \cdot \sigma \leq A_{n,d} \leq \overline{A_{n,d}} + 2 \cdot \sigma.$$

Here,  $\overline{A_{n,d}}$  is the mean value of all the areas measured for the group  $n$  on the day  $d$ , and  $\sigma$  is their standard deviation. In this way, outliers are excluded. After that, sunspot areas for individual groups are summed up to get the daily value. Also averaged are latitudes and longitudes of each sunspot group recorded by those observatories whose data are

Table 2.1: Data provided by the different observatories

Observatory	Observation Period	Observing technique	Coverage [%]	Min. area reported [ppm solar hemisph.]
RGO	1874 – 1976	photographic plates	98	1
Russia	1968 – 1991	photographic plates	96	1
SOON	1981 – 2005	drawings	98	10
Catania	1978 – 1987	drawings	81	3
Rome	1958 – 1999	photographic plates	50	2
Yunnan	1981 – 1992	photographic plates	81	2

employed to get the averaged sunspot area.

These three data sets (RGO, Russia and SOON) are the prime sources of data that we consider, since they are the most complete, being based on observations provided by multiple stations. A number of further observatories have also regularly measured sunspot areas during the past decades. Rome Astronomical Observatory, whose measurements began in 1958, covers more than three consecutive and complete solar cycles. It has several years of observations in common with Russia and SOON as well as with RGO. This is perhaps the only source of data with a long period of overlap with all three prime data sets. The database from Rome is used to compare the results obtained from the other observatories and also to fill in remaining gaps whenever possible. Unfortunately, its coverage is limited by weather conditions and instrumentation problems. Whenever available, data from Yunnan Observatory in China and Catania Astrophysical Observatory in Italy are also used to fill in the remaining gaps. In Catania, daily drawings of sunspot groups were made at the Cooke refractor on a 24.5 cm diameter projected image from the Sun, while the measurements provided by the Chinese observatory are based on good quality white light photographs. Table 2.1 summarizes the information provided by each observatory: the period in which observations were carried out, the observing technique, the coverage (i.e. the percentage of days on which measurements were made) and the minimum area reported by each observatory. Areas corrected for foreshortening are provided in all the cases while directly observed areas, or projected areas, can be derived using the heliographic positions for sunspot groups, and hence heliocentric angle,  $\theta$ , or  $\mu$ -values ( $\cos \theta$ ). All the data used in this work were extracted from <http://www.ngdc.noaa.gov/stp/SOLAR/>.

## 2.4 Analysis

Daily sunspot areas from two different observatories are directly compared on each day on which both had recorded data. We deduced multiplication factors needed to bring all data sets to a common scale, namely that of RGO, which is employed as fiducial data set.

For this, the spot areas from one data set are plotted vs. the other (see left panels of Fig. 2.1). The slope of a linear regression forced to pass through the origin (see Section 2.4.1) can be used to calibrate the sunspot area record considered auxiliary,  $A^{aux}$ , to the areas of another basic data set,  $A^{bas}$ :

$$A^{bas} = b \cdot A^{aux}. \quad (2.1)$$

First, this analysis is applied to all the points. The obtained  $b_1$  is taken to be the initial estimate for a second analysis where not all the points are taken into account. Only areas lying above the line joining the points  $(0, 3\sigma)$  and  $(3\sigma, 0)$ , with  $\sigma$  being the standard deviation from the fit are considered, so that points close to the origin are excluded since they introduce a bias. Moreover, outliers are excluded by taking only points within  $3\sigma$  from the first fit.

The same procedure is repeated now interchanging the data sets taken as a basis and taken as auxiliary. For the reasons outlined in Section 2.4.1, the inverse value of the slope now obtained,  $b'$ , differs from the slope  $b$  obtained in the first place. Therefore, the final calibration factor is then calculated by averaging these two values:  $b$  and  $1/b'$ .

Table 2.2 shows the results of the comparison between the sunspot areas, both the projected areas (PA) and those corrected for foreshortening (corrected areas, CA) measured by the different observatories. The observatories whose data is taken as the basis are indicated as Obs.1, while the observatories whose data is recalibrated are indicated as Obs.2.

Table 2.2: Calibration factors for the different observatories

Obs.1	Obs.2	Overlap Period	Calibration Factor PA	Calibration Factor CA	Correl. Coeff. PA	Correl. Coeff. CA
SOON	Rome	1982 – 1999	$0.791 \pm 0.105$	$0.846 \pm 0.138$	0.946	0.902
RGO	Rome	1958 – 1976	$1.095 \pm 0.086$	$1.097 \pm 0.084$	0.969	0.963
Russia	Rome	1968 – 1990	$1.169 \pm 0.058$	$1.227 \pm 0.107$	0.947	0.907
SOON	Yunnan	1982 – 1992	$0.913 \pm 0.113$	$0.907 \pm 0.131$	0.948	0.955
Russia	Yunnan	1968 – 1990	$1.321 \pm 0.215$	$1.365 \pm 0.242$	0.959	0.947
SOON	Catania	1982 – 1987	$0.948 \pm 0.042$	$0.925 \pm 0.097$	0.967	0.949
Russia	Catania	1978 – 1987	$1.236 \pm 0.052$	$1.226 \pm 0.059$	0.959	0.909
Russia	SOON	1982 – 1991	$1.402 \pm 0.131$	$1.448 \pm 0.148$	0.953	0.942
RGO	Russia	1968 – 1976	$1.019 \pm 0.067$	$1.028 \pm 0.083$	0.974	0.961
RGO	SOON	via Russia	$1.429 \pm 0.163$	$1.489 \pm 0.194$	-	-
RGO	Catania	via Russia	$1.240 \pm 0.099$	$1.234 \pm 0.119$	-	-
RGO	Yunnan	via Russia	$1.346 \pm 0.237$	$1.403 \pm 0.273$	-	-

Data series that do not overlap in time can be intercalibrated using the Zurich sunspot number as a common index (Fligge and Solanki 1997, Vaquero et al. 2004). Since this

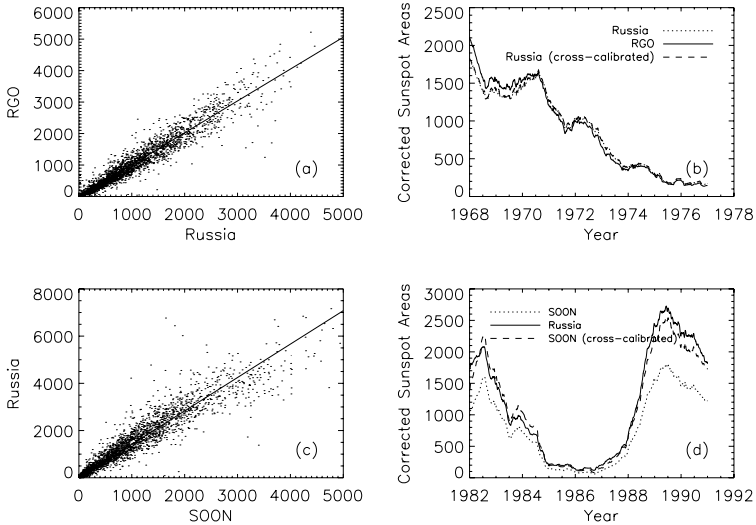


Figure 2.1: Comparison of sunspot areas corrected for foreshortening obtained by different observatories. Top: RGO vs. Russia, bottom: Russia vs. SOON. Left: scatter plots. Solid lines represent linear regressions to the data neglecting a possible offset (i.e., forced to pass through zero) as well as data points close to the origin and the outliers lying outside the  $\pm 3\sigma$  interval from the fit. Right: 12-month running means of sunspot areas vs. time. Solid curves show the data used as basis level and dot dashed the calibrated ones.

approach requires an additional assumption, namely that the size distribution of sunspots (Bogdan et al. 1988, Baumann and Solanki 2005) remains unchanged over time we avoid using it for calibration purposes. We use this comparison only for confirmation of the results obtained from the direct measurements, so that the new record is completely independent of the sunspot number time series.

#### 2.4.1 On the effect of including offset to calculate cross-calibration factors

Let us consider sunspot areas recorded by two different observatories, Obs.1 and Obs.2, during the same period. Let  $b$  be the slope of the linear regression when the area recorded by Obs.2 is the independent variable and  $b'$  the slope when the area recorded by Obs.1 is the independent variable. In the ideal case,  $b = 1/b'$ . However for real data sets this is not true. There are two reasons for this. Firstly, since sunspot areas cannot be negative, values close to zero introduce a bias into the regression coefficients. As a result, the slopes we obtain including an offset (dashed lines in Fig. 2.2) are typically lower than the ones

obtained by considering no offset (solid lines in Fig. 2.2). In particular, the obtained  $b$  is always lower than  $1/b'$ , whereas  $b'$  is lower than  $1/b$ . In order to overcome this, we force the fit to go through the origin (solid lines in Fig. 2.2). The corresponding slopes typically increase, such that values of  $b$  and  $1/b'$  become closer to each other, although still differ. Secondly, when looking for a relationship between the observatories, we assume measurements by one of them to be free of errors, whereas in reality both records are subjected to errors. This immediately produces different regressions depending on which data set is plotted on the ordinate. This is well illustrated by comparing the encircled data point in Figs. 2.2a and b (it corresponds to the same data point in both). In Fig. 2.2a, the point significantly lowers the regression slope, since there are hardly any data points at that location of the x-axis, while in Fig. 2.2b its influence is small, since it now lies at a well populated part of the x-axis. By removing such outliers, we further reduce the difference between  $b$  and  $1/b'$  but they are still not identical for purely statistical reasons. Therefore, as final factors we take the average between  $b$  and  $1/b'$ .

A more complicated case is the one when there is a significant offset between Obs.1 and Obs.2, for example due to the difference in the minimum area of the considered spots (see e.g. Fig. 2.2c and Table 2.1). In this case it may happen that  $b$  is not lower than  $1/b'$ . Then the slopes obtained by forcing the fit to go through zero do not necessarily improve the original ones. However, we apply the same procedure, neglecting the offset, for the following reasons: (1) the magnitude of the offset is rather uncertain due to the bias introduced by the positivity of the sunspot areas; (2) in doing this we may introduce some errors mainly at low values of sunspot areas, whereas values obtained during high activity levels which are of higher priority here are on average relatively reliable; (3) the real slope is still lying in the range  $[b, 1/b']$  (or  $[b', 1/b]$ ) so that an average of  $b$  and  $1/b'$  (or  $b'$  and  $1/b$ ) is a good approximation and finally (4), there are only few such cases (comparisons between areas from Russia and Rome and from Russia and Yunnan).

## 2.4.2 An alternative method to calculate cross-calibration factors

In addition to the method described in Section 2.4 and 2.4.1 to cross-calibrate different sunspot area data sets, we also performed the cross-calibration by varying a parameter  $f$  (defined below) in order to minimize a merit function  $\mathcal{M}$ , calculated over the  $N$ -days on which both  $A^{bas}$  and  $A^{aux}$  are available:

$$\mathcal{M} = \sum_{i=1}^N [A_{t_i}^{bas} - f \cdot A_{t_i}^{aux}]^2. \quad (2.2)$$

In order to find the absolute minimum of  $\mathcal{M}$  irrespective of the presence of any secondary minima, a genetic algorithm called Pikaia is used, which is available in the web: <http://www.hao.ucar.edu/public/research/pikaia/pikaia.html> (Charbonneau 1995).

In Fig. 2.3 an example of a comparison between two data sets and the difference between them after calibration using this technique is given. We show data from SOON and Rome, which overlap for a long period of time. 12-month running mean of the original data vs. time (upper panel) as well as the difference between them for both, original and calibrated data (lower panel) are shown.

In Table 2.3, values of the calibration factors for projected sunspot areas and for areas

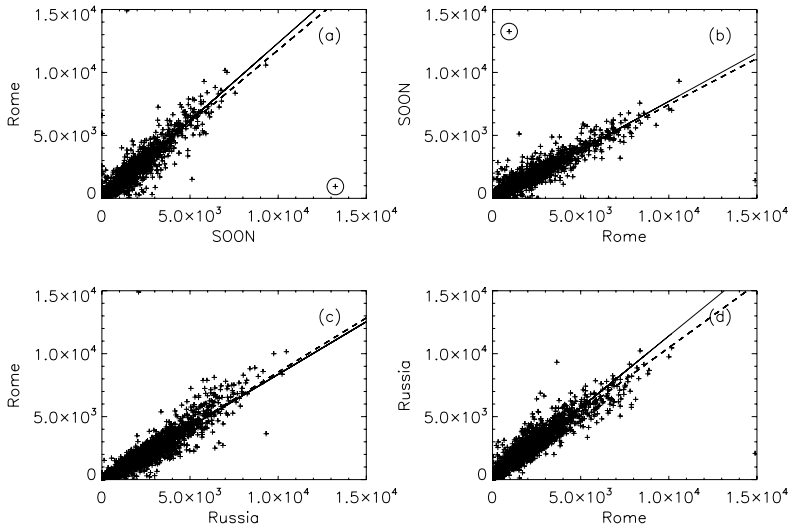


Figure 2.2: Comparison of sunspot areas for different observatories. Areas are in units of millionths of solar disk. The lines represent linear regressions to the data: standard (dashed) and forced to pass through the origin (solid). The encircled data point is discussed in the text.

corrected for foreshortening obtained using this technique are listed. The corresponding values for  $M$  are also tabulated. In all cases, these factors are lower than the ones found as explained in Section 2.4 and 2.4.1.

This technique differs from the one discussed in previous sections in that here the same weight is given to maximum and minimum phases of solar cycle. It can be seen from Fig. 2.3, that after calibration the difference between both data sets is very close to zero during activity minimum. However, during times of high solar activity this calibration technique does not give so accurate results. As mentioned before, one of the most important applications of sunspot areas data sets is irradiance reconstruction. So we intend to produce a homogeneous and as complete as possible time series of sunspot areas that can be used in irradiance models to describe adequately the variations. Since sunspots contribute to these variations mainly during times of high activity, we can neglect smaller areas in the comparisons in order to get a more appropriate calibration factor. For this reason, we suggest in this case to use the factors obtained with the method explained in the previous sections. Note, however, that in almost all cases factors obtained by the two methods agree within the given uncertainties.

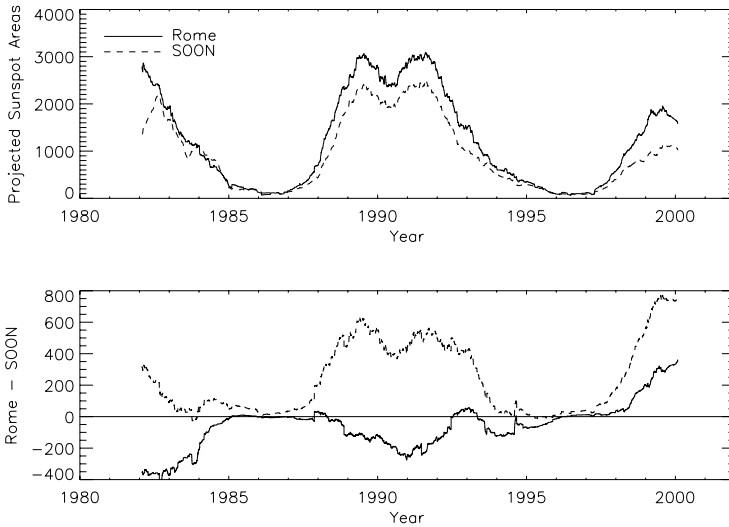


Figure 2.3: Upper panel: 12-month running means of projected sunspot areas. Areas are in units of millionths of the solar disk. They correspond to original values without any calibration. The solid line represents data from the Rome Observatory, the dashed line represents data from SOON. Lower panel: The solid line represents the 12-month running mean of the difference between data from these two observatories after calibrating the data. The dashed line is the difference between the original data from both observatories.

### 2.4.3 Error estimates

A single calibration factor is calculated for the whole period of overlap between two given data sets. In some cases however, the relation between two data sets was found to evolve with time. This can be seen in the right panels of Fig. 2.1(b and c), in which the 12-month running means of sunspot area records are plotted. Therefore factors for different sub-intervals are also calculated, in order to estimate the uncertainties of the final factors. This is performed by separating different solar cycles. When the whole interval of overlap does not cover more than one cycle, then the division is made when a change in the behaviour is observed (see e.g., the comparison between RGO and Russian data in the upper right panel of Fig. 2.1). The uncertainties of the factors result from the cycle-to-cycle variations (different factors for different cycles and/or subintervals), from the difference between  $b$  and  $1/b'$  and from the errors in determining the slopes. The main source of uncertainties come from the fact that the relationship between two given observatories during the period they overlap is not uniform. Therefore, the smallest errors are obtained when this period is short (see e.g., Russia - Catania, SOON - Catania in Table



Table 2.3: Calibration factors for projected and corrected sunspot areas measured by different observatories obtained by minimizing  $\mathcal{M}$ 

Obs.1	Obs.2	Calibration Factor PA	Calibration Factor CA	$\mathcal{M}$ PA	$\mathcal{M}$ CA
SOON	Rome	0.764	0.733	215.8	157.6
RGO	Rome	1.083	1.073	61.3	70.3
Russia	Rome	1.121	1.106	220.5	185.9
SOON	Yunnan	0.895	0.882	75.6	87.9
Russia	Yunnan	1.279	1.326	111.5	130.6
SOON	Catania	0.924	0.853	197.5	244.5
Russia	Catania	1.205	1.197	202.1	164.5
Russia	SOON	1.352	1.399	136.1	242.7
RGO	Russia	1.014	1.012	68.9	94.6

2.2). On the other hand, the largest errors are found in the comparison between Russia and Yunnan. This is discussed in more detail in the next Section.

## 2.5 Results and discussion

### 2.5.1 Comparison between sunspot areas

The results of the analysis described in in Section 3 are summarized in Table 2.2. The first two columns give the names of the data sets being compared, the third column the interval over which they overlap. In the following two columns we list the calibration factors by which the data of Obs.2 have to be multiplied in order to match those of Obs.1. In column 5 the factors for the originally measured areas (projected areas, PA) are given, while the next column lists the factors for the areas corrected for foreshortening (CA). The last two columns list the correlation coefficients between the two data sets.

With one exception the correlation coefficients for the projected areas are larger than for the ones corrected for foreshortening. This is not unexpected, since errors in the measured position of a sunspot increases the scatter in the areas corrected for foreshortening while leaving the projected areas unaffected.

In the following we discuss the results in greater detail. First consider the last three lines of the Table 2.2. Here we provide the factors by which SOON, Catania and Yunnan data need to be multiplied in order to match the RGO data. Since none of these data sets overlap with RGO we have used the Russian books as intermediary. Of course, correlation coefficients can not be determined in this case.

The comparison between RGO and Russia is made for the period from 1968 to 1976 when the data series overlap. As can be seen from Figs. 2.1 (a and b) the measurements

from RGO and Russia agree rather well with each other. The factor calculated from the comparison between these two observatories is very close to unity, although the difference between the two data sets displays a trend with time. Before 1970, areas from RGO are larger (6% for PA, 8% for CA) than Russian measurements and after that time areas from the Russian data set are 8% larger (see Fig. 2.1b) for both, PA and CA. This trend remains also after recalibrating the Russian data, because a single factor is not sufficient to remove this effect. Since it is not clear which (or both) of these two data sets contains an artificial drift, we do not try to correct for it.

Russian and SOON areas display more significant differences (see Fig.2.1 c and d). The overlap covers the period from 1982 to 1991, or cycles 21 and 22. During the whole time interval, SOON areas appear to be smaller (40 for PA, 45% for CA) than those of the Russian data. This is mainly due to the significant difference in the minimum values of the counted sunspots (1 ppm of the solar hemisphere for Russia vs. 10 ppm of the solar hemisphere for SOON, see Table 2.1). As can be seen from the Fig. 2.1d, the data from these two records also do not run in parallel, exhibiting quite a significant trend relative to each other (compare solid and dashed curves).

SOON and Rome measurements overlap between 1982 and 1999 covering three solar cycles: parts of cycles 21 and 23 and the whole of cycle 22. Similarly to the SOON vs. Russia case, the difference between these data sets varies strongly with time. During the declining phase of cycle 21, both observatories present similar values for the areas. However, SOON areas in cycle 22 are about 20% smaller than Rome data while during the ascending phase of cycle 23 they are about 40% smaller in both cases, for PA and CA.

Rome and RGO measurements overlap during the declining phase of cycle 19 and the whole of cycle 20. During the whole period, Rome provides smaller areas than RGO. The difference is only about 9% for PA (10% for CA) for the whole period of overlap. During cycle 20 the difference is of 15–18%, in agreement with the value found by Fligge and Solanki (1997). Russia and Rome present the longest period of overlap from 1962 to 1985, covering three solar cycles. The difference between these two data sets varies from cycle to cycle from about 15 to 17% in PA.

Projected areas measured by Catania Observatory are ~20–27% smaller than Russian measurements during solar cycle 21, and similar values are found for areas corrected for foreshortening. They are ~5–10% bigger than SOON measurements in the case of PA and ~4–7% in the case of CA. These data do not overlap in time with RGO measurements. The data provided by Yunnan overlap during parts of solar cycles 21 and 22 with Russia and with SOON. In the whole period Yunnan areas are smaller by about 32% for PA (36% for CA) with respect to the Russian books. Meanwhile PA are 6% (8% for CA) smaller than SOON areas during cycle 21, but ~14% larger in cycle 22.

In general, it was found that areas measured by the SOON network as well as the one measured by the Rome, Catania and Yunnan observatories are on average smaller than those reported by RGO and Russian stations, which agrees with the fact that the minimum areas of individual spots included into these two records are the smallest. For the same reason, SOON areas are smaller on average than the measurements from other observatories: as seen from Table 2.1, smallest spot areas recorded by other observatories analyzed here are not included in this time series.

The factor needed to calibrate SOON data to the RGO data set (10th row of Table 2.2) is 1.43 for projected areas in good agreement with the results by Hathaway et al. (2002)

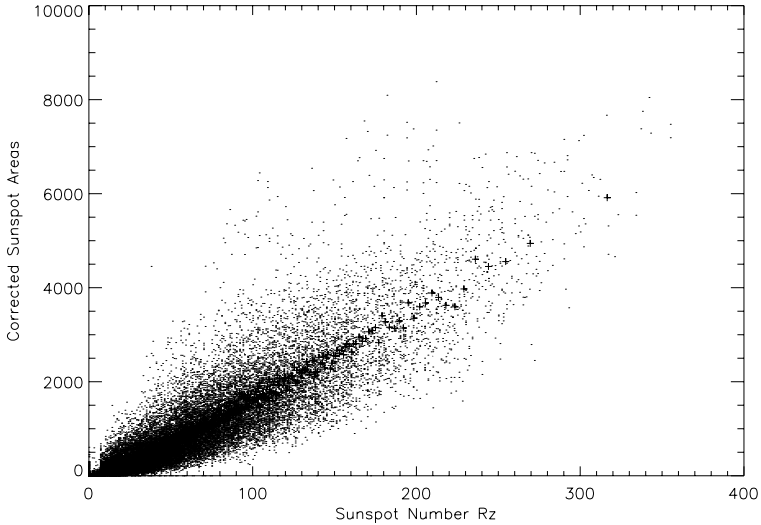


Figure 2.4: Sunspot areas corrected for foreshortening vs. sunspot number,  $R_z$ , for measurements made by RGO. The dots represent daily values between 1874 and 1976. Each '+' symbol represents an average over bins of 50 points.

and Foster (2004), who give 1.4 in both cases. However, in the case of areas corrected for foreshortening the factor is  $\sim 10\%$  larger, being 1.49.

### 2.5.2 Comparison with sunspot number

The relationship between both parameters, the Zürich relative sunspot number,  $R_z$ , and sunspot area shows a roughly linear trend with a large scatter. In Fig. 2.4 we plot sunspot areas corrected for foreshortening,  $A_S$ , for RGO measurements vs  $R_z$ . We have chosen  $A_S$  from RGO since they correspond to the longest running data set. The plus signs represent data points binned in groups of 50. These points indicate that the relationship is roughly, but not exactly linear. In particular at low  $R_z$  values,  $A_S$  appears to be too small, possibly because of the cutoff in the  $A_S$  measurements. However, this behaviour may reflect also the particular definition of  $R_z$ . It is observed from this plot that a given value of  $R_z$  corresponds to a range of values of sunspot areas. However, the scatter due to points within a single cycle is larger than the scatter from cycle to cycle.

When studying the relationship between  $A_S$  and  $R_z$  for individual cycles, it was observed that in some cases the scatter is significantly high. In such cycles, large areas are observed while  $R_z$  remains low. In particular, the shape of  $A_S$  cycles resembles that of  $R_z$  cycles, but individual peaks are more accentuated in  $A_S$ . This could be also a consequence

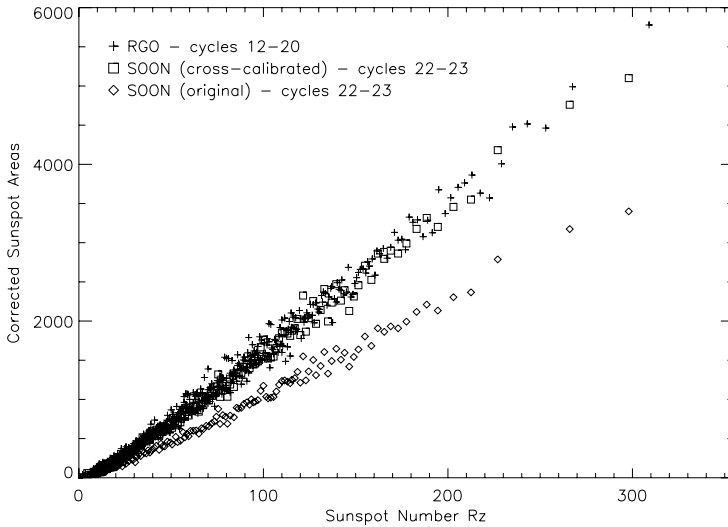


Figure 2.5: Sunspot areas corrected for foreshortening vs. Zürich relative sunspot number,  $R_z$ , for measurements made by RGO and SOON. Each symbol represents an average over bins of 50 points. The original data from SOON are represented by diamonds, after multiplication by a calibration factor of  $\sim 1.5$  in order to match RGO data, represented by squares.

of the definition of  $R_z$ , regarding the groups identification.

Fligge and Solanki (1997) already showed that in general, the relationship between  $A_s$  and  $R_z$  changes only slightly from one cycle to the next, with the difference being around 10%. This is illustrated in their Figure 5, where the slopes for different cycles is plotted. The biggest difference was observed between cycles 15 and 16, when the slope increased abruptly for about 25-30%. Fligge and Solanki (1997) argued that it might be more likely that the sun has undergone a change in its magnetic activity during these cycles and not in recent cycles.

Fig. 2.5 shows the comparison between sunspot areas corrected for foreshortening measured by RGO and by SOON with sunspot number. We have binned the data from each observatory every 50 points according to the sunspot number. The corrected areas from SOON lie significantly below the ones from RGO. In order to match RGO data, it is necessary to multiply SOON data by a calibration factor of  $\sim 1.5$  in agreement with the factor found by comparing the different data sets.

### 2.5.3 Cross-calibrated sunspot area records

In a next step we create records of projected and corrected sunspot areas covering the period from 1874 to present that are consistently cross-calibrated to the RGO values. We use RGO, Russia and SOON measurements as the primary sources of data. As shown by Table 2.1, these sources provide the most complete sets of sunspot area measurements, i.e., with only few gaps.

The individual periods of time over which each of these is taken as the primary source are:

1874 - 1976	RGO
1977 - 1985	Russia
1986 - present	SOON

The final sunspot area composite is plotted in Fig. 2.6. We have chosen to use the Russian data set until 1985 for the simple reason that this year corresponds to the solar minimum. In this way, each data set describes a different solar cycle (see Fig. 2.6). This is only approximately correct since sunspots from consecutive cycles overlap during a short period of time, but this is a second order effect. In this combination we opt to multiply the post-RGO measurements by the factors obtained here since RGO areas data set is by far the longest running and relatively homogeneous source. Any data gaps in the primary source are filled using data from one of the other two primary records (if available).

In this way, the final composite has only  $\sim 8\%$  of gaps over 47719 days. Using data from Rome and Yunnan, properly recalibrated, it was possible to fill in the gaps over a total of 115 days.

## 2.6 The Photometric Sunspot Index

When sunspots pass across the solar disk, a noticeable decrease in the measured total solar irradiance (TSI) is observed. TSI is the observed total power integrated over all wavelengths per unit normal area in the ecliptic plane received at 1 AU. To quantify the effect of sunspots on TSI, Willson et al. (1980), Foukal (1981) and Hudson et al. (1982) introduced the Photometric Sunspot Index,  $P_S$ . This index depends on the positions of the sunspots on the visible solar disc and on the fraction of the disk covered by the spots, i.e. on the sunspot area. It is thus clear that appropriately cross-calibrated sunspot areas are required for accurate reconstructions of solar irradiance, as already pointed out by Fligge and Solanki (1997), Froehlich et al. (1994).

Therefore we now calculate the daily  $P_S$  index following Foukal (1981) from the area  $A_S$  and the heliocentric positions  $\mu$ , of the sunspots present on the solar disk:  $\mu = \cos \theta$ , with  $\theta$  being the heliocentric angle. First, the deficit of radiative flux,  $\Delta S_S$ , due to the presence of a sunspot of area  $A_S$  is calculated as:

$$\frac{\Delta S_S}{S_Q} = \frac{\mu A_S (C_S - 1)(3\mu + 2)}{2}. \quad (2.3)$$

This value is expressed in units of  $S_Q$ , the solar irradiance for the quiet Sun (i.e. solar surface free of magnetic fields).  $S_Q = 1365.5 \text{ Wm}^{-2}$  is taken from the PMOD Composite of measured solar irradiance (Fröhlich 2003, 2006). The residual intensity contrast of the sunspot relative to that of the background photosphere  $C_S - 1$  is taken from Brandt

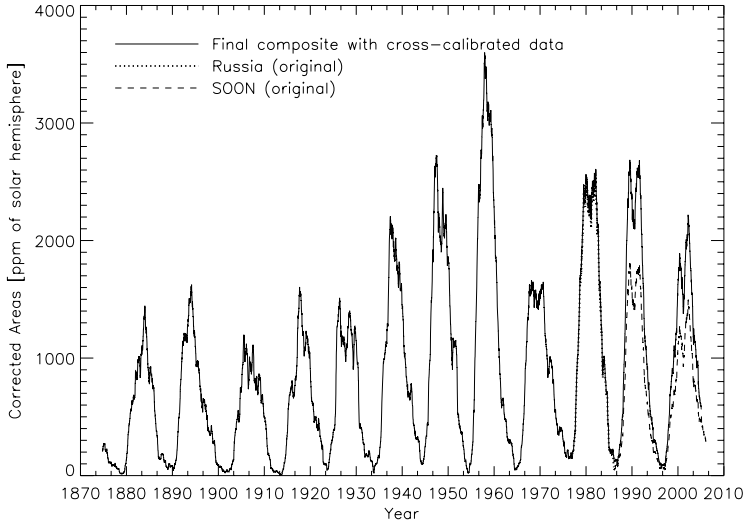


Figure 2.6: 12-month running means of sunspot areas corrected for foreshortening of the final composite using the factors given in Table 2.2 (solid curve). Also plotted are the Russian and SOON data entering the composite prior to calibration.

et al. (1992). It takes into account the dependence of sunspot residual intensity contrast on sunspot area, i.e., larger sunspots are darker than smaller spots:

$$C_S - 1 = 0.2231 + 0.0244 \cdot \log(A_S). \quad (2.4)$$

The bolometric sunspot blocking function,  $P_S$  is then obtained by summing the effects from all the sunspots present on the disk:

$$P_S = \sum_{i=1}^n \left( \frac{\Delta S_s}{S_Q} \right)_i. \quad (2.5)$$

Figure 2.7 shows the time series of 12-month running mean  $P_S$  index obtained as explained here for the period 1874-2004.

The technique to reconstruct solar irradiance involving  $P_S$  was first developed by Foukal and Lean (1986). The first step consists of subtracting the sunspot darkening described by the  $P_S$  index from the measured solar irradiance. These residuals are considered as an estimate of the facular contribution, so then they are compared to a facular proxy (10.7cm flux, Ca K plage data, sunspot number) in order to reconstruct the irradiance for longer timescales. Thus, any uncertainty in  $A_S$  affects directly the calculation of  $P_S$  index and consequently the estimate of facular contribution. In turn, results based on

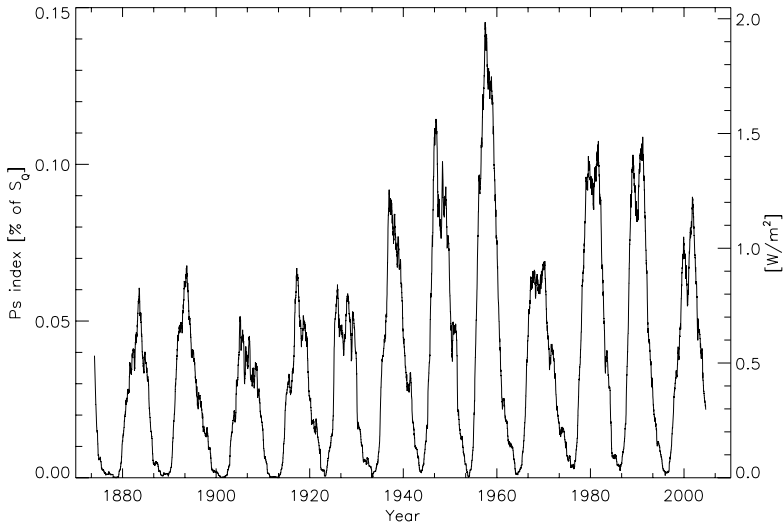


Figure 2.7: 12-month running mean of the photometric sunspot index,  $P_S$ , computed using the sunspot areas composite produced here. The y-axis is expressed in percents of  $S_0$ .

inappropriately combined sunspot areas data sets can suggest misleading interpretations when studying, for instance, the possible link between solar irradiance variability and Earth's climate changes.

## 2.7 Summary and conclusions

We have investigated here the relationship between sunspot areas from different observatories by comparing them during the time when they overlap with each other. We found a good agreement between sunspot areas measured by Russian stations and RGO, while a comparison of sunspot areas measured by the SOON network with Russian data shows a difference of about 40% for projected areas and 44% in areas corrected for foreshortening. This is at least partly due to the different minimum areas of sunspots taken into account in these data sets: smallest areas included in the RGO and Russian records are 10 times smaller than those in the SOON series (see Table 2.1). SOON sunspot areas are combined with those from RGO and Russia by multiplying them by a factor of 1.43 in the case of projected areas and 1.49 in the case of areas corrected for foreshortening. Data from other observatories are employed to fill in some of the remaining gaps. In this manner, a consistent sunspot area database is produced from 1874 to present. We expect it to contribute to the improvement of studies on longer time-scales of, e.g., the total and spectral solar irra-

diance until more accurate measurements become available such as those from Debrecen Observatory in Hungary (Győri et al. 1998, 2000).



# 3 Reconstruction of solar total and UV irradiance from the sunspot and plage areas

## 3.1 Abstract

In order to study the possible influence of solar variability on the Earth's climate, accurate long-term series of reconstructed solar irradiance are required. These, in turn, need reliable data to describe the irradiance depletion produced by sunspots and the enhancement caused by faculae and network. Sunspot areas are available since 1874, with continuous records being kept by the Royal Greenwich Observatory up to 1976 and continued by other ground-based observatories around the world. The use of these data sets then requires a careful cross-calibration, as pointed out by diverse authors, to correctly describe the irradiance variations. In this Chapter, we make use of these improved indices of solar activity to reconstruct total and UV solar irradiance for the period 1915-1999. We show that since UV and total irradiance depend quite differently on sunspot areas. Any error in this quantity, e.g., due to incorrect intercalibration of  $A_S$  time series from different sources leads to systematic differences between reconstructed total and UV irradiance. Our results show that the use of properly intercalibrated sunspot areas results in very similar time series for both solar total and UV irradiance. Diverging results in the literature are found to be due to the use of inadequately intercalibration of sunspot area time series. Consequently, claims that solar UV irradiance is less important than total solar irradiance for climate are baseless.

## 3.2 Introduction

Similarities among various records of climate and solar activity suggest that the climate variability may be partly attributed to the solar variations. Some climate records, for instance, show periodicities of 11 and 22 years, as solar activity does (Labitzke and van Loon 1995, White et al. 1997, van Loon and Labitzke 2000, Marsh and Svensmark 2000). In addition, good correlations have been found between proxies of solar activity and climate records on timescales of decades and centuries (Eddy 1976, Friis-Christensen and Lassen 1991, Friis-Christensen 2000, Lean et al. 1995). In particular, solar irradiance and global or northern hemisphere temperature show a high correlation (Solanki and Fligge 1998, Solanki and Krivova 2003).

It is known that solar irradiance variability can influence the Earth's climate in different ways, e.g., via changing the total energy input into the geosystem (which is determined by the behaviour of the total solar irradiance), or via influences on the stratospheric chemistry, which is determined mainly via solar UV irradiance variability (Haigh 1999, Haigh et al. 2005, Larkin et al. 2000, Rind 2002, Egorova et al. 2004, Rozanov et al. 2004).

Hence the correlation between total or UV solar irradiance with global temperature is a possible tool to distinguish between these two mechanisms. Attempts to do this have given opposite results, however. Thus Solanki and Krivova (2003) found that both total solar irradiance and UV-irradiance evolve in almost the same manner and give nearly identical correlations with climate time series. Foukal (2002), however, obtained two rather different time series for total and UV irradiance, of which the former showed a much better correspondence with climate. In particular, his reconstructed total solar irradiance displays a strong increase since 1970.

Irradiance variations are due to solar surface magnetism. If the evolution of the solar surface flux is known (either from direct measurements or proxies), it is possible to reconstruct the cyclic component of the past irradiance changes. Here, we reconstruct total and UV solar irradiance from different proxies of the magnetic field distribution, namely the sunspot areas and plages plus enhanced network areas. We redo the analysis of Foukal (2002), but employing a carefully intercalibrated series of sunspot areas.

In Section 3.3, we estimate the contribution of active regions to the irradiance variations. In Section 3.4, we reconstruct total and UV irradiance for the period 1915-1999. In Sections 3.5 and 3.6 we discuss the relation of the reconstructed irradiance records to the global temperature and finally we summarize the conclusions in Section 3.7.

## 3.3 Quantifying the active-region contribution to the solar irradiance variations

### 3.3.1 Sunspot darkening

Reductions in the total solar irradiance are caused by the passage of dark sunspots across the solar disc. To describe the effect of sunspots on the total solar irradiance, Willson et al. (1980), Foukal (1981), Hudson et al. (1982) introduced the Photometric Sunspot Index (PSI or  $P_S$ ). The  $P_S$  index is calculated following Foukal (1981) from the sunspot area in units of the solar hemisphere,  $A_S$ , and heliocentric position  $\mu$  of the sunspots present on the solar disc.  $P_S$  is given in percents of  $S_\odot$ , the mean quiet sun irradiance taken from the PMOD irradiance composite (Fröhlich 2000, 2006). We have taken the sunspot areas and the  $\mu$ -values from the composite of RGO/Russia/SOON data, after a careful cross-calibration (Balmaceda et al. 2005). Fig. 3.1 shows the time series of 12-month running mean  $P_S$  index for the period 1915 – 1999 calculated from original data from the RGO and the SOON network (dashed black line) and from cross-calibrated (gray solid line) sunspot areas. It is clear from this plot that the cross-calibrated areas measured after 1977 (post RGO measurements) are considerably larger than the original ones. The need of a proper cross-calibration of different data sets of sunspot areas was first reported by Fligge and Solanki (1997) after comparing them with the Zurich relative sunspot number. Over the period 1874 – 1976, these two indices run parallel to each other but in the following solar

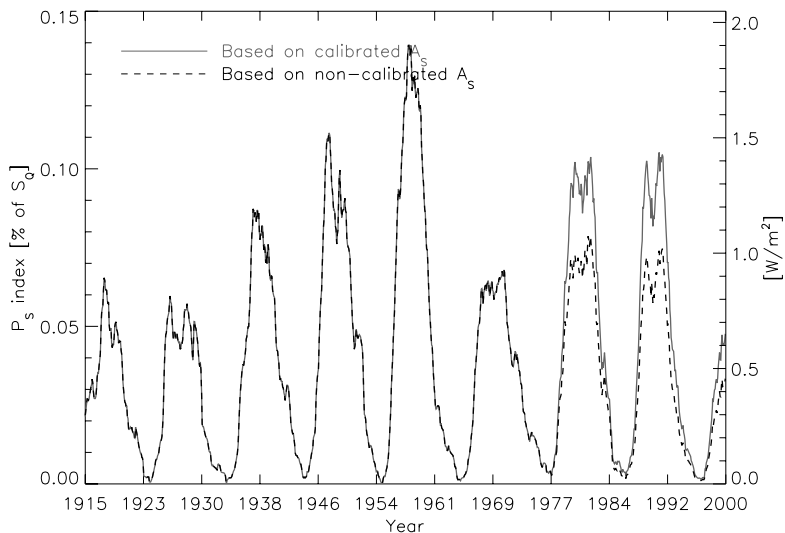


Figure 3.1: 12-month running mean of  $P_S$  index using sunspot areas composite (gray solid line) and the original data without proper cross-calibration (black dashed line). The y-axis is expressed in percentage of  $S_{\odot}$ .

cycles sunspot areas appeared to be significantly smaller. The cross-calibrated sunspot areas time series does not display this anomalous behaviour. The use of the carefully cross-calibrated sunspot areas time series, instead of simply the raw data is the main difference between our work and that of Foukal (2002).

### 3.3.2 Facular brightening

The facular contribution to the solar irradiance is more difficult to assess, because of their low contrast, especially at disc center. Areas of plages observed in the Ca II K line chromospheric emission are a good proxy for direct facular measurements (Caccin et al. 1998).

We employ the same proxy as Foukal (2002), a monthly mean time series of plage plus enhanced network areas,  $A_{PN}$ . This data set was kindly provided by P. Foukal (see Fig. 3.2). Areas were measured from spectroheliograms and photoheliograms in the K-line of Ca II obtained at Mt. Wilson, McMath-Hulbert and Big Bear observatories in the period 1915 – 1984 (Foukal 1996, 1998). Later, this time series was extended until 1999 using data from Sacramento Peak Observatory (SPO). The data covers the period August 1915 – December 1999 inclusive. The identification of plages and enhanced network was

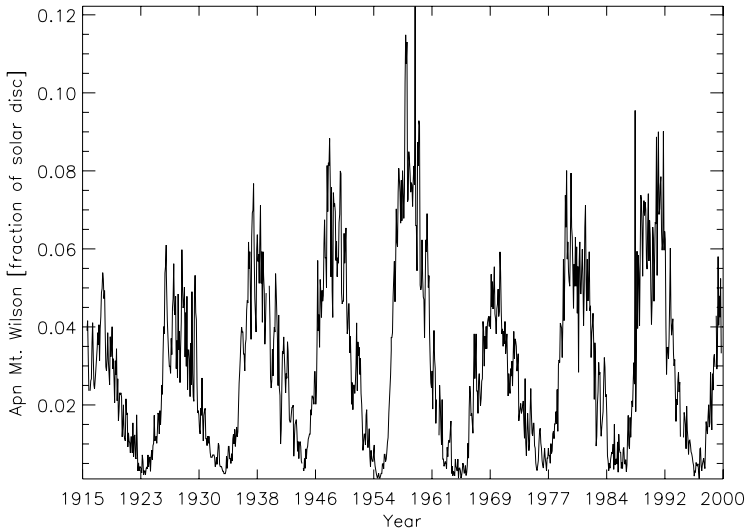


Figure 3.2: Monthly mean values for plage areas plus enhanced network in units of the projected disc.

performed by several observers and it was based on a density threshold criterion.  $A_{PN}$  are expressed in fractions of the solar disc. The 1915 – 1984 data are taken from daily images, but after 1984 data are based on four evenly-spaced images per month. The monthly values are only an intermediate data product that is relatively noisy. Since the lifetime of plages and network are larger than the solar rotation timescale, monthly averages are sufficient to study long-term variations in solar irradiance. The data also contain few gaps that are smoothed out by calculating the 12-month running means. Furthermore, the reduction procedure to derive the  $A_{PN}$  index was carried out on images of photographic density instead of photometrically calibrated intensity (Foukal 1996). Consequently effects introduced by, for instance, the blanchening curves of the film used, are not accounted for. Such a calibration would be necessary when doing quantitative studies of the long-term trend in plage or network evolution. The data may well contain inaccuracies due to this. However, unlike the sunspot areas,  $A_{PN}$  enters in both total and UV irradiance equally, so that any errors should affect both reconstructed time series by roughly the same amount and thus should not affect the main result.

### 3.4 Reconstruction of irradiance from plage and sunspot areas

Total and UV solar irradiance time series are reconstructed following Foukal (2002). Enhancements in total solar irradiance are proportional to the difference in plage,  $A_{PN}$ , and sunspot areas,  $A_S$ , whereas enhancements in UV irradiance are proportional to the plage areas alone. As a first step, residuals of solar irradiance and the sunspot darkening  $S - P_S$  (a measure of facular contribution to the total irradiance) are calculated for the time when irradiance measurements are available, i.e. from 1978 till the present. Total solar irradiance measurements are taken from the PMOD composite derived from different instruments with best allowance for their degradation and inter-calibration (Fröhlich 2000, 2006). Then, a regression relation of the form:  $S - P_S = b \cdot A_{PN} + a$  is constructed between the monthly mean values of these residuals and of the plage areas,  $A_{PN}$  (see upper panel of Fig. 3.3). The regression relation is then used to reconstruct the residuals  $(S - P_S)_{rec}$  between 1915 and 1999 when values of  $A_{PN}$  are available (see Fig. 3.3, middle panel). The reconstructed total solar irradiance is finally obtained by just adding back the time series of  $P_S$  over this period as shown in bottom panel of Fig. 3.3.

Residuals  $S - P_S$  and  $A_{PN}$  time series are compared in different periods:

- 1980 – 1988 (as used by Foukal 2002)
- 1990 – 1998 (when the irradiance measurements are more reliable)
- 1979 – 1998 (whole period of overlap of irradiance measurements and  $A_{PN}$ )

The regression parameters, as well as their uncertainties and the correlation coefficients for each of these comparisons are shown in Table 3.1. In all the cases, the offset values,  $a$ , are very small (of the order of  $10^{-2}$ ) and the slopes,  $b$ , do not vary too much from each other, so that the reconstructed total solar irradiance using any of the 3 sets of parameters is relatively similar. The correlation coefficients are high in all cases ( $> 0.93$ ), but the highest correlation coefficient is obtained for period 1990–1998, in which irradiance measurements are more accurate. For this reason, we choose the parameters from this comparison to reconstruct the irradiance back to 1915. Fig. 3.3 shows the result of this reconstruction. The variability of the solar flux at wavelengths shorter than 250 nm is determined mainly by the bright magnetic plages and enhanced network in active regions. Its reconstruction follows the same steps as of the total solar irradiance, except that the last step (adding back the  $P_S$ ) is not carried out.

Table 3.1: Regression parameters from the comparison between  $S - P_S$  and  $A_{PN}$  for different periods

Period	b	a	$R_c$	$\sigma_b$	$\sigma_a$
1980 – 1988	2.9	$-5.0 \cdot 10^{-3}$	0.93	$1.2 \cdot 10^{-1}$	$3.9 \cdot 10^{-3}$
1990 – 1998	2.5	$-1.1 \cdot 10^{-2}$	0.95	$8.3 \cdot 10^{-2}$	$3.0 \cdot 10^{-3}$
1979 – 1998	2.7	$-6.3 \cdot 10^{-3}$	0.93	$6.9 \cdot 10^{-2}$	$2.7 \cdot 10^{-3}$

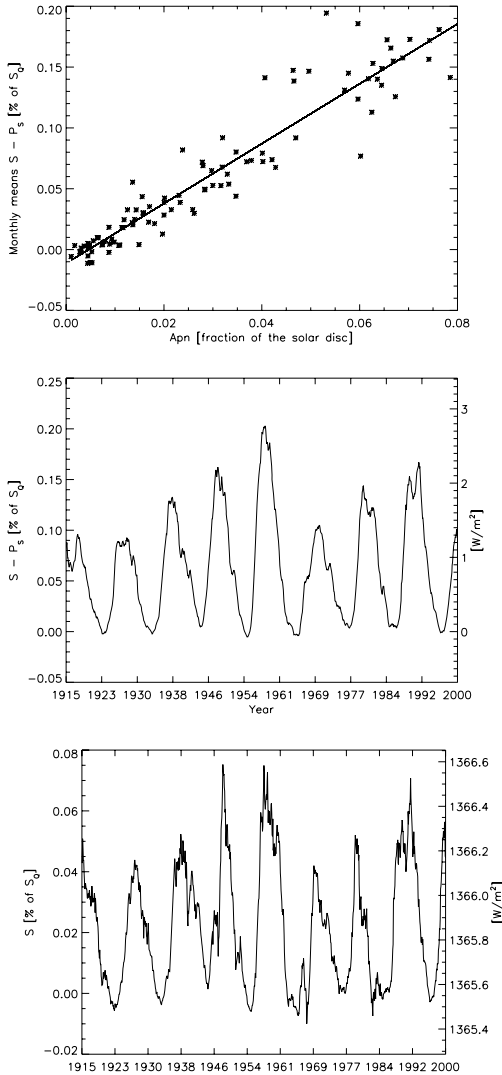


Figure 3.3: Top:  $A_{PN}$  vs. residuals  $S - P_S$  for the period 1990 - 1998. Middle: 12-month running means of the residuals  $S - P_S$  reconstructed from the relation regression of top panel. Bottom: 12-month running means of the reconstructed total irradiance  $S$ .

### 3.5 Comparison with climate records

In order to test whether the total solar irradiance really correlates better with Earth's climate than UV irradiance, we compare both irradiance time series reconstructed here with the global sea surface temperature records compiled by the Climatic Research Unit of the University of East Anglia. This data set extends from 1856 to 2005 and provides the anomalies from the mean temperature calculated for the best period of coverage: 1961-1990 (Jones 1994, Jones and Moberg 2003). This is to account for the differences introduced by methods, formulae and altitudes of the stations distributed all over the world. Fig. 3.4 displays the comparison between the global temperature,  $T$ , and the UV irradiance, whose variation is given mainly by the variation in the plage areas,  $A_{PN}$ . The correlation coefficient from this comparison for the whole period (1915-1999) is 0.59. No lag is observed between both time series. In Fig. 3.5 the 11-yr running mean of total irradiance reconstructed here,  $S$  (dashed line), and the global temperature,  $T$  (solid line), are compared. The correlation coefficient is in this case very similar (0.57) to that found in the comparison of temperature and UV-irradiance and there is also no lag between both records.

In Table 3.2 a summary of these results is presented. Correlation coefficients for the comparison between temperature and total and UV-irradiance are shown. The values in parenthesis correspond to the comparison of total irradiance using uncalibrated sunspot areas.

Table 3.2: Correlation coefficients for the comparison between solar irradiance and temperature

Period	Reconstructed Solar Irradiance	
	Total	UV
< 1970	0.54 (0.42)	0.62
< 1999	0.57 (0.87)	0.59

### 3.6 Discussion

In Foukal (2002), the reconstruction of total irradiance shows a clear upward trend after year 1970 due to the strong presence of faculae not balanced by increased sunspot area. This result was interpreted as an evidence for a difference in the behaviour between the total irradiance and UV-irradiance and consequently a very different influence on the Earth's climate. However, it was shown here that this result was obtained by using uncalibrated data when quantifying the effect of sunspots in the solar irradiance. Compare the 11-yr running mean of the reconstructed total irradiance in Fig. 3.5 from sunspot areas before (dotted line) and after calibration (dashed line). The steep increase of the total irradiance

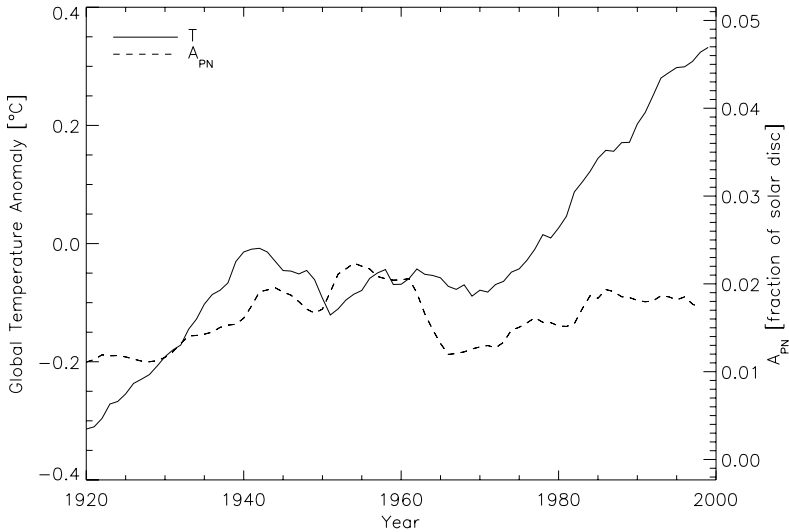


Figure 3.4: 11-yr running mean of UV solar irradiance given by the variation of the plage areas (dashed line) and Global Temperature Anomalies (solid line).

after 1970 observed in the curve from uncalibrated sunspot areas is no longer observed when an appropriate calibration is performed. The increase in the 11-yr running mean of the total solar irradiance between 1920 and 1999 is  $\sim 0.013\%$ . When uncalibrated sunspot areas are used, the total increase is  $0.006\%$  larger. Meanwhile, the increase in the UV-irradiance is  $\sim 0.009\%$ . The shape of the total irradiance estimated from calibrated data now follows closely the shape of the variation in  $A_{PN}$ , shown in Fig. 3.4.

The differences in the scales between this Figure and Fig. 2 of Foukal (2002) are due to the choice of a different period of comparison to get the regression relation.

We would like to stress that the total and UV solar irradiance reconstructed here are not necessarily correct, since this approach has some shortcomings. One concerns the  $A_{PN}$  time series, which is based on uncalibrated spectroheliograms. Film calibration in photographic plates and variable image quality are some of the factors that introduce uncertainties in the extraction of the features and need to be taken into account. They affect the correct identification of different features in the Ca II K images which is based on criteria of decreasing intensity, decreasing size or decreasing filling factors (Worden et al. 1998). Another concerns the simplicity of the model assumed here, which does not contain a secular trend, unlike recently developed models, for instance: Foster (2004), Wang et al. (2005). Such a secular trend can be produced by long-term changes in the network, which is very poorly sampled by the  $A_{PN}$  data employed here.

In Fig. 3.2 the  $A_{PN}$  are seen to drop nearly to zero at solar activity minimum (very



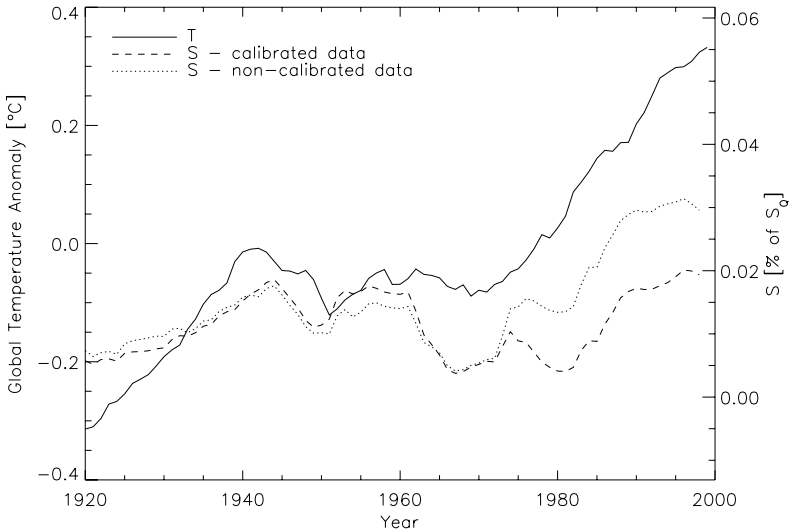


Figure 3.5: Comparison of Global Temperature Anomalies (solid line) and the reconstructed total solar irradiance  $S$  based on calibrated data (dashed line) and non-calibrated data (dotted line).

similar to what occurs with sunspots) indicating that the network contribution is not totally accounted.

The argument used by Foukal (2002) to neglect any secular variation was based on the work of Foukal and Milano (2001), who noted no change in the network during activity minima at different times in the 20th century. Recently, however, it has been shown that the absence of calibration of the employed data make the results of this analysis highly doubtful (Ermolli et al. 2007).

### 3.7 Concluding remarks

We have presented here a reconstruction of total and UV solar irradiance based on sunspot and plage areas for the period 1915 – 1999. We would like to stress two main points. First, it is worthy to note the importance of using appropriately calibrated data. The number of instruments has increased with time, providing long time series of different solar indexes. However, since their methods and observation techniques differ, intercalibration of the data is essential. It was proved here that the use of data of different sources directly combined can suggest erroneous conclusions. If the correct sunspot areas are used then total and UV irradiance behave very similarly in agreement with more careful reconstructions

(e.g. Fligge et al. 2000). The total solar irradiance now also does not display a rapid rise in the last 30 years. This result is important since it is now possible to distinguish between total and UV solar irradiance regarding their influence on climate on the basis of their correlation with temperature records.

However, we need to warn that comparisons of simply cyclic irradiance variations with temperature may not be appropriate. There is evidence for a secular change in the magnetic flux of the Sun, and therefore in the solar irradiance. Models based only on statistical relationship between different proxies of solar activity describe successfully the cyclic variation of the past irradiance. However it is necessary also to include reliable estimates of the secular change in the irradiance models. These aspects should be taken into account to compare irradiance with climate records, such as temperature.

# 4 Reconstruction of solar total irradiance from the surface magnetic flux

## 4.1 Abstract

Total solar irradiance changes by about 0.1% between solar activity maximum and minimum. Accurate measurements of this quantity are only available since 1978 and do not provide information on longer-term secular trends. In order to reliably evaluate the Sun's role in recent global climate change, longer time series are, however, needed. They can only be assessed with the help of suitable models. The total solar irradiance is reconstructed from the end of the Maunder minimum to the present based on variations of the surface distribution of the solar magnetic field. The latter is calculated from the historical record of the sunspot number using a simple but consistent physical model. Our model successfully reproduces three independent data sets: total solar irradiance measurements available since 1978, total photospheric magnetic flux since 1974 and the open magnetic flux since 1868 empirically reconstructed using the geomagnetic *aa*-index. The model predicts an increase in the solar total irradiance since the Maunder minimum of  $1.3_{-0.4}^{+0.2} \text{ Wm}^{-2}$ .

## 4.2 Introduction

Variations in solar total (i.e. integrated over all wavelengths) and spectral irradiance have been measured by a number of partly overlapping space experiments since 1978 and 1991, respectively (e.g., Willson and Hudson 1988, 1991, Brueckner et al. 1993, Woods et al. 1996, Floyd et al. 2003, Fröhlich 2003, and references therein). There is strong interest in this quantity due to its potential influence on global climate. Many investigations have considered whether and how the observed variations in solar irradiance influence the Earth's climate (e.g., Haigh 1996, 1999, Kodera and Kuroda 2002, Coughlin and Tung 2004, Arnold 2005, Kuroda and Kodera 2005, Egorova et al. 2005, Langematz et al. 2005, Sinnhuber et al. 2005, Dameris et al. 2006a,b). Variations of solar irradiance on longer time scales, which have not been directly measured, are possibly of even greater importance for the global climate change (e.g., Eddy 1976, Reid 1987, Bond et al. 2001, Haigh 2001, Shindell 2001, Rind 2002, Stott et al. 2003), since the coupled system of the Earth's atmosphere and oceans reacts rather slowly to the varying solar signal (but see

Foukal et al. 2006). Hence understanding the mechanisms of solar impact on the Earth's environment is plagued by the inadequate length of the directly measured time series of solar irradiance. Only a reconstruction of solar irradiance for the pre-satellite period with the help of models can aid in gaining further insight into the nature of this influence.

A number of long-term (up to 300–400 years) reconstructions, both purely empirical and more physics-based, have been produced in the last two decades (for more details and references see the overviews by, e.g., Solanki and Krivova 2004, Lockwood 2005). Such reconstructions are usually split into two parts: reconstruction of a cyclic component and the secular variation. The reconstruction of the cyclic component is relatively straightforward from various historical proxy records of solar magnetic activity, such as the (Group and Zurich) sunspot number, sunspot areas, white-light facular areas, Ca II plage areas, etc. (e.g., Foukal and Lean 1990, Hoyt and Schatten 1993, Lean et al. 1995, Lean 2001, Solanki and Fligge 1998, 1999, Fligge et al. 2000, Preminger and Walton 2005).

The magnitude of the secular change in the irradiance is far more speculative. Evidence for such a long-term trend was initially provided by stellar data. Baliunas and Jastrow (1990) found that the distribution of Ca II H and K emission in field stars fell into two groups. They argued that stars with the lowest Ca II brightness do not show any cyclic modulations and are thus in a state similar to the Maunder minimum. On the other hand, the Sun's Ca II level at recent activity minima remained markedly higher than that of most other late-type stars in the Baliunas & Jastrow sample (White et al. 1992). This could mean that the Sun during the Maunder minimum was much more quiet than during current minima, e.g. due to disappearance of the network. Assuming that the relationship between solar Ca II brightness and irradiance did not change, estimates of the irradiance increase since that time encompassed the range between 2 and  $16 \text{ Wm}^{-2}$  (Lean et al. 1992, Zhang et al. 1994, Mendoza 1997).

The stellar evidence is indirect and based on a number of assumptions. For example, extrapolation of the relation between Ca II flux and the irradiance measured for recent cycles to lower levels of activity is based on the assumption that this relationship is the same for the quiet Sun and active regions (which differ, e.g., in the absence and presence of sunspots). Also, recent measurements of carefully selected samples of stars suggest that many of the 'Maunder minimum' stars in the Baliunas & Jastrow sample had, in fact, evolved from the main sequence (Wright et al. 2004). In addition, stars in a Maunder minimum-like state do not always exhibit Ca II emission brightness below that of solar minimum (Hall and Lockwood 2004).

The problems faced by the stellar approach have recently led to the development of alternative methods. Thus, assuming that faculae are located near sunspots, Foster (2004), cf. Lockwood (2005), reconstructed the butterfly diagram for faculae using the historical record of sunspot areas and positions. He then employed averaged functions for the centre-to-limb variations of the facular contrasts derived by Ortiz et al. (2002), in order to model facular brightening. Analysing the distribution of the magnetic field in the recent period and assuming that the Sun was magnetically quiet during the Maunder minimum he set an upper limit of  $\approx 1.7 \text{ Wm}^{-2}$  on the secular variation since that time. This limit increases to approx  $2.1 \text{ Wm}^{-2}$  if the weak magnetic flux escaping registration in the Michelson Doppler Imager (MDI) magnetograms due to insufficient spatial resolution (Krivova and Solanki 2004) is taken into account. Additional uncertainty in this model is introduced by the fact that the contrasts derived at a single wavelength are used instead of

more realistic facular models.

A yet lower value of about  $1 \text{ Wm}^{-2}$  for the increase in the cycle-averaged total solar irradiance (TSI) since the beginning of the 18th century was published by Wang et al. (2005), who used a flux transport model to simulate the evolution of the solar magnetic flux and then the TSI. Solanki et al. (2000, 2002) presented a simple physical model that allows a reconstruction of the solar total and open magnetic flux from the sunspot number and provides an explanation for the origin of the secular variation displayed by the open flux. Here we use this model to reconstruct the solar total irradiance variations back to 1700 using the Zurich sunspot number and to 1610 using the Group sunspot number. In our approach we follow the successful irradiance modelling by, e.g., Wenzler et al. (2006) as closely as possible and extend it to longer times. We also constrain our reconstructions by requiring them to reproduce the available time series of total solar irradiance as well as total and open magnetic flux. We describe our approach in Sect. 4.3, present and discuss the results in Sect. 4.4 and sum up our conclusions in Sect. 4.5.

## 4.3 Approach

Our model describes irradiance changes on time scales of days to centuries that are due to the evolution of the solar surface magnetic flux. Models based on this assumption explain about 90% of all irradiance changes observed on time scales of a day to decades (Krivova et al. 2003, Wenzler et al. 2004, 2005, 2006). Of course, we cannot rule out that other effects also influence irradiance on longer time scales (e.g., changes in convection or thermal shadows from subsurface flux Parker 1987, 1995), but since there is no observational evidence for that, we here ignore all other possible influences.

The success of the model by Krivova et al. (2003) and Wenzler et al. (2005, 2006) implies that if the evolution of the magnetic flux is known for each photospheric component (sunspots, faculae and the network), then it is also possible to calculate irradiance variations. Unfortunately, measurements of the magnetic flux are not available prior to the second half of the 20th century, so that it has to be computed based on some proxy. A model that allows a reconstruction of the solar magnetic flux from the sunspot number has been worked out by Solanki et al. (2002). We outline the idea of this model in Sect. 4.3.1, describe how we use it for the irradiance reconstructions in Sect. 4.3.2 and review the model parameters and the available observational data that need to be reproduced by a successful model in Sect. 4.3.3.

### 4.3.1 Photospheric magnetic flux

For simplicity, we divide the continuous spectrum of sizes of magnetic structures on the solar surface into active and ephemeral regions. Active regions (AR) are larger bipolar structures emerging in the activity belts at latitudes below approximately  $\pm 30^\circ$  and living up to several weeks. They generally contain one or more sunspots. The flux emergence rate in active regions can be estimated from the historical record of the sunspot number.

Ephemeral regions (ER) emerge at all latitudes in the form of smaller, short-lived bipoles. They do not contain sunspots. Due to their high emergence rate (Harvey 1993, Hagenaar 2001) their contribution to the total photospheric magnetic flux is significant.

ER evolve over a cycle which is extended with respect to the sunspot cycle (e.g., Harvey 1992, 1994). In order to describe their evolution in time, we assume that the length and the amplitude of the ER cycle are related to the properties of the corresponding sunspot cycle, i.e. we assume that they are produced by the main dynamo, just like the active regions.

Most of the emerged photospheric flux forms closed loops until it decays due to cancellation with flux of opposite polarity. A small part of it is, however, dragged outward by the coronal gas and reaches far into the heliosphere. This is called the open magnetic flux. Both active and ephemeral regions contribute to the open flux, which can survive on the solar surface for several years, since it is located in often large regions with a dominant magnetic polarity (e.g., at the poles).

A set of three coupled ordinary differential equations has been shown to describe the evolution of the three flux components (Solanki et al. 2002):

$$\frac{d\phi_{\text{act}}}{dt} = \varepsilon_{\text{act}}(t) - \frac{\phi_{\text{act}}}{\tau_{\text{act}}} - \frac{\phi_{\text{act}}}{\tau_{\text{ta}}}, \quad (4.1)$$

$$\frac{d\phi_{\text{eph}}}{dt} = \varepsilon_{\text{eph}}(t) - \frac{\phi_{\text{eph}}}{\tau_{\text{eph}}} - \frac{\phi_{\text{eph}}}{\tau_{\text{te}}}, \quad (4.2)$$

$$\frac{d\phi_{\text{open}}}{dt} = \frac{\phi_{\text{act}}}{\tau_{\text{ta}}} + \frac{\phi_{\text{eph}}}{\tau_{\text{te}}} - \frac{\phi_{\text{open}}}{\tau_{\text{open}}}. \quad (4.3)$$

Here  $\phi_{\text{act}}$ ,  $\phi_{\text{eph}}$  and  $\phi_{\text{open}}$  refer to the magnetic flux of AR, ER and open components, respectively, and their sum represents the total photospheric magnetic flux,  $\phi_{\text{tot}}$ :

$$\phi_{\text{tot}} = \phi_{\text{act}} + \phi_{\text{eph}} + \phi_{\text{open}}. \quad (4.4)$$

The main ingredients entering the model are the flux emergence rates,  $\varepsilon_{\text{act}}$  and  $\varepsilon_{\text{eph}}$ , of AR and ER, respectively, the decay time scales for the three flux components,  $\tau_{\text{act}}$ ,  $\tau_{\text{eph}}$ ,  $\tau_{\text{open}}$ , and the time scales for flux transfer from active and ephemeral regions to the open flux,  $\tau_{\text{ta}}$  and  $\tau_{\text{te}}$ , respectively. Equations 4.1–4.3 are solved following Solanki et al. (2002).

The flux emergence rate in active regions,  $\varepsilon_{\text{act}}$ , is chosen to vary with time,  $t$ , linearly with the sunspot number,  $R$ , and is scaled according to the observations of Schrijver and Harvey (1994) for cycle 21:

$$\varepsilon_{\text{act}}(t) = \varepsilon_{\text{act,max,21}} \frac{R(t)}{R_{\text{max,21}}}, \quad (4.5)$$

with  $\varepsilon_{\text{act,max,21}} = 2.3 \times 10^{24} \text{ Mx yr}^{-1}$  and  $R_{\text{max,21}} = 150$ .

Following Harvey (1993) we prescribe that  $\varepsilon_{\text{eph}}(t)$  also varies cyclically, with the amplitude and the length of this cycle being related to the properties of the corresponding AR cycle:

$$\varepsilon_{\text{eph},i}(t) = X\varepsilon_{\text{act,max},i} \sin^2(t'), \quad (4.6)$$

with

$$t' = [t - t_i + \tau_x] \frac{\pi}{\tau_i + 2\tau_x}. \quad (4.7)$$

Here  $\tau_i = t_{i+1} - t_i$  is the length of the  $i$ th sunspot cycle ( $t_i$  and  $t_{i+1}$  refer to the times of the adjacent sunspot minima) and  $\tau_i + 2\tau_x$  is the length of the corresponding ER cycle,

which is, in line with observations (Harvey 1993), stretched by the interval  $\tau_x$  in each direction with respect to the sunspot cycle. The value of  $\tau_x$  depends on the length of the sunspot cycle:  $\tau_x = \tau_i - c_x$ , with  $c_x$  lying in the range 5–9 years.

The time-independent amplitude factor  $X$  in Eq. (4.6) can be estimated in the following manner:

$$X = \frac{\varepsilon_{\text{eph,max}} \varepsilon_{\text{eph,min}}}{\varepsilon_{\text{eph,min}} \varepsilon_{\text{act,max}}}. \quad (4.8)$$

Here  $\varepsilon_{\text{eph,min}} = 1.8 \times 10^{26} \text{ Mx yr}^{-1}$  (Hagenaar 2001),  $\varepsilon_{\text{act,max}} = 2.3 \times 10^{24} \text{ Mx yr}^{-1}$  (Schrijver and Harvey 1994), and values of  $\varepsilon_{\text{eph,max}}/\varepsilon_{\text{eph,min}}$  found in the literature lie in the range 1–2 (Harvey 1993, 1994, Hagenaar et al. 2003). These values result in  $X \approx 80 - 160$ .

The decay time of the AR flux can be assessed by assuming a balance between flux emergence and decay:  $\tau_{\text{act}} = \phi_{\text{act}}/\varepsilon_{\text{act}}$ . Employing the values  $\phi_{\text{act,max}} \approx 6 \times 10^{23} \text{ Mx}$  and  $\varepsilon_{\text{act,max}} = 2.3 \times 10^{24} \text{ Mx yr}^{-1}$  for the maximum of cycle 21, which is the best estimate obtained from the plots in Harvey (1994), Schrijver and Harvey (1994), we arrive at an estimate of  $\tau_{\text{act}} \approx 0.25 \text{ yr}$ . For the decay time of the ER flux we take the value of  $\tau_{\text{eph}} = 14 \text{ h}$  as found by Hagenaar (2001).

The transfer times from AR and ER flux to the open flux,  $\tau_{\text{ta}}$  and  $\tau_{\text{te}}$ , are considerably longer ( $\gtrsim 10 \text{ yr}$ ) than the corresponding decay times and are not expected to influence the evolution of  $\phi_{\text{act}}$  and  $\phi_{\text{eph}}$  significantly. We varied  $\tau_{\text{ta}}$  within the range 10 to 14 years, and take  $\tau_{\text{te}} = 6\tau_{\text{ta}}$  according to Harvey (1994). These parameters only affect the open flux together with the decay time of the open flux,  $\tau_{\text{open}}$ , lying in the range 2–6 years.

### 4.3.2 Solar irradiance

Our approach to the irradiance reconstruction is similar in concept to that of the SATIRE models (Spectral And Total Irradiance REconstructions; see Solanki et al. 2005, Krivova and Solanki 2005) used to calculate solar irradiance on time scales of days to the solar cycle (Krivova et al. 2003, Wenzler et al. 2004, 2005, 2006). We divide the solar photosphere into 5 components: quiet Sun (index  $q$  from here on), sunspot umbrae ( $u$ ) and penumbrae ( $p$ ), faculae ( $f$ ) and the network ( $n$ ). The time-independent brightness of each component  $F_{q,u,p,f,n}(\lambda)$ , where  $\lambda$  is the wavelength, is calculated using the ATLAS9 code of Kurucz from plane-parallel model atmospheres (for details, see Unruh et al. 1999). Note that we use the same model for faculae and the network:  $F_f = F_n$ . The variation of the solar irradiance with time is described by the corresponding filling factors,  $\alpha_{q,u,p,f,n}(t)$ , which define the fraction of the solar surface covered by each component at a given time. Since magnetograms, from which the  $\alpha$  values have in the past mainly been determined, are not available for most of the time since the Maunder minimum, we need to consider other sources for  $\alpha$ .

Evaluation of filling factors for sunspots is straightforward. In the period since 1874 the sunspot areas were directly recorded at a number of observatories. The longest and most complete time series is that of the Royal Greenwich Observatory (1874–1976), which is used as a basis for our compilation. For the period 1977–1985, we use the data obtained in the former USSR and for the most recent period (since 1986) those compiled by the USAF (US Air Force) network including the data from Mt. Wilson Observatory. The remaining gaps are filled in with the data from Rome, Yunnan and Catania observatories. Since records by different stations show systematic differences, they have

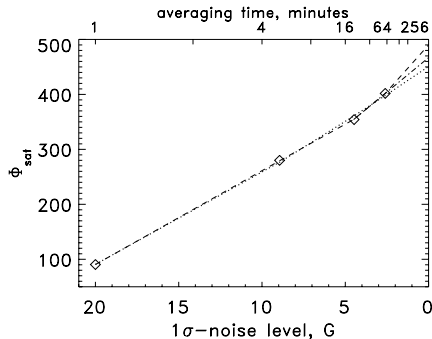


Figure 4.1: Dependence of the saturation flux,  $\phi_{\text{sat}}$ , on the noise level of the employed magnetograms. Values of  $\phi_{\text{sat}}$  obtained with the original 1-minute magnetograms and their 5-, 20- and 59-minute averages (having the  $1\sigma$  noise level of approximately 20 G, 8.9 G, 4.5 G and 2.6 G, respectively) are marked by diamonds. The lines show three different fits to these points and their extrapolation to the zero noise level: a linear fit (dot-dashed line) based on 2 points with the lowest noise ( $\sigma = 2.6$  G and 4.5 G) gives an estimate of  $\phi_{\text{sat}}(0)=467$  G for  $\sigma = 0$  G, whereas quadratic (dotted) and cubic (dashed) fits to all points yield  $\phi_{\text{sat}}(0)=451$  G and 490 G, respectively.

been carefully analysed and cross-calibrated (see Balmaceda et al. 2005 for further details). Before 1874 sunspot area measurements are not available, but can easily be extrapolated through a correlation analysis with the sunspot number. We alternately use the Zurich sunspot number,  $R_Z$  (Waldmeier 1961), and the Group sunspot number,  $R_G$  (Hoyt and Schatten 1993), provided by the National Geophysical Data Center (NGDC, <http://www.ngdc.noaa.gov/stp/SOLAR/solar.html>). Only yearly values of  $R_Z$  are available for 1700–1818, monthly records are accessible for 1819–1848, whereas daily numbers have been stored since 1849. We use a fixed ratio between umbral and penumbral areas,  $\alpha_u/(\alpha_u + \alpha_p) = 0.2$  as obtained by Wenzler et al. (2005) for recent cycles and in agreement with other estimates reported in the literature (for an overview see Solanki and Krivova 2003).

The filling factors of other photospheric components are obtained from the magnetic flux calculated as outlined in Sect. 4.3.1. The sum of the ER and open fluxes describes the evolution of the network:  $\phi_n = \phi_{\text{eph}} + \phi_{\text{open}}$ , whereas  $\phi_{\text{act}}$  represents the variation of the magnetic flux in sunspots and faculae. The magnetic flux in sunspots (the sum of the umbral,  $\phi_u$ , and penumbral,  $\phi_p$ , components) can be calculated from the sunspot areas:

$$\phi_u + \phi_p = \alpha_u \langle B_{z,u} \rangle + \alpha_p \langle B_{z,p} \rangle, \quad (4.9)$$

where the area-averaged vertical components of the magnetic flux strength in umbrae,  $\langle B_{z,u} \rangle$ , and penumbrae,  $\langle B_{z,p} \rangle$ , are about 1800 G and 550 G, respectively, according to the measurements of Keppens and Martinez Pillet (1996). Subtraction of  $\phi_u$  and  $\phi_p$  from  $\phi_{\text{act}}$  gives the evolution of the facular magnetic flux,  $\phi_f$ .



Table 4.1: Key features of the models providing best fits to the 3 considered data sets. (1) Main parameters (i.e. those that are also varied in the standard model). These include  $c_x = \tau_i - \tau_x$  (where  $\tau_i$  is the length of the AR cycle and  $\tau_i + 2\tau_x$  is the length of the corresponding ER cycle), the amplitude factor  $X$  [see Eqs. (4.6 and (4.8)], the flux transfer time from AR to the open flux,  $\tau_{\text{tr}}$ , and the decay time for the open flux,  $\tau_{\text{open}}$ . In models ‘antiphase (2)’ and ‘const.  $\phi_{\text{eph}}$  (2)’, an optional parameter is the saturation flux in faculae,  $\phi_{\text{sat},f}$ , which is otherwise fixed to 300 G. Also listed are (2) the corresponding values of the variance (i.e.  $\chi^2$  normalised by the number of points) for the TSI,  $\sigma_{\text{TSI}}^2$ , total magnetic flux,  $\sigma_{\text{TMF}}^2$  and the open flux,  $\sigma_{\text{open}}^2$ , their mean,  $\sigma^2 = (\sigma_{\text{TSI}}^2 + \sigma_{\text{TMF}}^2 + \sigma_{\text{open}}^2)/3$ , the correlation coefficient,  $R_{c,\text{TSI}}$ , between the modelled and measured TSI and (3) the estimated increase in the TSI since 1700. In the last row, ranges within which all parameters have been varied are listed.

model	Sect.	(1) parameters				(2) fit quality				(3) predicted $\Delta I$ , $\text{Wm}^{-2}$ since 1700		
		$c_x$ , yr	$X$	$\tau_{\text{tr}}$ , yr	$\tau_{\text{open}}$ , yr	$\phi_{\text{sat},f}$ , G	$\sigma_{\text{TSI}}^2$	$\sigma_{\text{TMF}}^2$	$\sigma_{\text{open}}^2$		$\sigma^2$	$R_{c,\text{TSI}}$
standard $R_Z$	4.4.1	7.6	117	13.5	3.5	300*	0.048	0.0062	0.041	0.032	0.78	$\approx 1.3$
antiphase <sup>+</sup> (1)	4.4.2	5.0	80	10.0	2.6	300*	0.113	0.0071	0.041	0.054	0.64	.....
antiphase <sup>+</sup> (2)	4.4.2	7.4	80	13.9	3.9	168	0.055	0.0086	0.036	0.033	0.77	$\approx 1.5$
const. $\phi_{\text{eph}}$ (1)	4.4.3	-#	-#	10.0	2.5	300*	0.116	0.0072	0.038	0.054	0.63	.....
const. $\phi_{\text{eph}}$ (2)	4.4.3	-#	-#	13.5	3.6	182	0.049	0.0074	0.035	0.031	0.77	$\approx 0.9$
standard $R_G$	4.4.4	7.6	117	13.5	3.5	300*	0.049	0.0062	0.035	0.030	0.75	$\approx 1.3$
ranges	4.3	5–9	80–160	10–14	2–6	150–400						

\* this parameter has been deduced independently of the current modelling and its value was not varied in order to fit the data.

<sup>+</sup> in the antiphase model, the shift between the emergence rate of AR and ER was varied between 2 and 8 years (ER preceding AR), so that it becomes an additional free parameter. For the best-fit models presented here, the shift is 5 years.

# in the const.  $\phi_{\text{eph}}$  model,  $c_x$  and  $X$  are replaced by one free parameter:  $\phi_{\text{eph}} = 3.0 \times 10^{15}$  Wb for model (1) and  $\phi_{\text{eph}} = 2.8 \times 10^{15}$  Wb for model (2).

Next, we convert the network,  $\phi_n$ , and facular,  $\phi_f$ , magnetic fluxes into corresponding filling factors,  $\alpha_n$  and  $\alpha_f$ . For this, we use the same conversion scheme as in previous applications of the SATIRE models (Krivova et al. 2003, Wenzler et al. 2004, 2005, 2006):  $\alpha_n$  and  $\alpha_f$  are proportional to  $\phi_n$  and  $\phi_f$ , respectively, until a saturation limit  $\phi_{\text{sat}}$  is reached where  $\alpha = 1$  (see previous papers for more details). Above  $\phi_{\text{sat}}$  they remain constant.  $\phi_{\text{sat}}$  is a free parameter of the SATIRE models, which depends on the resolution and the noise level of the employed magnetic field maps. The smaller the fraction of the true magnetic flux visible in the magnetograms, the smaller the  $\phi_{\text{sat}}$  needs to be.

In order to reproduce solar irradiance variations in cycle 23 on the basis of MDI magnetograms, Krivova et al. (2003) found  $\phi_{\text{sat}} = 280$  G (no distinction was made between faculae and the network). For a reconstruction of solar irradiance in cycles 21–23 based on National Solar Observatory Kitt Peak (NSO KP) data, Wenzler et al. (2005, 2006) found  $\phi_{\text{sat}} = 310 - 320$  G to be more adequate. The large  $\phi_{\text{sat}}$  is consistent with the fact that KP magnetograms have a lower noise level than those from the MDI. Since magnetic field strengths in faculae are higher than the noise level of either of these 2 sets of images, we do not expect a considerable difference in the  $\phi_{\text{sat},f}$  value and used the value of 300 G as our primary estimate. In some extreme cases (see Sects. 4.4.2 and 4.4.3), however, we allowed  $\phi_{\text{sat},f}$  to vary.

At the same time, the weakest network elements are lost within the noise level and, since they are often present as mixed polarity features, they are also lost due to apparent cancellation of polarities caused by insufficient spatial resolution of the MDI or KP magnetograms (Krivova and Solanki 2004). Consequently, in case of noise-free high resolution data, their saturation flux could lie significantly higher than 300 G deduced from MDI and KP magnetograms. In order to estimate  $\phi_{\text{sat},n}$  for such ideal ‘noise-free’ data, we utilised MDI magnetograms with different noise levels to reconstruct solar irradiance on 70 days between the minimum of cycle 23 in 1996 and its maximum in 2000 following Krivova et al. (2003). For this, we consecutively averaged MDI magnetograms over 5, 20 or 59 minutes (which reduced the  $1\sigma$  noise level down to approximately 8.9 G, 4.5 G and 2.6 G, respectively) and employed these together with the original 1-minute data (having the  $1\sigma$  noise level of about 20 G) for the reconstruction. In each case, the value of  $\phi_{\text{sat}}$  was found from a comparison with the irradiance variations measured by the VIRGO instrument on SoHO (Fröhlich and Finsterle 2001). The dependence of the  $\phi_{\text{sat}}$  on the noise level of the employed magnetograms is shown in Fig. 4.1. An extrapolation to the 0-noise level (see Fig. 4.1) suggests a value of  $\phi_{\text{sat},n}$  of around 500 G, which we use in this work.

The area not covered by sunspots, faculae or the network is assumed to be free of magnetic field and is considered to be quiet Sun. The corresponding filling factor is  $\alpha_q = 1 - \alpha_u - \alpha_p - \alpha_f - \alpha_n$ , and the final formula for the solar radiative flux at a given wavelengths,  $\lambda$ , is:

$$\begin{aligned}
 F(\lambda, t) = & \alpha_q(t)F_q(\lambda) + \alpha_u(t)F_u(\lambda) \\
 & + \alpha_p(t)F_p(\lambda) + [\alpha_f(t) + \alpha_n(t)]F_f(\lambda).
 \end{aligned}
 \tag{4.10}$$

Integration over all wavelengths gives the total solar irradiance.

### 4.3.3 Parameters and optimization

Our model, outlined in Sects. 4.3.1 and 4.3.2, contains a number of parameters, which are constrained by independent observations to lie within a given range rather than to a unique value. The main parameters suffering from such an uncertainty are  $c_r$  and the amplitude factor,  $X$ , which relate the length and the amplitude of the ER cycles, respectively, to the corresponding values for the AR cycles. To a lesser extent the transfer time from AR to the open flux,  $\tau_{\text{ia}}$ , and the decay time of the open flux,  $\tau_{\text{open}}$ , which mainly influence the evolution of the open flux, are also affected. In some cases, as described in the next section, we also vary the saturation magnetic flux,  $\phi_{\text{sat}}$ , in order to test the sensitivity and the limits of our model. Table 4.1 provides an overview of all parameters, their values for the 4 models discussed below in more detail and the ranges within which the parameters have been varied.

We believe that it is important to constrain the output of the model using as many data sets as possible. Our model is tested against 3 independent data sets. Firstly, the reconstructed total irradiance should reproduce direct space based measurements which are available since 1978. For a comparison with the model, we use the composite from the Davos Observatory (PMOD composite, Fröhlich 2006). Secondly, almost daily observations of the solar global photospheric field have been carried out at the Mt. Wilson Solar Observatory (MWO), KP NSO and Wilcox Solar Observatory (WSO) over cycles 21–23. Arge et al. (2002) present a compilation of these data, whereby they have introduced corrections to the older NSO KP data, which suffered from instrumental problems. This reduces the magnetic flux in cycle 21 to roughly the level in cycle 22 (cf. Wenzler et al. 2006). The total magnetic flux derived from these measurements can thus be compared to the modelled one. When doing so, we take into account the finding by Krivova and Solanki (2004) that more than half of the photospheric flux from ER may go uncounted in the employed synoptic charts due to their relatively low spatial resolution. Therefore, the measured flux is compared to the value  $\phi_{\text{act}} + 0.4\phi_{\text{eph}} + \phi_{\text{open}}$ . Finally, the heliospheric magnetic flux has been reconstructed by Lockwood et al. (1999) based on the geomagnetic *aa*-index, and we compare the calculated open magnetic flux to their empirical reconstruction.

In order to find a solution which provides as close fits to all 3 sets of data as possible, we take advantage of the PIKAIA software (Charbonneau 1995) available from the ftp archive of the High Altitude Observatory: <http://www.hao.ucar.edu>. PIKAIA is a general purpose function optimization routine based on a genetic algorithm, which is particularly efficient in finding absolute extrema of multimodal optimization problems. We employ PIKAIA to find a set (or sets) of parameters minimizing the mean of  $\chi^2$  values between the modelled and measured TSI,  $\chi_{\text{TSI}}^2$ , total photospheric magnetic flux,  $\chi_{\text{TMF}}^2$ , and solar open magnetic flux,  $\chi_{\text{open}}^2$ , all normalised by the number of points,  $N$ , in the corresponding data set. In other words, we search for the minimum of the mean variance:

$$\sigma^2 = \frac{1}{3}(\sigma_{\text{TSI}}^2 + \sigma_{\text{TMF}}^2 + \sigma_{\text{open}}^2), \quad (4.11)$$

where  $\sigma_{\text{data set}}^2 = \chi_{\text{data set}}^2 / N_{\text{data set}}$ . In order to compare the three  $\sigma^2$  values directly, we scale the total and open magnetic fluxes to the absolute level of the TSI before computing the appropriate  $\sigma^2$ .

## 4.4 Results

### 4.4.1 Standard model

We first ran PIKAIA by allowing the 4 main free parameters listed in Table 4.1 to vary within the ranges suggested by different observational data (see Sect. 4.3.1). The results for the model providing the smallest  $\sigma^2$  are presented in Figs. 4.2–4.4: Fig. 4.2a compares the calculated total photospheric magnetic flux with the measurements since 1974, Fig. 4.3 the modelled open flux with the *aa*-based reconstruction of Lockwood et al. (1999) and Fig. 4.4 the reconstructed TSI with the PMOD composite. The estimated values of the free parameters as well as the  $\sigma^2$  values for the TSI,  $\sigma_{\text{TSI}}^2$ , total magnetic flux,  $\sigma_{\text{TMF}}^2$ , and the open flux,  $\sigma_{\text{open}}^2$ , are summarised in Table 4.1. Also given is the correlation coefficient,  $R_{c,\text{TSI}}$ , between the modelled and observed variations of the TSI.

Figure 4.2a shows the total photospheric magnetic flux for each Carrington rotation between 1974 and 2002 measured using the WSO (circles), NSO KP (triangles) and MWO (squares) synoptic charts and calculated with our model (solid curve). Figures 4.2b and c illustrate the evolution of the magnetic flux of each photospheric component (AR, ER and the open flux) as well as their sum (total magnetic flux) since 1975 and 1700, respectively. Note that the effect of the spatial resolution on the visibility of the small ER is taken into account in Fig. 4.2a by considering the quantity  $\phi_{\text{act}} + 0.4\phi_{\text{eph}} + \phi_{\text{open}}$  rather than just  $\phi_{\text{act}} + \phi_{\text{eph}} + \phi_{\text{open}}$ . The calculated curve lies in Fig. 4.2a well within the scatter of the data and reproduces both the amplitude of the variations and the cycle length quite well. In particular, the amplitudes of cycles 21 and 22 are comparable to each other whereas cycle 23 is somewhat weaker. Note that a similar comparison by Solanki et al. (2002) showed a strong disparity between the measurements (raw NSO KP data, without the corrections proposed by Arge et al. 2002) and the model in cycle 21. As Fig. 4.2a shows, this disparity has now disappeared. It turns out that it was due to problems with the data rather than to a shortcoming of the model.

Since the open flux controlled in the model by the transfer time from AR,  $\tau_{\text{ta}}$ , and the decay time,  $\tau_{\text{open}}$ , contributes rather little to the total flux ( $\approx 10 - 15\%$ , see Figs. 4.2b and c), the main two parameters determining the evolution of the total photospheric magnetic flux are  $c_x$  and  $X$ , relating the length and the amplitude of the ER cycles, respectively, to the corresponding values for the AR cycles. Encouragingly, values of  $c_x = 7.6$  yr and  $X = 117$  found by the optimization procedure lie within the respective limits suggested by observations.

Since the ER cycles partly overlap, the ER flux varies much less over the cycle than the AR flux, only by approximately a factor of 2 (see Figs. 4.2b and c). Thus, whereas the flux in ER is only slightly lower than that in AR at activity maxima (cf. Krivova and Solanki 2004), it clearly dominates at minima. For recent cycles (Fig. 4.2b), the minimum flux in ER is reached slightly ( $\approx 1 - 2$  years) before sunspot minimum (note that, in contrast to the model described in Sect. 4.4.2, no shift is imposed here, see Eq. 4.6). All this is in good agreement with the conclusions of Harvey (1993, 1994).

The decay time of the open flux,  $\tau_{\text{open}}$ , only enters Eq. 4.3 and the transfer time from AR to the open flux,  $\tau_{\text{ta}}$ , is significantly longer ( $\gtrsim 10$  yr) than the decay times of AR and ER ( $\sim 3$  months and 14h, respectively). Thus, as mentioned above, these two parameters mainly affect the evolution of the open flux component (see Fig. 4.3). Solanki et al.

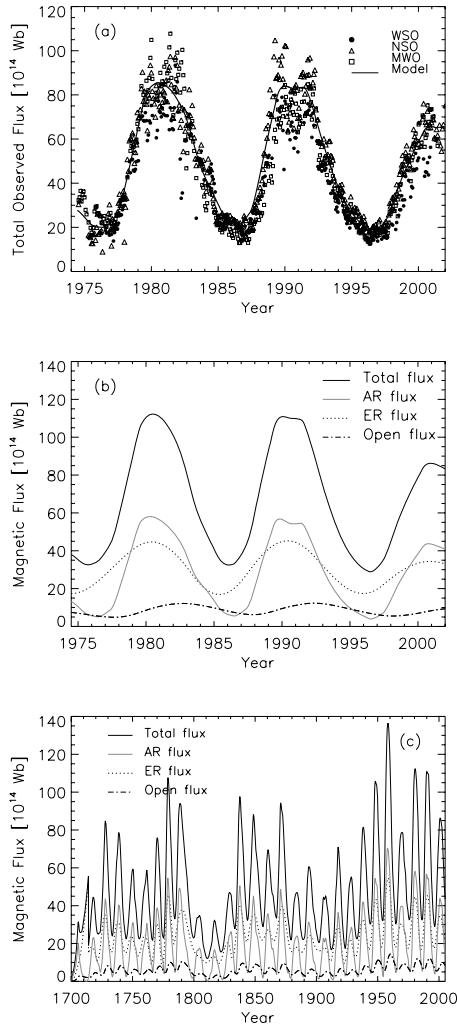


Figure 4.2: **(a)**: Measured (symbols) and modelled (standard model; solid line) total magnetic flux between 1974 and 2002. Each data point is an integral over a synoptic chart for one Carrington rotation. Different symbols are used for different data sets: filled circles represent the WSO data, open triangles the KP NSO data and open squares the MWO measurements (cf. Arge et al. 2002, Wenzler et al. 2006). For the modelled flux the value  $\phi_{\text{act}} + 0.4\phi_{\text{eph}} + \phi_{\text{open}}$  is given (see Sect. 4.3.3). **(b)** and **(c)**: Reconstructed magnetic flux in AR (grey solid curve), ER (dotted), as well as the open (dot-dashed) and total (black solid) flux since 1974 and 1700, respectively.

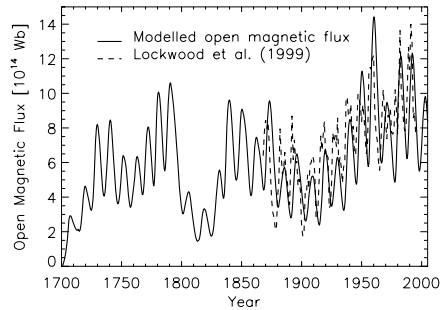


Figure 4.3: Evolution of the open flux since 1700: calculated with the standard model (solid curve) and reconstructed by Lockwood et al. (1999) from the geomagnetic  $aa$ -index (dashed).

(2000) modelled the evolution of the open flux considering only AR and obtained values of  $\tau_{\text{ta}} = 12$  yr and  $\tau_{\text{open}} = 4$  yr from a comparison with the reconstruction by Lockwood et al. (1999). Inclusion of ER led to a slightly lower value of  $\tau_{\text{open}} = 3$  yr (Solanki et al. 2002), although it should be noted that the contribution of ER to the open flux is rather uncertain. The values we obtain with the standard model,  $\tau_{\text{ta}} = 13.5$  yr and  $\tau_{\text{open}} = 3.5$  yr are close to the previously obtained values (cf. Lockwood 2003).

The modelled (dots) and measured (grey solid line; PMOD composite by Fröhlich 2006) variations of the total solar irradiance are compared in Fig. 4.4. Figure 4.4a shows daily values, Fig. 4.4b the 3-month running means and Fig. 4.4c the difference between the model and the data (dots mark daily values and the bigger filled circles the 30-day averages). Similarly to the total magnetic flux, the modelled TSI is mainly driven by the 2 parameters,  $c_x$  and  $X$  describing the ER cycle (the length and the amplitude) via characteristics of the corresponding AR cycle (known from the historical sunspot record). Obviously, the coarse model used to calculate the evolution of the magnetic flux on the solar surface is not designed to match the observed shorter-term variations down to the last detail. In particular, the sine approximation of the shape of the ER cycle is relatively rough, which is clearly seen during the ascending and descending phases of cycle 22<sup>1</sup>. Nevertheless, both the amplitude and the phase of the variations are adequately reconstructed and the agreement between the model and the observations is fairly good with a correlation coefficient of  $R_c = 0.78$ . Both the short-term (rotation time scale) and longer-term (solar cycle) variations are equally well reproduced.

We now use the same model to calculate the variations of the TSI since the end of the Maunder minimum. The reconstructed irradiance since 1700 is presented in Fig. 4.5 (based on the Zurich sunspot number). The quality of the reconstruction improves with time: only yearly values of the sunspot number (and thus of the resulting TSI) are avail-

<sup>1</sup>We also tried using the shape of the (correspondingly stretched) sunspot cycle for the ER cycle. This did not improve the correspondence of the modelled to the observed irradiance.

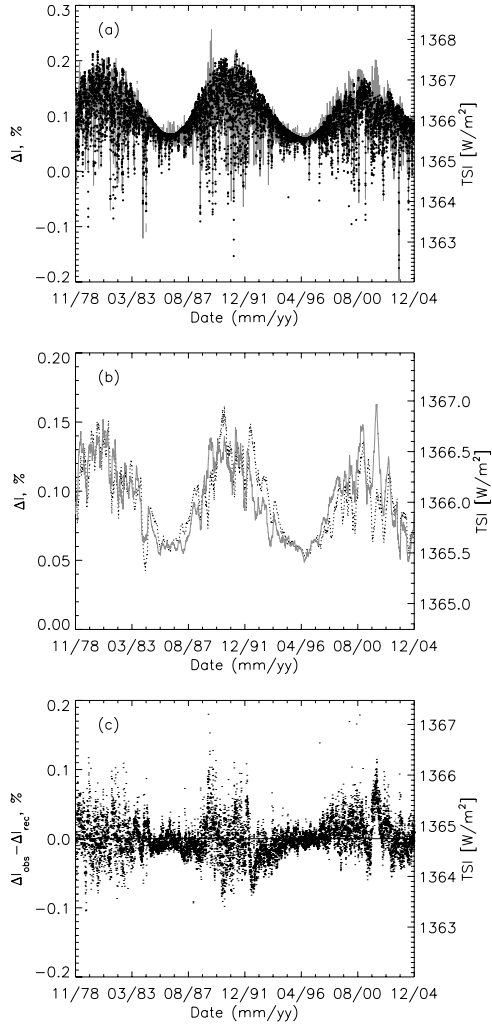


Figure 4.4: Modelled (standard model; dots) and observed (PMOD composite, grey solid line) variations of the total solar irradiance in cycles 21–23. **(a)**: daily values; **(b)**: 3-month running means; **(c)**: the difference between the model and the data (each dot represents a daily value, the bigger filled circles 30 day averages).

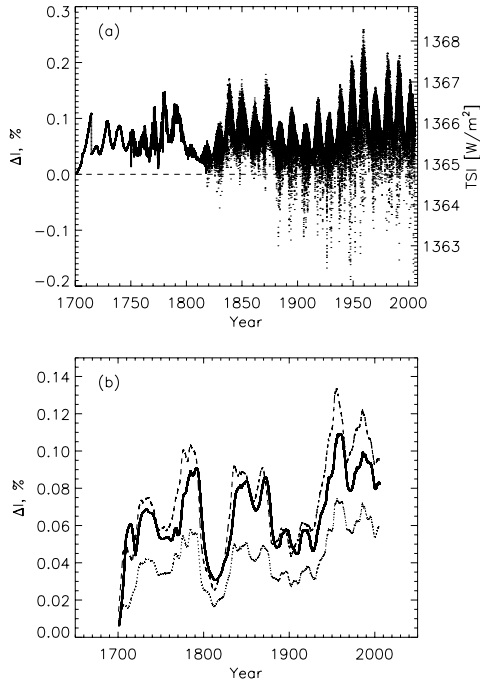


Figure 4.5: **(a)**: Reconstructed TSI since 1700 for the standard model. **(b)**: 11-yr running mean of the reconstructed TSI for the standard (solid line), ‘antiphase (2)’ (dashed) and ‘constant  $\phi_{\text{eph}}(2)$ ’ (dotted) models.

able before 1749, monthly averages can be calculated for the period between 1749 and 1818, whereas daily sampling is possible after 1818 (see panel a of Fig. 4.5). The longer-term trend is better evident in panel b of this figure, where an 11-year running mean of the reconstructed TSI is shown (solid line). Thus if we require that the model agrees as well as possible with all available observational data, it predicts an increase in the cycle averaged TSI of about 0.095% or  $1.3 \text{ Wm}^{-2}$  between the end of the Maunder minimum and the present (where present-day level is taken as an average over last 30 years). Note that this estimate of the secular change is fairly stable in the sense that if we vary the free parameters within the reasonable ranges, we typically arrive at values close to those listed above (within about  $\pm 0.2 - 0.3 \text{ Wm}^{-2}$ ). Below we discuss two extreme cases in more detail. It is also worth noting that none of the reasonable combinations of the parameters led to a higher level of the irradiance at the minimum of cycle 23 than at the minimum of cycle 22 as proposed by Willson (1997).



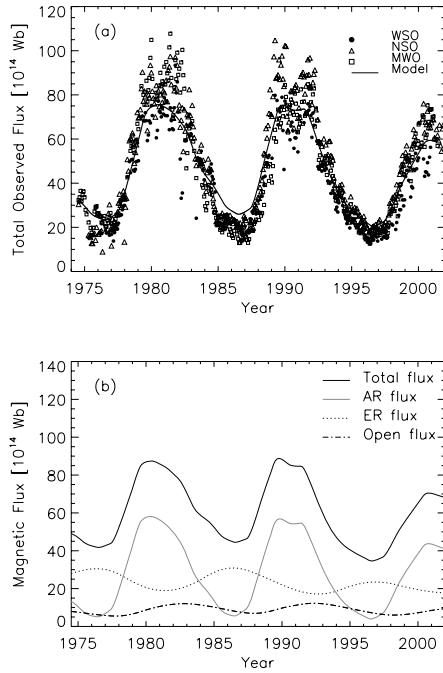


Figure 4.6: Same as Figs. 4.2a and b but for the model with ER running 5 years ahead of AR (model ‘antiphase (2)’ in Table 4.1).

#### 4.4.2 A possible shift between the ER and AR evolution

The main uncertainty in our model is introduced by the unknown temporal evolution of the emergence rate of the ER. Although it is evidently related to the emergence rate of AR, the exact form of this relationship is not well established. Based on the observational evidence outlined in Sect. 4.3.1, we assume that this relationship is described by Eqs. 4.5–4.8, which implies that although ER of a new cycle appear earlier on the solar surface than the corresponding AR cycle starts, the two components still evolve nearly in phase. Hagenaar et al. (2003) found, however, that the number density of emerging ER decreased by about a factor of 1.5 from 1997 (i.e. right after the sunspot minimum in 1996) to a minimum in 2000 (when the sunspot number reached its maximum). They concluded thus that the two components may progress in antiphase, or at least with a significant shift. Therefore we now investigate this possibility.

We introduced a shift between the emergence rates of AR and ER, with ER always preceding the AR. This shift was allowed to be between 2 and 8 years and was thus an

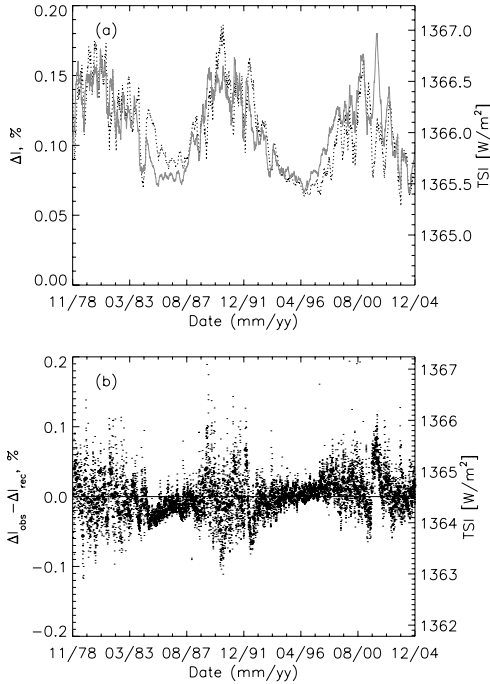


Figure 4.7: Same as Figs. 4.4b and c but for the model with ER running 5 years ahead of AR (model ‘antiphase (2)’ of Table 4.1).

additional parameter. A point that should be mentioned is that no good solution matching reasonably all 3 data sets (with TSI being the most critical) was initially found (see Table 4.1, model ‘antiphase(1)’). The contribution of ER to the total magnetic flux turned to be too strong, in particular during activity minima, and led to a heavily deformed shape of the irradiance cycles.

Only after introducing an additional parameter, i.e. after allowing one previously fixed parameter to vary, could reasonable fits be obtained. This new parameter is the saturation flux of faculae,  $\phi_{\text{sat},f}$ , which we now allow to vary within the range 150–400 G (see Table 4.1). Indeed, the value of 300 G that we use for faculae was adopted from our reconstructions based on MDI and KP NSO magnetograms with no distinction between faculae and the network. Since the value for the network saturation flux is somewhat higher than this (see Sect. 4.3.2), the value of  $\phi_{\text{sat},f}$  can, in principle, be somewhat (although hardly significantly) lower.

The best fit was obtained with  $\phi_{\text{sat},f} = 168$  G (see Table 4.1, model ‘antiphase (2)’). This low value indicates that the facular contribution to the cyclic variation needs to be

strongly amplified in this model, in order to compensate for the contribution of ER evolving in antiphase with the solar cycle (see Fig. 4.6b). Also, the ER amplitude parameter,  $X$ , dropped down to 80, which is the lowest possible value within the allowed range. This means that better fits are obtained when the antiphase variation of ER is dampened down. A shift of 5 years was found to be in best agreement with the observed records, which implies that ER and AR evolve nearly in antiphase. Note, however, that if a shift of 0 is also allowed, then the standard model is selected as the one providing the best possible fits to the data (with the smallest number of free parameters). In order to match the reconstruction of the heliospheric magnetic flux by Lockwood et al. (1999), we also had to increase the transfer time from AR to the open flux,  $\tau_{\text{ta}} = 13.9$  years, and the decay time of the open flux,  $\tau_{\text{open}} = 3.9$  years.

The model with these parameters reproduces the total photospheric magnetic flux measured in cycles 21–23 less well than the standard model (see Fig. 4.6a and Table 4.1). Particularly, the flux at the minima preceding cycles 22 and 23 appears too high compared to the observations due to the ER contribution as demonstrated by Fig. 4.6b.

The agreement of the reconstructed irradiance with the measured is also worse than in the standard model (Fig. 4.7 and Table 4.1). Specifically, the solar cycle trend in the model systematically lags behind that in the data by about a year. This concerns only the overall irradiance level, while the shorter-term (rotational time scales) changes due to AR occur simultaneously in the model and the data. The shift is probably due to the phase shift in the ER emergence rate, while the good short-term agreement is due to the active regions, in particular the sunspots. For the open flux, the results are rather similar in both cases, with  $\sigma_{\text{open}}^2$  values being even somewhat smaller in the ‘antiphase (2)’ model (Table 4.1). Note, however, that the antiphase model has 2 additional free parameters and the value of  $\phi_{\text{sat},f} = 168$  G required to reproduce the observed irradiance variations seems to be unreasonably low.

Although our preference is given to the standard model for the reasons outlined above, we cannot rule the antiphase model out and, in order to evaluate the uncertainty in the estimated secular change in the irradiance, we have reconstructed the TSI back to 1700 using this model as well. It is shown in Fig. 4.5b by the dashed line. The predicted increase in the cycle-averaged TSI since that time is about 0.11% or  $1.5 \text{ Wm}^{-2}$ , which is 15% higher than the value obtained with the standard model (see Table 4.1).

### 4.4.3 Constant ER flux

Observations suggest that during cycles 21–23 the emergence rate and the total magnetic flux of ER varied rather little, by no more than a factor of 2 and it might well be that this factor is very close to 1 (Harvey 1993, 1994, Hagenaar et al. 2003). Therefore we now also consider the important special case with no variation in the ER flux at all. If the magnetic flux of the so-called quiet Sun (i.e. the ER flux) does not change, then the only source of a possible secular variation remains the open flux, beyond variations in amplitude from one cycle to the next. In this way we should obtain a lower limit to the increase of the TSI since the end of the Maunder minimum.

Since the quiet Sun magnetic flux is not known accurately, it is considered to be another free parameter. It replaces the two parameters,  $c_x$  and  $X$ , used to describe the evolution of the ER flux with time. The facular saturation flux,  $\phi_{\text{sat},f}$ , also needs to be allowed

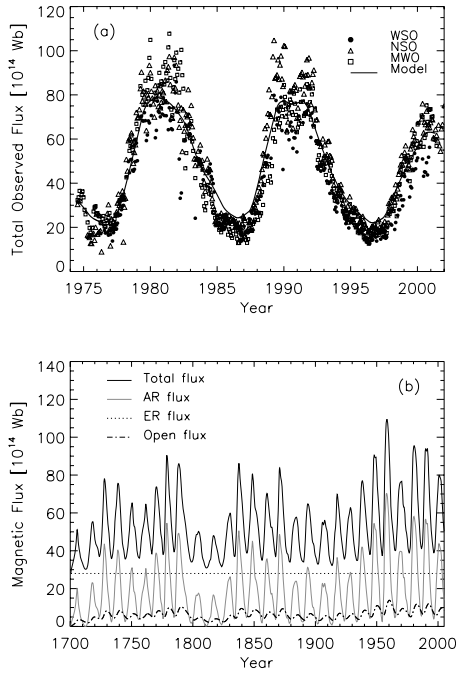


Figure 4.8: Same as Figs. 4.2a and c but for the model with the constant ER magnetic flux,  $\phi_{\text{eph}} = 2.8 \times 10^{15}$  Wb ('const.  $\phi_{\text{eph}}$  (2)' in Table 4.1).

to vary in order to obtain good fits (cf. models 'const.  $\phi_{\text{eph}}$  (1)' and 'const.  $\phi_{\text{eph}}$  (2)' in Table 4.1). Thus the number of free parameters in this model is the same as in the standard case.

The results for this model are shown in Figs. 4.8–4.9. The evolution of the total magnetic flux is reproduced less well by this model than by the standard model (cf. Table 4.1), and the flux is rather high during activity minima (Fig. 4.8). The variations of the TSI are reproduced slightly (although not significantly) less well than by the standard model (Table 4.1 and Fig. 4.9).

In order to put a lower limit on the secular change in the TSI since 1700, we utilise this model too to reconstruct irradiance variations back in time. The 11-year running mean of this reconstruction is shown by the dotted line in Fig. 4.5b. As expected, the resulting increase in the cycle averaged TSI is somewhat lower than in the other cases,  $0.9 \text{ Wm}^{-2}$  or  $\approx 0.065\%$  (see also Table 4.1), but is still noticeable. As seen from Fig. 4.8b, this increase has 2 sources: the large amplitude of recent AR cycles and a secular rise in the open flux.

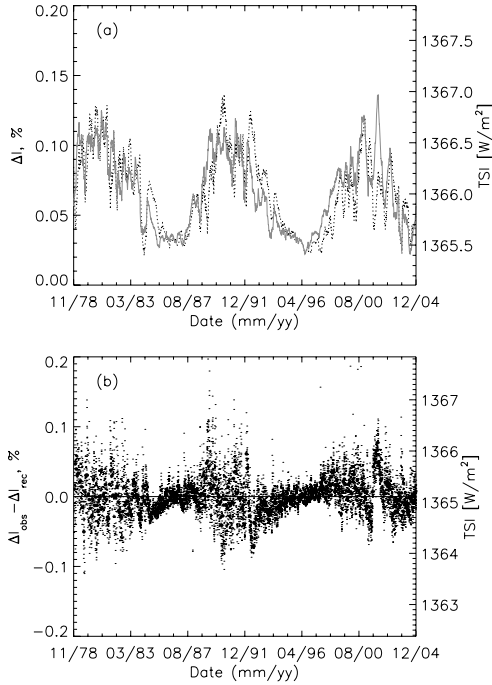


Figure 4.9: Same as Figs. 4.4b and c but for the model with the constant ER magnetic flux,  $\phi_{\text{eph}} = 2.8 \times 10^{15}$  Wb ('const.  $\phi_{\text{eph}}(2)$ ' in Table 4.1).

#### 4.4.4 Reconstruction based on the Group sunspot number

The reconstructions carried out in previous sections were based on the Zurich sunspot number,  $R_Z$ , available since 1700.  $R_Z$  is calculated using the number of both the individual sunspots and the sunspot groups present on the solar disc. In contrast, the Group sunspot number,  $R_G$  (Hoyt and Schatten 1998) takes into account only the number of sunspot groups and goes back to 1610, covering the whole Maunder minimum. A weighting factor was introduced by Hoyt and Schatten (1998), in order to scale the Group sunspot number to the Zurich number for the period 1874–1976. Prior to 1874, however, the Zurich number is, on average, higher than the Group number.

Using the Group sunspot number it is possible to reconstruct solar magnetic flux and solar irradiance for a period of more than 36 cycles, thus extending the model to the beginning of the Maunder minimum. We first ran PIKAIA using  $R_G$  instead of  $R_Z$ , and the 4 main free parameters were allowed to vary within the same ranges as listed in Table 4.1. The obtained set of parameters turned to be very similar to the one obtained in Sect. 4.4.1

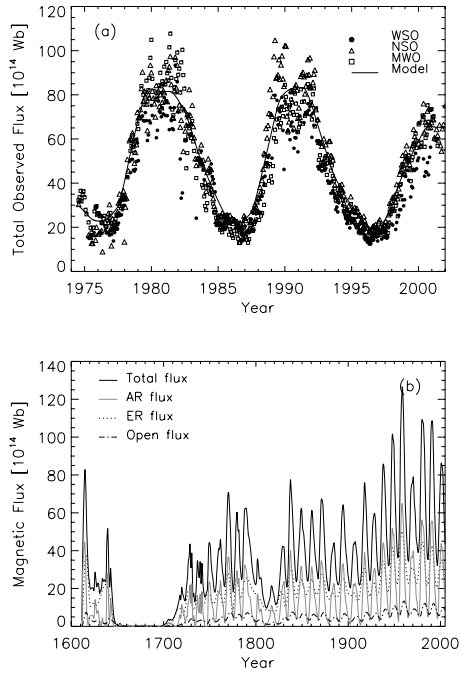


Figure 4.10: Same as Figs. 4.2a and c but for the model based on  $R_G$ .

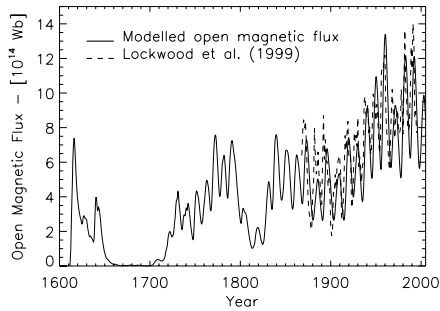


Figure 4.11: Same as Fig. 4.3 but for the model based on  $R_G$ .

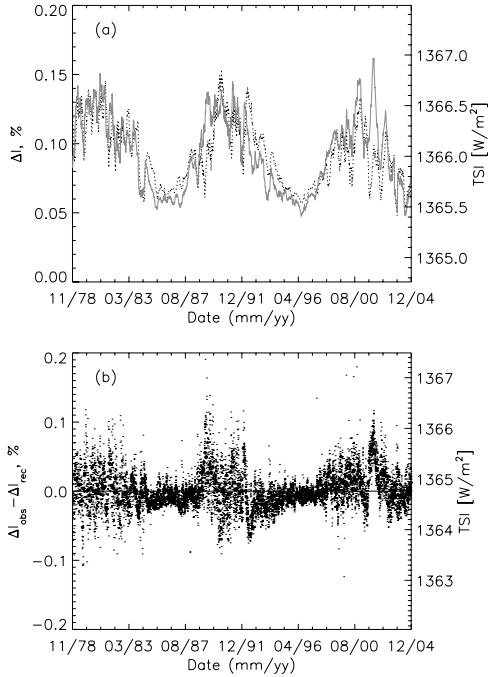


Figure 4.12: Same as Figs. 4.4b and c but for the model based on  $R_G$ .

with the Zurich sunspot number,  $R_Z$ , and the  $\sigma^2$  values changed only imperceptibly. This is due to the normalisation introduced by Hoyt and Schatten (1998) for the period after 1874. Therefore, for the  $R_G$ -based reconstruction we opt for the same set of values as in the standard  $R_Z$  model.

The reconstructed total magnetic flux is compared to the data from different observatories in Fig. 4.10a. The model reproduces both the cycle amplitude and cycle length of the observed magnetic flux, and the fit is about as good as in the case of the standard  $R_Z$  model (cf. Fig. 4.2a and Table 4.1). The evolution of the magnetic flux in active regions, ephemeral regions as well as the open and total magnetic flux are shown in Figure 4.10b.

During the Maunder minimum the sunspot number was extremely low, with extended periods without any sunspots at all. Therefore the magnetic flux in active regions dropped almost to zero. In our model, the evolution of the other two components of the magnetic flux (i.e. ER and open flux) is related to the evolution of the flux emerging in active regions. Thus flux in these components drops to zero as well. Of course, the lack of sunspots does not necessarily imply that also smaller bipolar regions stopped emerging at the solar surface. E.g., the  $^{10}\text{Be}$  data suggest that the open flux showed periodic fluctua-

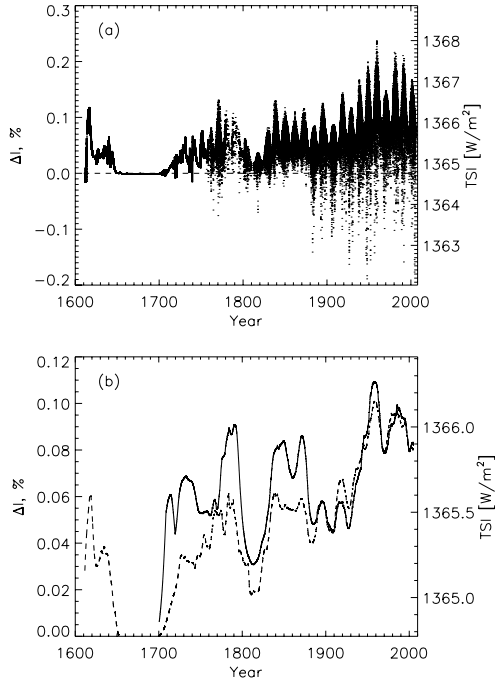


Figure 4.13: **(a)**: Reconstructed irradiance variations since 1610 for the standard model based on the Group sunspot number,  $R_G$ . **(b)**: 11-yr running mean of the reconstructed TSI for the standard models based on the Zurich (solid line) and Group (dashed) sunspot numbers.

tions during the Maunder minimum (Beer et al. 1998). Unfortunately, an estimate of the amount of flux emerging on the solar surface during this period is not straightforward and we assume for simplicity that all components of the magnetic flux drop to zero during the Maunder minimum.

In Fig. 4.11 the modelled open flux (solid line) is compared to that reconstructed by Lockwood et al. (1999) from the  $aa$ -index (dashed). Note that this component of the magnetic flux is better reproduced using the Group sunspot number (see Table 4.1).

In Fig. 4.12 the TSI reconstructed using  $R_G$  (dots) is compared to the PMOD composite of space measurements (solid line). Although the  $\sigma_{\text{TSI}}^2$  values are very similar for the models based on  $R_Z$  and  $R_G$ , the TSI reconstructed with  $R_G$  is somewhat higher than observed in the minima preceding cycles 22 and 23, and the corresponding correlation coefficient,  $R_c$ , is lower (0.75 vs. 0.78 for the standard  $R_Z$  model). This may be due to the fact, that by ignoring individual spots,  $R_G$  contains less information about the evolu-



tion of the weaker fields than  $R_Z$ , and is thus a worse proxy of the ER evolution. At the same time, the open flux is well described by the large-scale magnetic field and is well represented by  $R_G$ .

The long-term evolution of the solar irradiance since 1610 is shown in Fig. 4.13a. Note that it is almost identical with the reconstruction using the values of the free parameters obtained by running PIKAIA. In Fig. 4.13b, the 11-yr running mean of this reconstruction (dashed line) is plotted together with that obtained with the  $R_Z$  standard model (solid). This figure shows that during the period 1700–1874 the irradiance reconstructed from the Zurich sunspot number is higher than the one obtained from the Group number. This is because  $R_Z$  is higher than  $R_G$  at that time. The change in the TSI since the Maunder minimum is, however, almost the same in both cases,  $1.3 \text{ Wm}^{-2}$  (the difference between the 2 values is about 1.5% and is statistically insignificant).

## 4.5 Conclusions

Using the physical model of Solanki et al. (2002) to calculate the evolution of the solar photospheric magnetic flux we have reconstructed solar total irradiance back to 1700 (or even 1610 if the Group sunspot number is employed). In this model, the cyclic variation of ephemeral regions (ER) is related to the properties of the active region (AR) cycles, which are represented by the historical records of the sunspot number and sunspot areas. The change in the level of the quiet Sun magnetic flux caused by the partial overlap of the ER cycles leads to a secular variation in the solar total magnetic flux and irradiance.

Our basic model has 4 free parameters. They are estimated by fitting simultaneously 3 independent time series which are the total photospheric magnetic flux in cycles 21–23, the heliospheric magnetic flux since 1868 empirically reconstructed by Lockwood et al. (1999) and the space-borne measurements of the TSI since 1978. Two of the free parameters, the transfer time from AR to the open flux,  $\tau_{\text{ta}}$ , and the decay time of the open flux,  $\tau_{\text{open}}$ , mainly influence the evolution of the open flux and do not affect the total magnetic flux and irradiance. The 2 others,  $c_x$  and  $X$ , link the properties of the ER cycles to those of the AR cycles and control the evolution of the ER magnetic flux (which is a significant part of the total photospheric flux) and the irradiance variations. The obtained values of these parameters are in good agreement with independent observational estimates.

Both historical sunspot records, the Zurich and Group sunspot numbers, have been employed. The irradiance reconstructed from the Group sunspot number is on average somewhat lower during 1700–1874. However, the predicted secular increase in the cycle averaged TSI since 1700 is almost the same in both models and is about  $1.3 \text{ Wm}^{-2}$ . In order to understand the reliability and uncertainty of this estimate we also consider two extreme cases, one assuming that ER progress in antiphase with AR, and one assuming that the ER magnetic flux does not change in time.

Since both of these models initially produced noticeably worse fits to, at least, one of the considered independent time series, we extended the set of free parameters. Then, fairly good fits were obtained for these alternative models. The reconstructed TSI since 1700 looks quite similarly for all the cases (see Fig. 4.5b). The model with the ER cycles being in antiphase with those of the AR provides the highest rise in the cycle averaged

TSI of about  $1.5 \text{ Wm}^{-2}$ , whereas the model with a constant ER flux puts a lower limit of about  $0.9 \text{ Wm}^{-2}$  to this quantity.

This low value is in agreement with findings of Foster (2004), Lockwood (2005) and Wang et al. (2005). This is not surprising. Wang et al. (2005) neglected the extended length of the ephemeral region cycle. Therefore, the increase in TSI since the Maunder minimum they find ( $1 \text{ Wm}^{-2}$ ) is expected to be similar to that which we obtain when we do not allow the ephemeral region flux to change with time. Foster (2004), cf. Lockwood (2005), did take the network into account and obtained an upper limit of  $1.7 \text{ Wm}^{-2}$  on the TSI change by assuming that the network disappeared during the Maunder minimum. This is close to the value of  $1.5 \text{ Wm}^{-2}$  we obtain for our extreme model showing the largest  $\Delta\text{TSI}$ . They then assume that half of the network was still present in the Maunder minimum, which gives a  $\Delta\text{TSI} \approx 1 \text{ Wm}^{-2}$ . This lies between the values of  $\approx 0.9 \text{ Wm}^{-2}$  and  $\approx 1.3 \text{ Wm}^{-2}$  obtained for our constant ER flux and standard models. The  $\Delta\text{TSI}$  obtained in this paper thus cover the range found from independent recent reconstructions. However, all the values we obtain are significantly below the  $\Delta\text{TSI}$  values deduced from stellar data and used in older TSI reconstructions.

# 5 Outlook: First steps towards a millennial reconstruction of solar irradiance

## 5.1 Abstract

Reconstruction of total solar irradiance is of great importance for the study of the possible link between the Sun and the Earth's climate because of the lack of observational data for the period prior to 1978. However, the available models are based on records of solar activity which cover only centuries, while millennial timescales are necessary in order to study the evolution of the climate system with robust statistics. By using records of cosmogenic isotopes, a reconstruction of the sunspot number for a period of ~11000 years recently became available. In the present work, we search for a relationship between different proxies of solar activity that allow us to reconstruct the total solar irradiance from these data.

## 5.2 Introduction

In Chapter 4, we have presented a reconstruction of the long term variations of total solar irradiance. By using a simple physical model the solar magnetic flux and solar irradiance could be reconstructed from the sunspot number for a period of more than three centuries. The next step, naturally implies the extension of this model to earlier times. In particular, millennial time scales are essential for investigating the influence of the Sun on the Earth's climate. Unfortunately, some indices of solar activity such as sunspot numbers, necessary for such reconstructions, have been recorded only since the invention of telescope in the 17th century. They represent the only direct long term measurements of past solar variability. Cosmogenic isotopes, in turn, provide indirect estimates of solar activity but they extend to earlier times, covering periods of thousands of years. By combining physics-based models for each of the processes connecting the isotope concentration at the Earth's atmosphere with solar activity, a reconstruction of sunspot number recently became available (Usoskin et al. 2003, Solanki et al. 2004, Usoskin et al. 2006). The sunspot number is obtained as follows: first, the production rate of a given isotope in the Earth's atmosphere is determined from the measured relative abundance in natural reservoirs such as tree-rings in the case of  $^{14}\text{C}$  (Stuiver and Braziunas 1989, 1998) or ice cores in the case of  $^{10}\text{Be}$  (Beer et al. 1990, Beer 2000). Then, from the production rate, the galactic cosmic

ray flux can be obtained by using a model which describes its transport and modulation in the heliosphere (Usoskin et al. 2002a). After this, it is possible to estimate the Sun's open flux since it modulates the transport of cosmic rays in the heliosphere (Usoskin et al. 2002b). Finally, by using this estimate of open flux as an input, the sunspot number can be derived by inverting the model which describes its evolution for given sunspot number from Solanki et al. (2000, 2002). A detailed description of the procedure is given by Usoskin et al. (2004). Unfortunately, the sunspot number thus reconstructed from  $^{14}\text{C}$  concentration is only available at decadal samples. For this reason, it is not straightforward to use it directly in the model to reconstruct the photospheric magnetic flux and the total solar irradiance. In the present work, we use a simple approach consisting of investigating the possible relation between different proxies of solar activity, in particular sunspot number, photospheric magnetic flux and total irradiance. If we assume that these relationships remain the same for longer periods, we could in principle get an estimate of the variation of solar irradiance at millennial time scales.

### 5.3 Description of the data

In the first place, we employ the two time series of sunspot number (SN): Zurich Sunspot Number (ZSN) and Group Sunspot Number (GSN). ZSN was introduced by Rudolf Wolf and it is obtained by counting the number of individual sunspots and groups present on the solar disc, combining them by weighting the result by an observer-dependent factor (Waldmeier 1961). GSN was introduced to provide a homogeneous record of solar activity from 1610 to 1995 (Hoyt et al. 1994, Hoyt and Schatten 1997, 1998). It is based on group counts alone and is extended back in time with respect to ZSN by including data from additional historical sources. GSN and ZSN differ mainly for the period prior to 1880. By using these two records of sunspot activity, Solanki et al. (2000, 2002) reconstructed the time evolution of the open and total surface magnetic flux of the Sun. Thus, it was possible to estimate the contribution of closed active regions flux and open flux (i.e. the fraction of the solar total magnetic flux that reaches out into interplanetary space) to the total flux for a period covering more than 28 solar cycles. Variations in the total solar irradiance were shown to be of magnetic origin (Krivova et al. 2003, Wenzler et al. 2004, 2005, 2006). So, once the evolution of the solar magnetic flux is known, it is possible to estimate the changes in the solar irradiance for the same period of time (Krivova et al. 2006a, Balmaceda et al. 2007). In this work, we use the estimates of total and open magnetic flux and irradiance variations from ZSN and GSN described above. Fig. 5.1 shows the time evolution of these indicators of solar variability employed here. Additional observational data sets available only for shorter periods are also employed in order to evaluate the relationships found for longer time intervals. These are: PMOD composite of total solar irradiance for the period 1978 – present (Fröhlich 2006), photospheric magnetic flux from synoptic charts for the period 1974 – 2002 (Arge et al. 2002) and open flux reconstructed by (Lockwood et al. 1999) from 1868 to 1995.

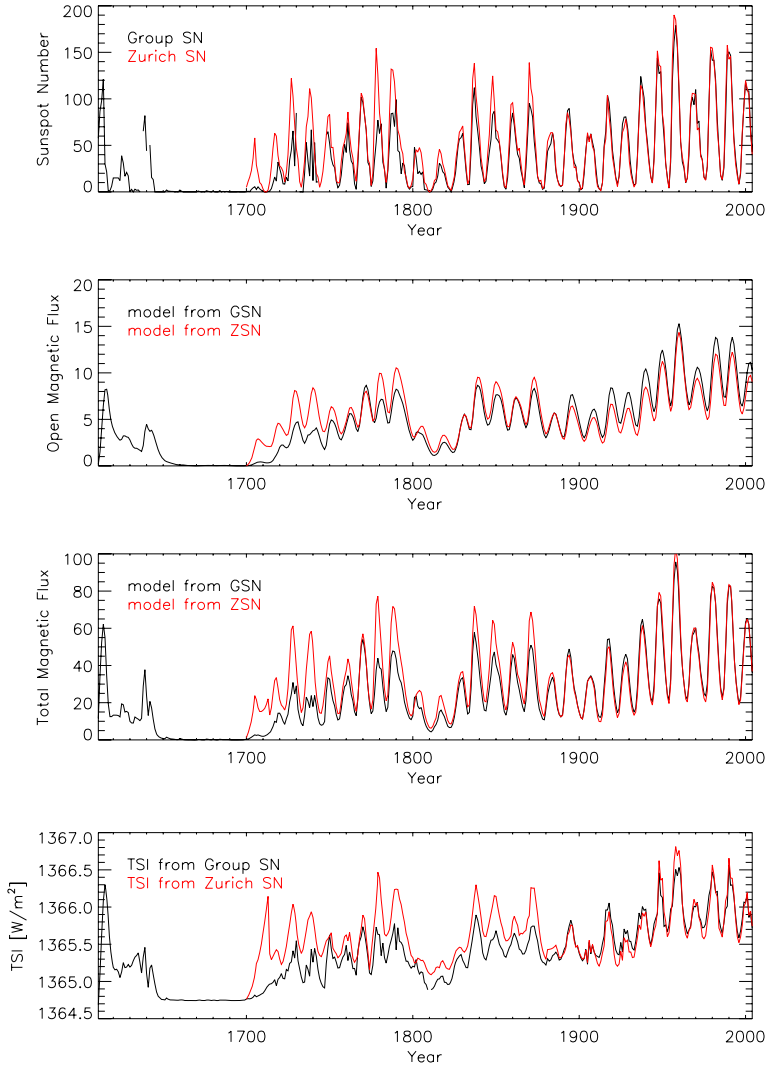


Figure 5.1: From top to bottom: time evolution of sunspot number, open magnetic flux [ $10^{14}$  Wb], total magnetic flux [ $10^{14}$  Wb] and total solar irradiance. In all cases annual are plotted vs. time.

## 5.4 Searching for relations

The relationships between different indices of solar magnetic activity differ on different time scales. In this section we look for relationships between total solar irradiance (TSI) and sunspot number (SN), open flux (OF) and total magnetic flux (TMF). To distinguish the quantities obtained from models using the two sunspot number time series available, we add (Z) and (G) for the ones derived from ZSN and GSN respectively. We mainly concentrate on studying the relationship for cycle averages. However, annual means of these quantities are also compared to study whether the relationship remains constant or changes from one cycle to the next.

### 5.4.1 Total solar irradiance and sunspot number

We compare annual and cycle averages of TSI and SN for a period of time since 1611 in the case of GSN and since 1700 in the case of ZSN (see Fig. 5.2, panels a-d). In all cases, the relationship was found to be linear with the form:  $\text{TSI} = \text{SN} \cdot b + a$ . In Table 5.1 we list the regression parameters ( $a$  and  $b$ ) for these comparisons with the respective error estimates ( $\sigma_a$  and  $\sigma_b$ ). The correlation coefficient,  $R_c$  is also shown. In the second column of this table we indicate whether the TSI time series used corresponds to measured values (obs.) or to the estimates from the model.

Table 5.1: Regression parameters for the comparison between TSI and SN

SN	TSI	Period	b	a	$R_c$	$\sigma_b$	$\sigma_a$
Annual means							
ZSN	obs.	1978 - 2005	$6.64 \times 10^{-3}$	1365.48	0.972	$3.25 \times 10^{-4}$	$3.09 \times 10^{-2}$
GSN	obs.	1978 - 2005	$6.77 \times 10^{-3}$	1365.47	0.974	$3.23 \times 10^{-4}$	$3.04 \times 10^{-2}$
ZSN	model	1700 - 2005	$6.49 \times 10^{-3}$	1365.32	0.729	$3.49 \times 10^{-4}$	$2.25 \times 10^{-2}$
GSN	model	1611 - 2005	$8.75 \times 10^{-3}$	1365.05	0.775	$3.64 \times 10^{-4}$	$1.88 \times 10^{-2}$
Cycle averages							
ZSN	model	1700 - 2005	$1.46 \times 10^{-2}$	1364.94	0.955	$9.28 \times 10^{-4}$	$4.77 \times 10^{-2}$
GSN	model	1611 - 2005	$1.66 \times 10^{-2}$	1364.79	0.980	$5.97 \times 10^{-4}$	$2.39 \times 10^{-2}$

When we use annual means on the interval longer than 1978 - 2005 the correlation coefficient are of the order of 0.7 - 0.8 (third and fourth rows in Table 5.1) and the scatter is large (see panels a and b of Fig. 5.2). The slope and the offset for the linear fit are different, depending on which SN time series is used. If we compare TSI measurements with SN only for the period where they are available the correlation improves significantly and the values for the slopes and offset obtained using ZSN and GSN are very similar (see first and second rows of Table 5.1). This is expected since both sunspot numbers are very similar for the period after 1874 and in particular, after 1996 they are calculated in the same way. The slope from the comparison with TSI data lies within the ones obtained for each of

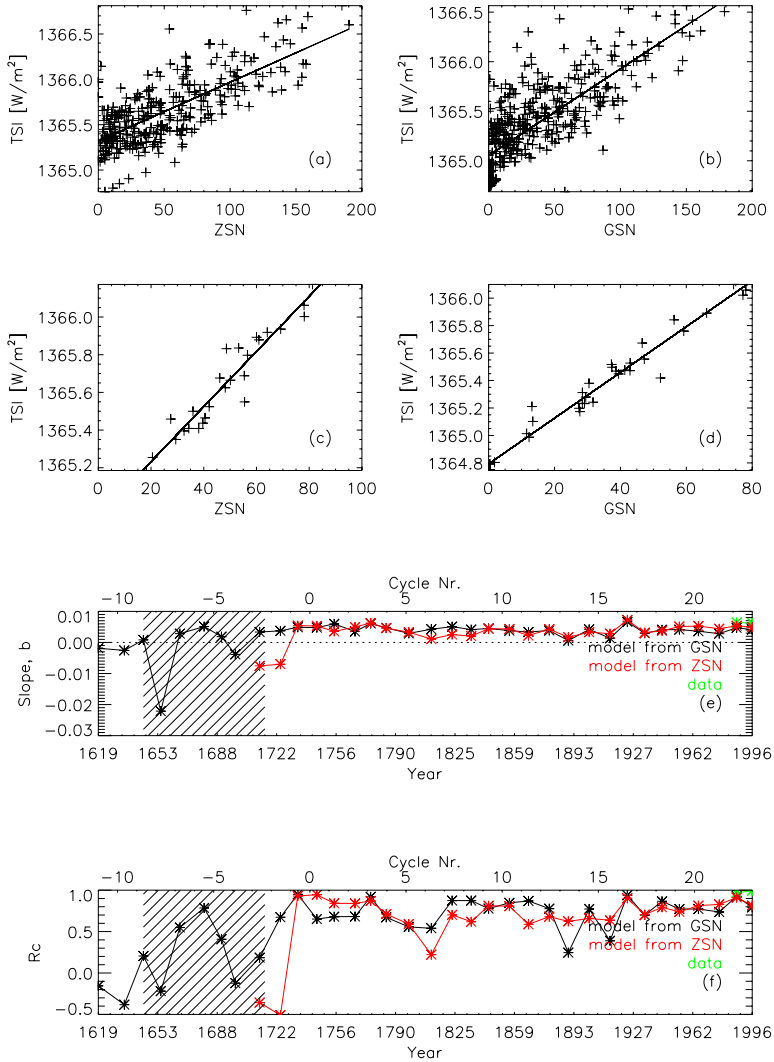


Figure 5.2: Comparison between annual means (a and b) and cycle averages (c and d) of TSI and SN. Variation of the relationship between TSI and SN from one cycle to another: slope of the linear regression for each solar cycle (e); correlation coefficient vs. time (f).

both sunspot numbers during the period since 1610 or 1700 respectively. However, it is closer to the value found when using ZSN.

We also investigate how the relationship between TSI and SN changes from one cycle to the next. For this, we compare the annual means of both quantities belonging to a given solar cycle. The value of the slope of the linear fit and the correlation coefficient for each cycle are shown in Fig. 5.2e and f. The slopes vary on average from about 20%, which increases to a relative variation of 40% in the case of GSN for the period after  $\sim 1709$ . The correlation with ZSN seems to be slightly more stable showing a smaller variation from cycle to cycle (about 32–38%) for the period after  $\sim 1729$ . TSI and SN seem to correlate well for the same period with a mean correlation coefficient of 0.74 for both, GSN and ZSN. However, at earlier times, the correlation drops considerably and the relation shows a very large variation from one cycle to the next. Some cycles during the Maunder Minimum (1645–1715) exhibit even an anti-correlation. As explained in our model described in Chapter 4, the different components of the total magnetic flux of the Sun (active regions, ephemeral regions and open flux) and thus, the different contributions to the solar irradiance variations (i.e., sunspot, faculae, network) are calculated from the sunspot number. In general, the shape of the modelled solar irradiance cycles is similar to that of the sunspot cycles. However during this period due to the lack of sunspots, the other contributions to the solar irradiance are difficult to estimate and the uncertainties are very high. Consequently, the cycles of the modelled solar irradiance are slightly deformed compared to that of sunspot number during the Maunder Minimum.

The correlation between TSI and SN improves significantly when we use cycle averages instead of annual means with correlations coefficients now being larger than 0.96 (see panels c and d of Fig. 5.2). However, the values of the slopes and the offset differ in large manner from those obtained using annual means. This is due to the fact that SN drops almost to zero during activity minima, while TSI does not, as can be seen in Fig. 5.1. When we average values per cycle, we only get the secular trend for both time series, while the relationship between the annual averages is dominated by the variations of both quantities over the solar cycle. Wang et al. (2005) found also a linear relationship between their reconstructed solar irradiance and sunspot number when comparing cycle averaged values. However the relationship changes to quadratic when yearly values are used. Also daily data show quadratic relationship with large scatter (Solanki and Fligge 1999). This is due to the fact that the ratio of faculae to sunspot areas decreases when sunspot activity increases (Foukal 1998, Chapman et al. 1997). When cycle averages are compared, instead, all these effects are smoothed out and the relationship between solar irradiance and sunspot number becomes linear.

### 5.4.2 Total solar irradiance and total magnetic flux

TSI and TMF are compared in Fig. 5.3(a-d) and the regression parameters for the linear fit obtained from this comparison ( $\text{TSI} = \text{TMF} \times b + a$ ) as well as the corresponding correlation ( $R_c$ ) coefficient and error estimates ( $\sigma_a$  and  $\sigma_b$ ) are listed in Table 5.2. TSI and TMF show very high correlations regardless of whether annual or cycle averages are used (see fourth column of Table 5.2). The correlation coefficients are in all cases larger than 0.88. We also compare annual values of the measured TSI and TMF, for the period they overlap (1978 - 2002), in order to evaluate these results. In this case, the slope is



somewhat smaller (20% in the case of ZSN and 30% in the case of GSN) than the slopes obtained from the comparison between the modelled TSI and TMF for the period of the reconstruction (see second and third rows of Table 5.2). This difference can be attributed to the shortcomings of the magnetic flux model that does not reproduce the observed short-term variations in detail, showing a more smooth variation compared to the real data.

Table 5.2: Regression parameters for the comparison between TSI and TMF

TMF	TSI	Period	b	a	$R_c$	$\sigma_b$	$\sigma_a$
Annual means							
observations		1978 - 2002	$1.49 \times 10^{-2}$	1365.27	0.987	$5.77 \times 10^{-4}$	$3.12 \times 10^{-2}$
model (Z)		1700 - 2005	$1.65 \times 10^{-2}$	1365.08	0.886	$4.97 \times 10^{-4}$	$1.94 \times 10^{-2}$
model (G)		1611 - 2005	$1.97 \times 10^{-2}$	1364.88	0.918	$4.31 \times 10^{-4}$	$1.34 \times 10^{-2}$
Cycle averages							
model (Z)		1700 - 2005	$2.37 \times 10^{-2}$	1364.85	0.982	$9.26 \times 10^{-4}$	$3.26 \times 10^{-2}$
model (G)		1611 - 2005	$2.50 \times 10^{-2}$	1364.77	0.992	$5.72 \times 10^{-4}$	$1.58 \times 10^{-2}$

In order to investigate the inter-cycle variations of the relationship between TSI and TMF we show in Fig. 5.3e and f the slopes of the regression relation and the correlation coefficient for each cycle vs time. High correlations ( $R_c > 0.8$ ) are found for the period after  $\sim 1722$ , with some exceptions. In particular, cycles 13 and 14 for the model derived from GSN and cycle 6 for the model derived from ZSN show a poor correlation ( $R_c < 0.5$ ). This behaviour was also observed in the comparison between TSI and SN (compare with Fig. 5.2).

The slopes determined by comparing annual means for each solar cycle show a variation from one cycle to the other larger than in the comparison between TSI and SN. For the models using ZSN, the slopes vary on average from 12 to 36% from one cycle to another. For the models from GSN the variation in the slopes ranges from 13 to 42% after  $\sim 1729$ . Before that year, the slopes vary strongly from one cycle to the next.

The slopes obtained from the comparison using cycle averages are about 20% (in the case of models derive from GSN) and 30% (in the case of models derived from ZSN) higher than the ones obtained using annual values.

### 5.4.3 Total solar irradiance and open magnetic flux

In Fig. 5.4 (a-d) the scatter plots of TSI vs OF are shown. The red diamonds represent annual values for the last three solar cycles. As in the analysis shown in previous sections, the dependence of TSI on OF is also linear. The results from this comparison are presented in Table 5.3. In this table we also include the comparison between the OF reconstructed by Lockwood et al. (1999), here denoted as L99, and the modelled TSI. Good correlations between TSI and OF are found when we consider the whole period covered

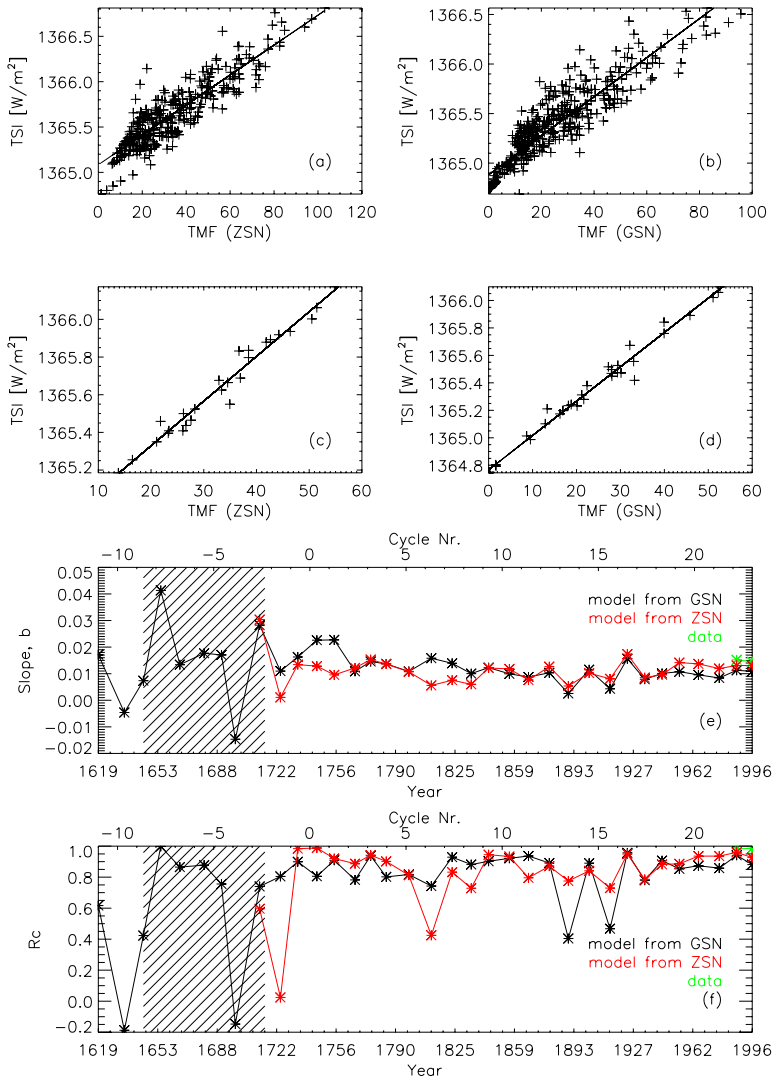


Figure 5.3: Scatter plots of TSI vs TMF: annual means (a and b), cycle averages (c and d). Inter-cycle variations of the relationship between TSI and TMF: slope vs. time (e); correlation coefficient for each solar cycle (f). The hatched area indicates the Maunder Minimum.

by the reconstruction in both cases, using annual or cycle means. The correlation coefficients from these comparisons are nearly as high as the ones of the comparison between TSI and TMF ( $R_c > 0.8$ ).

Table 5.3: Regression parameters for the comparison between TSI and OF

OF	TSI	Period	b	a	$R_c$	$\sigma_b$	$\sigma_a$
Annual means							
	model (Z)	1700 - 2005	$1.11 \times 10^{-1}$	1364.99	0.815	$4.55 \times 10^{-3}$	$2.92 \times 10^{-2}$
	model (G)	1611 - 2005	$1.11 \times 10^{-1}$	1364.83	0.912	$2.59 \times 10^{-3}$	$1.49 \times 10^{-2}$
L99	model(Z)	1868 - 1995	$1.13 \times 10^{-1}$	1364.93	0.747	$8.93 \times 10^{-3}$	$6.78 \times 10^{-2}$
L99	model(G)	1868 - 1995	$1.05 \times 10^{-1}$	1364.97	0.795	$7.14 \times 10^{-3}$	$5.42 \times 10^{-2}$
Cycle means							
	model (Z)	1700 - 2005	$1.30 \times 10^{-1}$	1364.88	0.971	$6.59 \times 10^{-3}$	$4.09 \times 10^{-2}$
	model (G)	1611 - 2005	$1.25 \times 10^{-1}$	1364.77	0.988	$3.41 \times 10^{-3}$	$1.87 \times 10^{-2}$
L99	model(Z)	1868 - 1995	$1.51 \times 10^{-1}$	1364.63	0.927	$1.52 \times 10^{-2}$	$2.15 \times 10^{-1}$
L99	model(G)	1868 - 1995	$1.47 \times 10^{-1}$	1364.69	0.954	$1.15 \times 10^{-2}$	$1.62 \times 10^{-3}$

However, as can be seen in Fig. 5.4e and f, the relationship between annual means of these two quantities changes significantly (more than 40%) from one cycle to another. The correlation coefficients for different cycles are generally smaller than 0.7 and in some cases even smaller than 0.5. Different from the comparisons of previous sections, this relationship does not show long periods where it remains stable. This is due to the fact that the OF lags about 1 year behind the solar irradiance.

In Fig. 5.5 we plot again the values for the slopes from the comparison using yearly means for different cycles but in this case shifting the OF time series so that it is in phase with the TSI. By removing this lag = 1yr the correlation for each cycle improves significantly ( $R_c > 0.8$ ). The variation in the slopes from one cycle to the next, however, is still large. We would like to stress this point because previous attempts to reconstruct solar irradiance back to earlier times from open flux were based on regression relations obtained by comparing only data of the recent solar cycles (see, e.g., Lockwood et al. 1999, Lockwood 2002). However, the behaviour observed in short periods may not be the same for longer time scales and the reconstructed irradiance can be significantly different. As can be seen in Fig. 5.4a and b, the values corresponding to the last cycles show a large scatter that is reduced but is still present after removing the lag between both time series, causing a variation in the slope from cycle to cycle.

The regression parameters after removing the lag are listed in Table 5.4. The values of the slope and offset for the comparison of annual means during the whole period get closer to the values obtained when cycle averages are compared. These values, in turn, remain approximately the same regardless of whether there is lag or not (they change only after the fourth place after the decimal point). For the annual means, the slope for

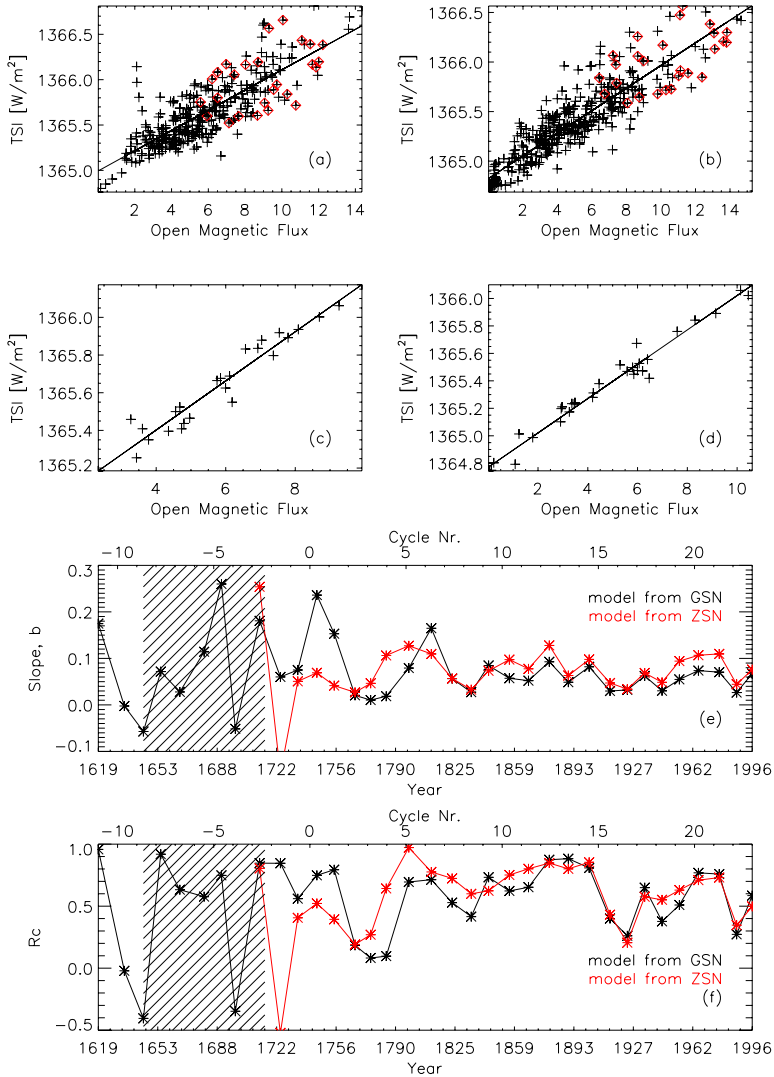


Figure 5.4: Comparison between TSI and OF. Top panel: annual means; the red diamonds correspond to values for the last three cycles. Bottom panel: cycle means. e: slope of the linear regression from the comparison between TSI and OF. f: variation of the correlation coefficient for different cycles. The hatched area corresponds to the Maunder Minimum period.

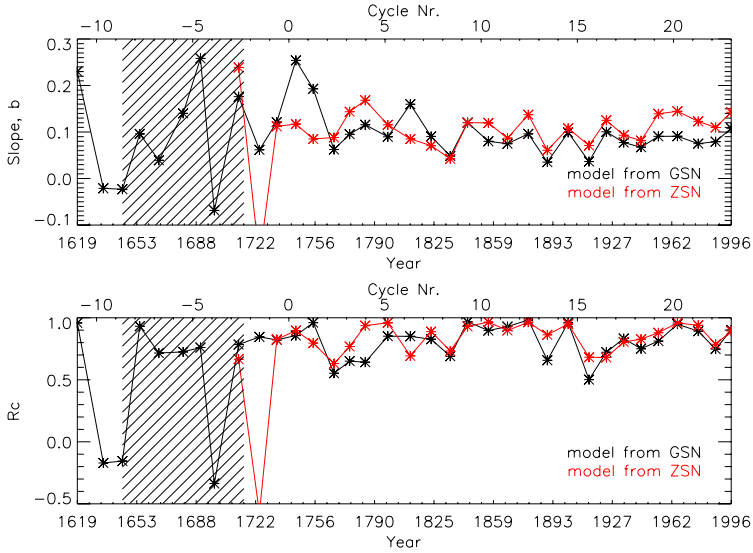


Figure 5.5: Same as Fig. 5.4e and f but including the lag of 1 year. It can be seen that the relationship now is more stable along different solar cycles.

the comparison between the OF (L99) and TSI from the model is lower than that one using the OF from the model. For cycle means, instead, the slope is larger.

When comparing cycle averages, the scatter is reduced and the correlation improves significantly ( $R_c > 0.97$ ). In spite of this result, unfortunately it is not yet clear whether there is a physical link between these two quantities that justifies the high correlation. There is, however, a physical link but indirectly through the surface flux, which is studied in the next section.

#### 5.4.4 Open magnetic flux and total magnetic flux

The comparison between OF and TMF is shown in Fig. 5.6 (a-d). Panels a and b show the comparison between annual values while in panels c and d cycle averages are compared. The relationship in this case is also linear. The slope ( $b$ ) and the offset ( $a$ ) of the linear relation found here, as well as the corresponding error estimates ( $\sigma_a$  and  $\sigma_b$ ) and the correlation coefficient ( $R_c$ ) are listed in Table 5.5.

For cycle averaged values of TMF and OF the correlation is very high during the period from 1611 or 1700 till present ( $R_c > 0.98$ ).

When annual means are used in the comparisons, the scatter is large and the correlation coefficients drop to 0.7 - 0.8. As in the case of the comparison between OF and TSI, here OF also lags behind TMF, this time by approximately 2 years. The correlation improves considerably when this lag of 2 years is removed (see red diamonds in the scat-

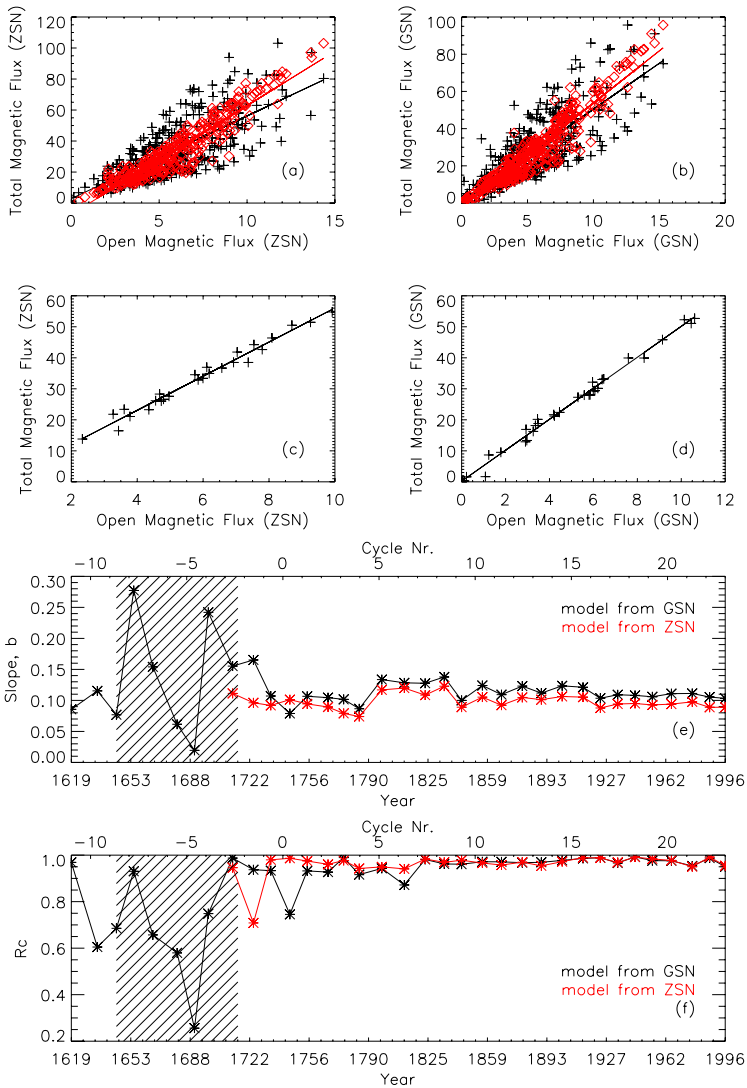


Figure 5.6: TMF vs. OF: yearly averages (a and b), the red diamonds correspond to values after correcting for the lag; cycle averages (c and d). Variation of the relationship between TMF and OF from one cycle to another: slopes of the linear relation for different solar cycles (e); correlation coefficient for those regressions (f). The hatched area indicates the Maunder Minimum.

Table 5.4: Regression parameters for the comparison between TSI and OF, considering lag = 1yr

OF	TSI	Period	b	a	$R_c$	$\sigma_b$	$\sigma_a$
Annual means							
	model (Z)	1700 - 2005	$1.25 \times 10^{-1}$	1364.91	0.908	$3.33 \times 10^{-3}$	$2.14 \times 10^{-2}$
	model (G)	1611 - 2005	$1.20 \times 10^{-1}$	1364.80	0.954	$1.90 \times 10^{-3}$	$1.09 \times 10^{-2}$
L99	model(Z)	1868 - 1995	$1.16 \times 10^{-1}$	1364.91	0.765	$8.73 \times 10^{-3}$	$6.61 \times 10^{-2}$
L99	model(G)	1868 - 1995	$1.06 \times 10^{-1}$	1364.96	0.801	$7.08 \times 10^{-3}$	$5.37 \times 10^{-2}$
Cycle means							
	model (Z)	1700 - 2005	$1.30 \times 10^{-1}$	1364.88	0.973	$6.33 \times 10^{-3}$	$3.93 \times 10^{-2}$
	model (G)	1611 - 2005	$1.25 \times 10^{-1}$	1364.77	0.989	$3.19 \times 10^{-3}$	$1.75 \times 10^{-2}$
L99	model(Z)	1868 - 1995	$1.50 \times 10^{-1}$	1364.64	0.946	$1.82 \times 10^{-2}$	$1.29 \times 10^{-1}$
L99	model(G)	1868 - 1995	$1.45 \times 10^{-1}$	1364.71	0.965	$1.39 \times 10^{-2}$	$9.92 \times 10^{-3}$

ter plots of panels a and b in Fig. 5.6). The correlation coefficients are in this case larger than 0.94. Since the lag is smaller than the cycle length ( $\sim 11$  yr), this does not cause any significant effect on the regression relation obtained using the cycle average values (compare the 3rd and 4th with the 7th and 8th rows in Table 5.5).

The inter-cycle variation of the relationship between TMF and OF is shown in Fig. 5.6. The value of the slope for the comparison using yearly values belonging to each solar cycle, after removing the lag between both time series, and the correlation coefficient for these relations are plotted vs time. The relationship between TMF and OF seems to remain stable along several solar cycles, specially after the Maunder Minimum. The correlation coefficient is high ( $> 0.9$ ) for most part of the period. Thus, the open flux seems to be a good proxy for the total magnetic flux on time scales longer than a solar cycle. Due to the good linear relationship, the OF can be considered to be an almost constant fraction of 10–15% of the TMF.

## 5.5 Discussion

The recently reconstructed time series of the sunspot number and open flux for a period extending through much of the Holocene offers an excellent opportunity to study solar irradiance variations for the same period of time. However, both records (SN and OF) are sampled only every 10 years, so that their use as direct input into the model presented in Chapter 4 is not straightforward.

As the first step for an alternative approach we have investigated in this chapter the relationship for the last 300 or 400 years between total solar irradiance and different proxies of solar activity, in particular the sunspot number and the quantities derived from it, i.e., total and open magnetic flux. We consider these relationships both for yearly and

Table 5.5: Regression parameters for the comparison between TMF and OF

OF	TMF	Period	b	a	$R_c$	$\sigma_b$	$\sigma_a$
Lag = 0							
annual means							
model (Z)		1700 - 2005	5.33	2.85	0.726	$2.90 \times 10^{-1}$	1.86
model (G)		1611 - 2005	4.93	1.10	0.847	$1.56 \times 10^{-1}$	0.90
Cycle means							
model (Z)		1700 - 2005	5.50	1.08	0.989	$1.70 \times 10^{-1}$	1.06
model (G)		1611 - 2005	4.99	0.19	0.996	$8.07 \times 10^{-2}$	0.44
Lag = 2 yr							
Yearly means							
model (Z)		1700 - 2005	7.01	-7.29	0.940	$1.46 \times 10^{-1}$	0.94
model (G)		1611 - 2005	5.59	-2.21	0.961	$8.21 \times 10^{-2}$	0.47
Cycle means							
model (Z)		1700 - 2005	5.54	0.56	0.996	$1.01 \times 10^{-1}$	0.65
model (G)		1611 - 2005	4.94	0.27	0.999	$4.49 \times 10^{-2}$	0.24

cycle averages. We find that the regression is different if we compare annual or cycle means because while the first ones are dominated by the solar cycle variation the latter are dominated by the century-scale drift.

The cycle means, needed for the reconstruction of the long term variation of the irradiance turn out to have a number of advantages. Firstly, the quantities are linearly related, quite unlike the daily data (e.g., Solanki and Fligge 1999). Secondly, all the short-term variations and the observed lags between the different time series seen when using yearly means are eliminated, so that only the upward trend observed in all the data sets employed here remains.

From the analysis presented in this Chapter it was observed that at time scales longer than a solar cycle all these proxies correlate very well with the modelled solar irradiance. So, in principle any of them would serve to estimate the general variation of this quantity for periods extending to millennia, although the best correlation is found between TSI and the total magnetic flux (which are also most closely related), followed by the open flux.

In Fig. 5.7 we present the results of the reconstructed irradiance since 1611 and 1700 by using the different regression relations presented in previous sections based on cycle averaged values. For comparison, the yearly values (black line) and the 11-yr running means (pink line) of the irradiance time series obtained from the physical model are also shown. It can be seen that the agreement is good for most part of the period and the reconstructions are in all cases very similar. In Table 5.6, we list the values for the variance,  $\sigma^2$ , as a measure of the error for each of these reconstructions. They are calculated



by comparing the reconstructed irradiance based on the model of magnetic flux with the irradiance obtained from the regression relation, as follows:

$$\sigma^2 = \chi^2/N, \quad (5.1)$$

$$\chi^2 = \sum_{i=1}^N (TSI_{i,model} - TSI_{i,regression})^2, \quad (5.2)$$

with  $N$  being number of data points.

Table 5.6: Goodness-of-fit for the reconstructions from different comparisons based on cycles averaged values

Comparison	$\sigma^2$
ZSN - TSI (Z)	$5.93 \times 10^{-3}$
GSN - TSI (G)	$5.78 \times 10^{-3}$
TMF - TSI (Z)	$2.40 \times 10^{-3}$
TMF - TSI (G)	$2.40 \times 10^{-3}$
OF - TSI (Z)	$3.84 \times 10^{-3}$
OF - TSI (G)	$3.36 \times 10^{-3}$

The cycle-by-cycle difference between the irradiance reconstructed using the physical model and the ones obtained by using the linear regressions analyzed in previous sections is plotted in the upper panel of Fig. 5.8 and 5.9 for models based on ZSN and GSN respectively. In both cases, the largest difference is observed in the period prior to 1800 for all the reconstructions. For the period after  $\sim 1880$ , the reconstructions based on ZSN and its products show the smallest difference, while in the case of GSN, the difference is larger.

Regarding the quality of the reconstruction depending on which proxy is used, the one based on sunspot number shows in general the largest difference during the whole period. TSI undergoes a cyclic variation caused by the magnetic activity superimposed to a long-term variation due to changes in the quiet Sun network. Sunspot number is a good proxy for the flux emerging in active regions (Solanki et al. 2000, 2002), so on time scales shorter than a solar cycle it correlates well with TSI. However, the sunspot record does not contain direct information about ephemeral regions which contribute to the network dominating during activity minima and are responsible for the secular change in solar irradiance. Thus, the upward trend observed in the cycle averaged values of SN is mainly caused by the increase in amplitude of individual solar cycles but some information on the slowly varying component due to the quiet Sun variations is lost. For this reason, the correlation between TSI and SN shows the lowest agreement when compared to the one of TSI with TMF or OF.

The frequency distribution of the errors for each of the reconstructions is also shown in the lower panel of the Fig. 5.8 and 5.9. From these plots, it is clear that the reconstructions

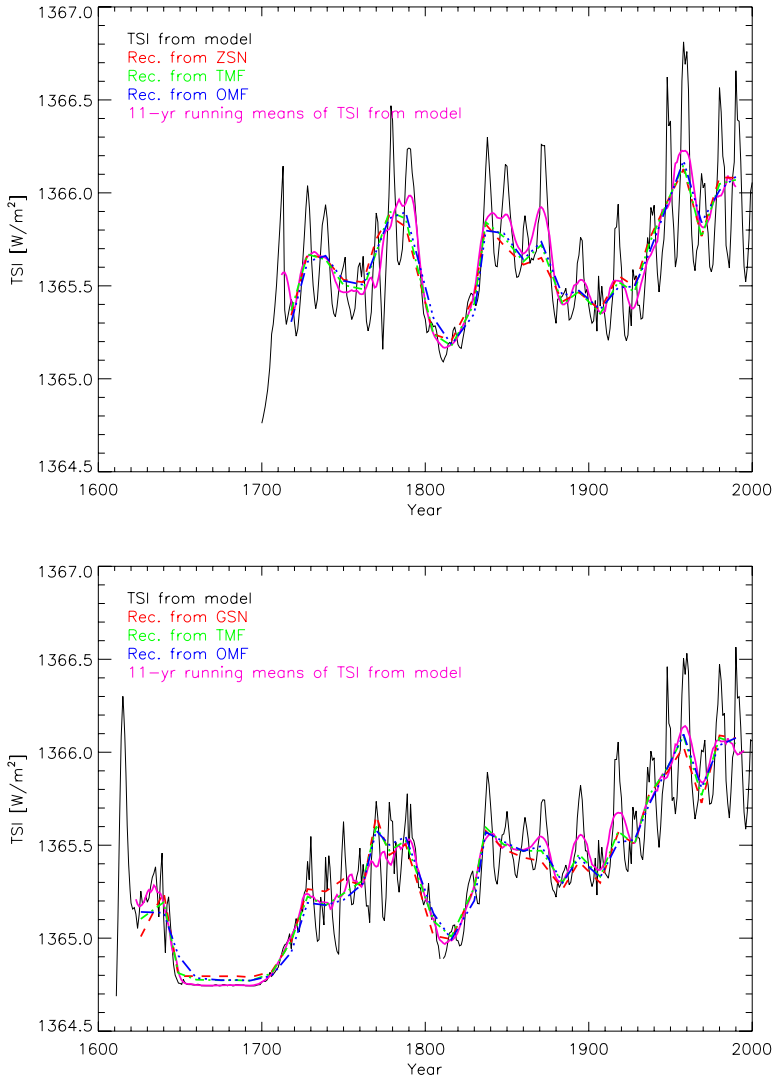


Figure 5.7: Comparison of the different reconstructions based on the relations studied here with ZSN (top panel) and GSN (bottom panel) and the quantities derived from them.

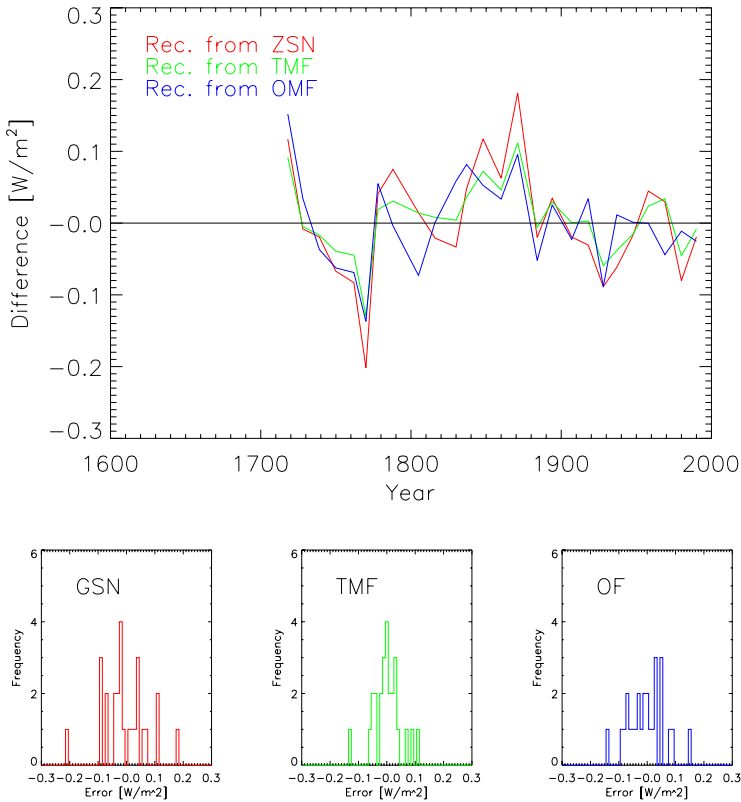


Figure 5.8: Top: Difference between the reconstructions based on the relations using ZSN and the quantities derived from it, TMF and OF, and the modelled irradiance. Bottom: distribution of the errors for each of these reconstructions.

based on total flux show a better agreement with the modelled irradiance than the ones from sunspot number or open flux. In fact, the lowest values for the variance are obtained for this reconstruction based on TMF. TMF consists of both, closed and open fields, but the OF comprises only a small fraction of it. Since irradiance variations are caused almost entirely by the competition between dark sunspots and bright plages areas, both associated with closed magnetic fields, it is not striking that TMF follows more closely TSI than OF does, specially at short time scales (Wang et al. 2000b,a).

It is important to note, however, that the reconstructions based on total and open mag-

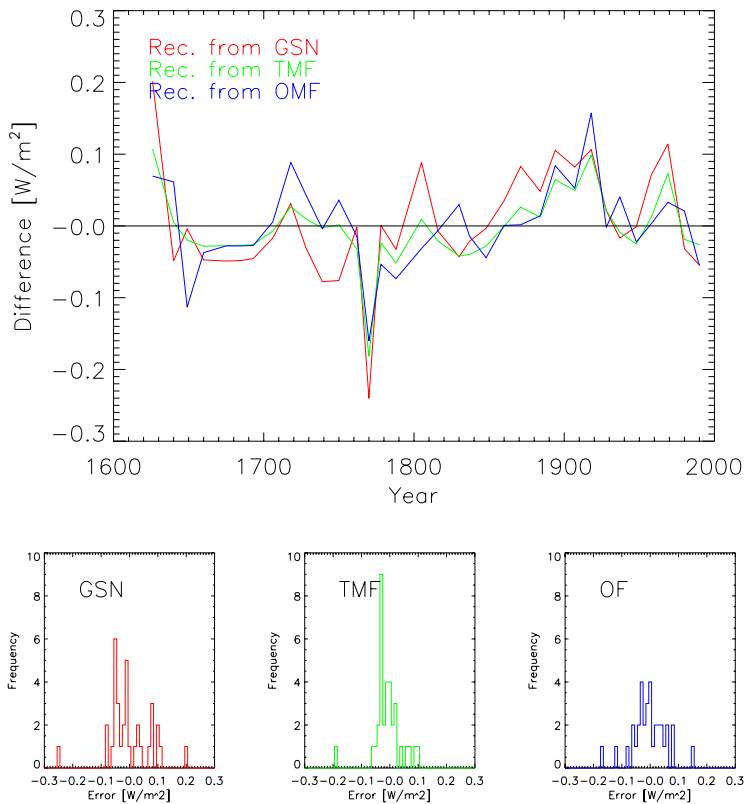


Figure 5.9: Same as Fig. 5.8 but using GSN and the quantities derived from it.

netic flux do not differ significantly. For this reason, the high correlation between solar irradiance and OF is not surprising. This result can be very useful since there is no available time series of TMF reaching further back than 1611, whereas OF could be taken as a reliable proxy for the total flux emerging at the solar surface in order to allow reconstructions of solar irradiance on longer time scales.

## 5.6 Summary and conclusions

It is currently known that solar irradiance variations affect the Earth's climate, in particular the energy balance, thermal structure and composition. However, how exactly and to which extent this occurs is not yet clear. For this reason, models of solar irradiance covering periods as long as possible are needed in order to study the evolution of the climate system. In the present Chapter we have presented a first step towards a reconstruction of solar irradiance covering millennial time scales. In particular, we have compared annual means and cycle averages of TSI, SN, OF and TMF and found that in all cases they show a linear relationship. Annual means of these quantities for separate cycles were also compared in order to study the variation at longer-time scales.

In the next step we intend to extrapolate the linear relationships found here back to the Holocene epoch by using the reconstructed time series of SN and OF obtained by Solanki et al. (2004). Since the reconstruction of the SN consists of multiple stages, it contains various sources of errors. Moreover, the time series of the different proxies of solar activity also contain uncertainties. The combination of these various indexes requires then a careful error analysis to be done in a further step.



## 6 Concluding remarks

In this dissertation we have studied aspects related to solar variability on long time scales. In particular, we have centered our attention on the irradiance variations from a solar cycle to centuries and millennia. Since the space-based record of irradiance measurements covers only the three most recent solar cycles, for prior periods irradiance variations can be estimated using models that account for the changes observed at present in combination with proxies of solar activity recorded in the past centuries. This requires as long as possible time series of reliable data that can serve as input in such models. In particular, sunspot areas and plage or facular areas are used to account for the depletion and increase of total solar irradiance respectively. Unfortunately, facular and plage area records are not available for extended periods of time. On the other hand, sunspot areas were continuously measured since 1874 at different observatories, providing a complete time series extending till the present. From a careful comparison between different data sets of sunspot areas we obtained cross-calibration factors in order to correct for systematic differences in the data recorded by diverse observatories. We used this revised time series of sunspot areas together with a plage area record to reconstruct total and UV solar irradiance back to 1915, by using a simple regression model. We found that the long-term behaviour of the total and UV irradiance is similar. Furthermore, the difference in the behaviour of these two quantities pointed out by other authors are only a consequence of the use of uncalibrated data in the reconstruction. In recent decades, a number of reconstructions extending back to the beginning of Maunder Minimum were developed for the cyclic component of the irradiance variations. The magnitude of the secular trend, however was more difficult to estimate. Based on a physical model of the evolution of the surface magnetic flux of the Sun (Solanki et al. 2000, 2002), we have set a long-term total irradiance increase from the Maunder Minimum to present in the range  $0.8 - 1.2 \text{ Wm}^{-2}$ . Relevant for studies of the evolution of the Earth's climate are even longer time series of solar irradiance. However, indirect proxies must be used to reconstruct solar activity over past millennia. In this dissertation we have also studied the relationship between different proxies of solar activity on time scales of centuries as a first step towards a millennial reconstruction of solar irradiance.

In spite of the progress observed in recent years in the quantitative knowledge and understanding of solar variability and its undoubted importance as a driver of climate changes there is still considerable work left to be done. On time scales of days to a solar cycle, the available SATIRE models (Krivova et al. 2003, Wenzler et al. 2004, 2005, 2006) can reproduce observed short-term solar total and spectral irradiance variations with high accuracy. However, the removal of the remaining free parameter is still an unresolved issue that hopefully will be tackled in the coming years. On time scales of a solar cycle to centuries Solanki et al. (2000, 2002) have found a process that can explain a secular change

in the solar magnetic field and thus in the total solar irradiance (Krivova et al. 2006b, Balmaceda et al. 2007). The next step includes also reliable reconstruction of spectral irradiance, in particular in the UV and IR. Variations of the solar irradiance longwards of 300 nm are well reproduced by SATIRE models (Unruh et al. 2000, Krivova et al. 2003). However a comparison on time scales longer than a few months is difficult due to the uncertain long-term trend in the data. On the other hand, at wavelengths shorter than 300 nm the LTE approximation used to calculate the model atmosphere fails and non-LTE modelling is then required. An alternative (and more empirical) approach consists of extrapolation of the existing models to shorter wavelengths based on the available measurements in the UV (Krivova and Solanki 2005, Krivova et al. 2006b). The extension of this empirical model further back in time is of great importance for Sun - climate studies. In the recent years, on even longer time scales (over millennia), Solanki et al. (2004) presented an improved time series of reconstructed sunspot number throughout the Holocene. We showed that a reconstruction of solar irradiance over this period can be also possible with the help of such data. The inclusion of this extended time series of solar irradiance in climate models would provide new insight into the understanding of the Sun - climate relationship.



# Bibliography

- Arge, C. N., Hildner, E., Pizzo, V. J., Harvey, J. W., 2002, Two solar cycles of nonincreasing magnetic flux, *Journal of Geophysical Research (Space Physics)*, 107, 16–1
- Arnold, N., 2005, Solar variability, coupling between atmospheric layers and climate change, pp. 391–417, *Advances in astronomy*
- Baliunas, S., Jastrow, R., 1990, Evidence for long-term brightness changes of solar-type stars, *Nature*, 348, 520–523
- Balmaceda, L., Solanki, S. K., Krivova, N., 2005, A cross-calibrated sunspot areas time series since 1874, *Memorie della Societa Astronomica Italiana*, 76, 929–932
- Balmaceda, L., Krivova, N., Solanki, S. K., 2007, Reconstruction of solar total irradiance using Group sunspot number, *Adv. Space Res.*, accepted
- Baranyi, T., Gyori, L., Ludmány, A., Coffey, H. E., 2001, Comparison of sunspot area data bases, *MNRAS*, 323, 223–230
- Baumann, I., Solanki, S. K., 2005, On the size distribution of sunspot groups in the Greenwich sunspot record 1874–1976, *A&A*, 443, 1061–1066, [astro-ph/0510516](#)
- Beer, J., 2000, Long-term indirect indices of solar variability, *Space Science Reviews*, 94, 53–66
- Beer, J., Blinov, A., Bonani, G., Hofmann, H. J., Finkel, R. C., 1990, Use of Be-10 in polar ice to trace the 11-year cycle of solar activity, *Nature*, 347, 164–166
- Beer, J., Tobias, S., Weiss, N., 1998, An Active Sun Throughout the Maunder Minimum, *Sol. Phys.*, 181, 237–249
- Belov, A., 2000, Large Scale Modulation: View From the Earth, *Space Science Reviews*, 93, 79–105
- Bogdan, T. J., Gilman, P. A., Lerche, I., Howard, R., 1988, Distribution of sunspot umbral areas - 1917–1982, *ApJ*, 327, 451–456
- Bond, G., Kromer, B., Beer, J., Muscheler, R., Evans, M. N., Showers, W., Hoffmann, S., Lotti-Bond, R., Hajdas, I., Bonani, G., 2001, Persistent Solar Influence on North Atlantic Climate During the Holocene, *Science*, 294, 2130–2136

- Brandt, P. N., Schmidt, W., Steinegger, M., 1992, Photometry of Sunspots Observed at Tenerife, in *Solar Electromagnetic Radiation Study for Solar Cycle 22*, (Ed.) R. F. Donnelly, pp. 130–134
- Brandt, P. N., Stix, M., Weinhardt, H., 1994, Modeling solar irradiance variations with an area dependent photometric sunspot index, *Sol. Phys.*, 152, 119–124
- Brueckner, G. E., Edlow, K. L., Floyd, IV, L. E., Lean, J. L., Vanhoosier, M. E., 1993, The solar ultraviolet spectral irradiance monitor (SUSIM) experiment on board the Upper Atmosphere Research Satellite (UARS), *J. Geophys. Res.*, 98, 10 695–10 711
- Caccin, B., Ermolli, I., Fofi, M., Sambuco, A. M., 1998, Variations of the Chromospheric Network with the Solar Cycle, *Sol. Phys.*, 177, 295–303
- Chapman, G. A., Cookson, A. M., Dobias, J. J., 1996, Variations in total solar irradiance during solar cycle 22, *J. Geophys. Res.*, 101, 13 541–13 548
- Chapman, G. A., Cookson, A. M., Dobias, J. J., 1997, Solar Variability and the Relation of Facular to Sunspot Areas during Solar Cycle 22, *ApJ*, 482, 541–545
- Charbonneau, P., 1995, Genetic Algorithms in Astronomy and Astrophysics, *ApJS*, 101, 309–334
- Coughlin, K., Tung, K. K., 2004, Eleven-year solar cycle signal throughout the lower atmosphere, *Journal of Geophysical Research (Atmospheres)*, 109, 21 105 (1–7)
- Cubasch, U., Voss, R., 2000, The Influence of Total Solar Irradiance on Climate, *Space Science Reviews*, 94, 185–198
- Dameris, M., Matthes, S., Deckert, R., Grewe, V., Ponater, M., 2006a, Solar cycle effect delays onset of ozone recovery, *Geophys. Res. Lett.*, 33, 3806 (1–4)
- Dameris, M., Matthes, S., Deckert, R., Grewe, V., Ponater, M., 2006b, Correction to “Solar cycle effect delays onset of ozone recovery”, *Geophys. Res. Lett.*, 33, 6821 (1–4)
- Dewitte, S., Crommelynck, D., Mekaoui, S., Joukoff, A., 2004, Measurement and Uncertainty of the Long-Term Total Solar Irradiance Trend, *Sol. Phys.*, 224, 209–216
- Eddy, J. A., 1976, The Maunder Minimum, *Science*, 192, 1189–1202
- Egorova, T., Rozanov, E., Manzini, E., Haberreiter, M., Schmutz, W., Zubov, V., Peter, T., 2004, Chemical and dynamical response to the 11-year variability of the solar irradiance simulated with a chemistry-climate model, *Geophys. Res. Lett.*, 31, 6119 (1–4)
- Egorova, T., Rozanov, E., Zubov, V., Schmutz, W., Peter, T., 2005, Influence of solar 11-year variability on chemical composition of the stratosphere and mesosphere simulated with a chemistry-climate model, *Advances in Space Research*, 35, 451–457
- Ermolli, I., Berrilli, F., Florio, A., 2003, A measure of the network radiative properties over the solar activity cycle, *A&A*, 412, 857–864

- Ermolli, I., Tlatov, A., Solanki, S. K., Krivova, N. A., 2007, Solar activity and irradiance studies with Ca II spectroheliogram time series: Potential problems and possible solutions, in *The Solar Chromosphere*, (Eds.) I. Dorotovic, R. Rutten, p. in press
- Fligge, M., Solanki, S. K., 1997, Inter-Cycle Variations of Solar Irradiance: Sunspot Areas as a Pointer, *Sol. Phys.*, 173, 427–439
- Fligge, M., Solanki, S. K., 1998, Long-term behavior of emission from solar faculae: steps towards a robust index, *A&A*, 332, 1082–1086
- Fligge, M., Solanki, S. K., 2000, The solar spectral irradiance since 1700, *Geophys. Res. Lett.*, 27, 2157–2160
- Fligge, M., Solanki, S. K., Unruh, Y. C., 2000, Modelling irradiance variations from the surface distribution of the solar magnetic field, *A&A*, 353, 380–388
- Floyd, L., Rottman, G., Deland, M., Pap, J., 2003, 11 years of solar UV irradiance measurements from UARS, in *ESA SP-535: Solar Variability as an Input to the Earth's Environment*, (Ed.) A. Wilson, pp. 195–203
- Fontenla, J., White, O. R., Fox, P. A., Avrett, E. H., Kurucz, R. L., 1999, Calculation of Solar Irradiances. I. Synthesis of the Solar Spectrum, *ApJ*, 518, 480–499
- Foster, S. S., 2004, Reconstruction of solar irradiance variations, for use in studies of global climate change: Application of recent SoHO observations with historic data from the Greenwich observations, Ph.D. thesis, Ph.D dissertation, 2004. England: University of Southampton (United Kingdom); 2004. Publication Number: AAT C820450. DAI-C 66/02, p. 430, Summer 2005
- Foukal, P., 1981, Comments on the thermodynamic structure and dynamics of the cool solar corona over sunspots, in *The Physics of Sunspots*, (Eds.) L. E. Cram, J. H. Thomas, pp. 191–209
- Foukal, P., 1996, The behavior of solar magnetic plages measured from Mt. Wilson observations between 1915-1984, *Geophys. Res. Lett.*, 23, 2169–2172
- Foukal, P., 1998, Extension of the F10.7 index to 1905 using Mt. Wilson Ca K spectroheliograms, *Geophys. Res. Lett.*, 25, 2909–2912
- Foukal, P., 2002, A comparison of variable solar total and ultraviolet irradiance outputs in the 20th century, *Geophys. Res. Lett.*, 29, 4–1
- Foukal, P., Lean, J., 1986, The influence of faculae on total solar irradiance and luminosity, *ApJ*, 302, 826–835
- Foukal, P., Lean, J., 1988, Magnetic modulation of solar luminosity by photospheric activity, *ApJ*, 328, 347–357
- Foukal, P., Lean, J., 1990, An empirical model of total solar irradiance variation between 1874 and 1988, *Science*, 247, 556–558

- Foukal, P., Milano, L., 2001, A measurement of the quiet network contribution to solar irradiance variation, *Geophys. Res. Lett.*, 28, 883–886
- Foukal, P., Fröhlich, C., Spruit, H., Wigley, T. M. L., 2006, Variations in solar luminosity and their effect on the Earth's climate, *Nature*, 443, 161–166
- Friis-Christensen, E., 2000, SOLAR VARIABILITY AND CLIMATE - A Summary, *Space Science Reviews*, 94, 411–421
- Friis-Christensen, E., Lassen, K., 1991, Length of the solar cycle: an indicator of solar activity closely associated with climate., *Science*, 254, 698–700
- Fröhlich, C., Pap, J. M., Hudson, H. S., 1994, Improvement of the photometric sunspot index and changes of the disk-integrated sunspot contrast with time, *Sol. Phys.*, 152, 111–118
- Fröhlich, C., 2000, Observations of Irradiance Variations, *Space Science Reviews*, 94, 15–24
- Fröhlich, C., 2003, Solar irradiance variations, in *ESA SP-535: Solar Variability as an Input to the Earth's Environment*, (Ed.) A. Wilson, pp. 183–193
- Fröhlich, C., 2006, Solar Irradiance Variability Since 1978, *Space Science Reviews*, pp. 90 (1–13)
- Fröhlich, C., Finsterle, W., 2001, VIRGO Radiometry and Total Solar Irradiance 1996–2000 Revised, in *IAU Symposium*, (Eds.) P. Brekke, B. Fleck, J. B. Gurman, pp. 105–110
- Giampapa, M. S., 2005, Stellar analogs of solar activity: the Sun in a stellar context, in *Saas-Fee Advanced Course 34: The Sun, Solar Analogs and the Climate*, (Eds.) J. D. Haigh, M. Lockwood, M. S. Giampapa, I. Rüedi, M. Güdel, W. Schmutz, pp. 307–415
- Györi, L., Baranyi, T., Csepura, G., Gerlei, O., Ludmany, A., 1998, Debrecen Photoheliographic Data for 1986 with image supplements, *Journal of Astronomical Data*, 4, 2 (1–6)
- Györi, L., Baranyi, T., Csepura, G., Gerlei, O., Ludmany, A., 2000, Debrecen Photoheliographic Data for 1987 with image supplements, *Journal of Astronomical Data*, 6, 1 (1–6)
- Haberreiter, M., Krivova, N. A., Schmutz, W., Wenzler, T., 2005, Reconstruction of the solar UV irradiance back to 1974, *Advances in Space Research*, 35, 365–369
- Hagenaar, H. J., 2001, Ephemeral Regions on a Sequence of Full-Disk Michelson Doppler Imager Magnetograms, *ApJ*, 555, 448–461
- Hagenaar, H. J., Schrijver, C. J., Title, A. M., 2003, The Properties of Small Magnetic Regions on the Solar Surface and the Implications for the Solar Dynamo(s), *ApJ*, 584, 1107–1119

- Haigh, J. D., 1996, The Impact of Solar Variability on Climate, *Science*, 272, 981–984
- Haigh, J. D., 1999, Modelling the impact of solar variability on climate, *Journal of Atmospheric and Terrestrial Physics*, 61, 63–72
- Haigh, J. D., 2001, The Impact of Solar Variability on Climate, *Science*, 272, 981–984
- Haigh, J. D., 2003, The effects of solar variability on the Earth's climate, *Royal Society of London Philosophical Transactions Series A*, 361, 95–111
- Haigh, J. D., Lockwood, M., Giampapa, M. S., Ruedi, I., Güdel, M., Schmutz, W. (Eds.), 2005, *The Sun, Solar Analogs and the Climate*
- Hall, J. C., Lockwood, G. W., 2004, The Chromospheric Activity and Variability of Cycling and Flat Activity Solar-Analog Stars, *ApJ*, 614, 942–946
- Harvey, K. L., 1992, The Cyclic Behavior of Solar Activity, in *ASP Conf. Ser. 27: The Solar Cycle*, (Ed.) K. L. Harvey, pp. 335–367
- Harvey, K. L., 1993, *Magnetic dipoles on the Sun*, Ph.D. thesis, Univ. Utrecht, (1993)
- Harvey, K. L., 1994, The solar magnetic cycle, in *Solar Surface Magnetism*, (Eds.) R. J. Rutten, C. J. Schrijver, pp. 347–364
- Hathaway, D. H., Wilson, R. M., Reichmann, E. J., 2002, Group Sunspot Numbers: Sunspot Cycle Characteristics, *Sol. Phys.*, 211, 357–370
- Hickey, J. R., Stowe, L. L., Jacobowitz, H., Pellegrino, P., Maschhoff, R. H., House, F., Vonder Haar, T. H., 1980, Initial Solar Irradiance Determinations from NIMBUS-7 Cavity Radiometer Measurements, *Science*, 208, 281–283
- Hoyt, D. V., Schatten, K. H., 1993, A discussion of plausible solar irradiance variations, 1700-1992, *J. Geophys. Res.*, 98, 18 895–18 906
- Hoyt, D. V., Schatten, K. H., 1997, The role of the sun in climate change, *The role of the sun in climate change / Douglas V. Hoyt, Kenneth H. Schatten*. New York : Oxford University Press, 1997. QC883.2.S6 H69 1997
- Hoyt, D. V., Schatten, K. H., 1998, Group Sunspot Numbers: A New Solar Activity Reconstruction, *Sol. Phys.*, 181, 491–512
- Hoyt, D. V., Schatten, K. H., Nesmes-Ribes, E., 1994, The one hundredth year of Rudolf Wolf's death: Do we have the correct reconstruction of solar activity?, *Geophys. Res. Lett.*, 21, 2067–2070
- Hudson, H. S., Silva, S., Woodard, M., Willson, R. C., 1982, The effects of sunspots on solar irradiance, *Sol. Phys.*, 76, 211–219
- IPCC, 2001, *Technical Summary of the Working Group I Report*, Intergovernmental Panel on Climate Change

- Jones, P. D., 1994, Hemispheric Surface Air Temperature Variations: A Reanalysis and an Update to 1993., *Journal of Climate*, 7, 1794–1802
- Jones, P. D., Moberg, A., 2003, Hemispheric and Large-Scale Surface Air Temperature Variations: An Extensive Revision and an Update to 2001., *Journal of Climate*, 16, 206–223
- Keppens, R., Martinez Pillet, V., 1996, The magnetic structure of pores and sunspots derived from Advanced Stokes Polarimeter data., *A&A*, 316, 229–242
- Kodera, K., Kuroda, Y., 2002, Dynamical response to the solar cycle, *Journal of Geophysical Research (Atmospheres)*, 107, 5–1
- Krivova, N., Balmaceda, L., Solanki, S. K., 2006a, Reconstruction of solar total irradiance since 1700 from the surface magnetic flux, submitted
- Krivova, N. A., Solanki, S. K., 2004, Effect of spatial resolution on estimating the Sun's magnetic flux, *A&A*, 417, 1125–1132
- Krivova, N. A., Solanki, S. K., 2005, Reconstruction of solar UV irradiance, *Advances in Space Research*, 35, 361–364
- Krivova, N. A., Solanki, S. K., Fligge, M., Unruh, Y. C., 2003, Reconstruction of solar irradiance variations in cycle 23: Is solar surface magnetism the cause?, *A&A*, 399, L1–L4
- Krivova, N. A., Solanki, S. K., Floyd, L., 2006b, Reconstruction of solar UV irradiance in cycle 23, *A&A*, 452, 631–639
- Kuhn, J. R., Libbrecht, K. G., 1991, Nonfacular solar luminosity variations, *ApJ*, 381, L35–L37
- Kuhn, J. R., Stein, R. F., 1996, Accounting for the Solar Acoustic and Luminosity Variations from the Deep Convection Zone, *ApJ*, 463, L117–L119
- Kuhn, J. R., Libbrecht, K. G., Dicke, R. H., 1988, The surface temperature of the sun and changes in the solar constant, *Science*, 242, 908–911
- Kuroda, Y., Kodera, K., 2005, Solar cycle modulation of the Southern Annular Mode, *Geophys. Res. Lett.*, 32, 13 802 (1–4)
- Labitzke, K., van Loon, H., 1995, Connection between the troposphere and stratosphere on a decadal scale, *Tellus Series A*, 47, 275–286
- Langematz, U., Matthes, K., Grenfell, J. L., 2005, Solar impact on climate: modeling the coupling between the middle and the lower atmosphere, *Memorie della Societa Astronomica Italiana*, 76, 868–875
- Larkin, A., Haigh, J. D., Djavidnia, S., 2000, The Effect of Solar UV Irradiance Variations on the Earth's Atmosphere, *Space Science Reviews*, 94, 199–214

- Lean, J., 2000a, Evolution of the Sun's spectral irradiance since the Maunder Minimum, *Geophys. Res. Lett.*, 27, 2425–2428
- Lean, J., Rind, D., 1998, Climate Forcing by Changing Solar Radiation., *Journal of Climate*, 11, 3069–3094
- Lean, J., Rind, D., 1999, Evaluating sun-climate relationships since the Little Ice Age, *Journal of Atmospheric and Terrestrial Physics*, 61, 25–36
- Lean, J., Skumanich, A., White, O., 1992, Estimating the Sun's radiative output during the Maunder Minimum, *Geophys. Res. Lett.*, 19, 1591–1594
- Lean, J., Beer, J., Bradley, R., 1995, Reconstruction of solar irradiance since 1610: Implications for climate change, *Geophys. Res. Lett.*, 22, 3195–3198
- Lean, J. L., 2000b, Short Term, Direct Indices of Solar Variability, *Space Science Reviews*, 94, 39–51
- Lean, J. L., 2001, Solar Irradiance and Climate Forcing in the Near Future, *Geophys. Res. Lett.*, 28, 4119–4122
- Li, K., 1999, The shape of the sunspot cycle described by sunspot areas, *A&A*, 345, 1006–1010
- Li, K. J., Qiu, J., Su, T. W., Gao, P. X., 2005, Sunspot Unit Area: A New Parameter to Describe Long-Term Solar Variability, *ApJ*, 621, L81–L84
- Lockwood, M., 2002, An evaluation of the correlation between open solar flux and total solar irradiance, *A&A*, 382, 678–687
- Lockwood, M., 2003, Twenty-three cycles of changing open solar magnetic flux, *Journal of Geophysical Research (Space Physics)*, 108, 7–1
- Lockwood, M., 2005, Solar outputs, their variations and their effects on Earth, in *Saas-Fee Advanced Course 34: The Sun, Solar Analogs and the Climate*, (Eds.) J. D. Haigh, M. Lockwood, M. S. Giampapa, I. Rüedi, M. Güdel, W. Schmutz, pp. 109–306
- Lockwood, M., Stamper, R., Wild, M. N., 1999, A doubling of the sun's coronal magnetic field during the past 100 years., *Nature*, 399, 437–439
- Marsh, N. D., Svensmark, H., 2000, Low Cloud Properties Influenced by Cosmic Rays, *Physical Review Letters*, 85, 5004–5007, [physics/0005072](https://doi.org/10.1103/PhysRevLett.85.5004)
- Mendoza, B., 1997, Estimations of Maunder Minimum Solar Irradiance and Ca II H and K Fluxes Using Rotation Rates and Diameters, *ApJ*, 483, 523–526
- Nesme-Ribes, E., Ferreira, E. N., Sadourny, R., Le Treut, H., Li, Z. X., 1993, Solar dynamics and its impact on solar irradiance and the terrestrial climate, *J. Geophys. Res.*, 98, 18 923–18 935

- Ortiz, A., Solanki, S. K., Domingo, V., Fligge, M., Sanahuja, B., 2002, On the intensity contrast of solar photospheric faculae and network elements, *A&A*, 388, 1036–1047, astro-ph/0207008
- Parker, E. N., 1955, Hydromagnetic Dynamo Models., *ApJ*, 122, 293–314
- Parker, E. N., 1975, The generation of magnetic fields in astrophysical bodies. X - Magnetic buoyancy and the solar dynamo, *ApJ*, 198, 205–209
- Parker, E. N., 1987, The dynamical oscillation and propulsion of magnetic fields in the convective zone of a star. I - General considerations, *ApJ*, 312, 868–879
- Parker, E. N., 1995, Theoretical properties of Omega-loops in the convective zone of the sun. 2: The origin of enhanced solar irradiance, *ApJ*, 440, 415–420
- Peristykh, A. N., Damon, P. E., 2003, Persistence of the Gleissberg 88-year solar cycle over the last ~12,000 years: Evidence from cosmogenic isotopes, *Journal of Geophysical Research (Space Physics)*, 108, 1–1
- Preminger, D. G., Walton, S. R., 2005, A new model of total solar irradiance based on sunspot areas, *Geophys. Res. Lett.*, 32, 14 109 (1–5)
- Radick, R. R., Lockwood, G. W., Skiff, B. A., Baliunas, S. L., 1998, Patterns of Variation among Sun-like Stars, *ApJS*, 118, 239–258
- Reid, G. C., 1987, The nucleation and growth of ice particles in the upper mesosphere, *Nature*, 20, 1285–1291
- Reid, G. C., 1997, The nucleation and growth of ice particles in the upper mesosphere, *Advances in Space Research*, 20, 1285–1291
- Reid, G. C., 2000, Solar Variability and the Earth's Climate: Introduction and Overview, *Space Science Reviews*, 94, 1–11
- Rind, D., 2002, The Sun's Role in Climate Variations, *Science*, 296, 673–678
- Rind, D., Lean, J., Healy, R., 1999, Simulated time-dependent climate response to solar radiative forcing since 1600, *J. Geophys. Res.*, 104, 1973–1990
- Rottman, G. J., 1988, Observations of solar UV and EUV variability, *Advances in Space Research*, 8, 53–66
- Rottman, G. J., Woods, T. N., Spurn, T. P., 1993, Solar-Stellar Irradiance Comparison Experiment 1. I - Instrument design and operation, *J. Geophys. Res.*, 98, 10 667–10 677
- Roazanov, E. V., Schlesinger, M. E., Egorova, T. A., Li, B., Andronova, N., Zubov, V. A., 2004, Atmospheric response to the observed increase of solar UV radiation from solar minimum to solar maximum simulated by the University of Illinois at Urbana-Champaign climate-chemistry model, *Journal of Geophysical Research (Atmospheres)*, 109, 1110 (1–16)



- Schimel, D. S., Braswell, B. H., McKeown, R., Ojima, D. S., Parton, W. J., Pulliam, W., 1996, Climate and nitrogen controls on the geography and timescales of terrestrial biogeochemical cycling, *Global Biogeochemical Cycles*, 10, 677–692
- Schmitt, D., 1993, The Solar Dynamo, in *IAU Symp. 157: The Cosmic Dynamo*, (Eds.) F. Krause, K. H. Radler, G. Rudiger, pp. 1–12
- Schrijver, C. J., Harvey, K. L., 1994, The photospheric magnetic flux budget, *Sol. Phys.*, 150, 1–2
- Schrijver, C. J., Zwaan, C., 2000, *Solar and Stellar Magnetic Activity, Solar and stellar magnetic activity / Carolus J. Schrijver, Cornelius Zwaan*. New York : Cambridge University Press, 2000. (Cambridge astrophysics series ; 34)
- Schüssler, M., Schmitt, D., Ferriz-Mas, A., 1997, Long-term Variation of Solar Activity by a Dynamo Based on Magnetic Flux Tubes, in *ASP Conf. Ser. 118: 1st Advances in Solar Physics Euroconference. Advances in Physics of Sunspots*, (Eds.) B. Schmieder, J. C. del Toro Iniesta, M. Vazquez, pp. 39–44
- Shindell, D. T., 2001, Climate and ozone response to increased stratospheric water vapor, *Geophys. Res. Lett.*, 28, 1551–1554
- Sinnhuber, B.-M., von der Gathen, P., Sinnhuber, M., Rex, M., König-Langlo, G., Oltmans, S. J., 2005, Large decadal scale changes of polar ozone suggest solar influence, *Atmospheric Chemistry & Physics Discussions*, 5, 12 103–12 117
- Sivaraman, K. R., Gupta, S. S., Howard, R. F., 1993, Measurement of Kodaikanal white-light images. I - A comparison of 35 years of Kodaikanal and Mount Wilson sunspot data, *Sol. Phys.*, 146, 27–47
- Sofia, S., Li, L. H., 2000, Irradiance or Luminosity Changes?, in *ESA SP-463: The Solar Cycle and Terrestrial Climate, Solar and Space weather*, (Ed.) A. Wilson, pp. 107–111
- Solanki, S. K., Fligge, M., 1998, Solar irradiance since 1874 revisited, *Geophys. Res. Lett.*, 25, 341–344
- Solanki, S. K., Fligge, M., 1999, A reconstruction of total solar irradiance since 1700, *Geophys. Res. Lett.*, 26, 2465–2468
- Solanki, S. K., Krivova, N. A., 2003, Can solar variability explain global warming since 1970?, *Journal of Geophysical Research (Space Physics)*, 108, 7–1
- Solanki, S. K., Krivova, N. A., 2004, Solar Irradiance Variations: From Current Measurements to Long-Term Estimates, *Sol. Phys.*, 224, 197–208
- Solanki, S. K., Schüssler, M., Fligge, M., 2000, Evolution of the Sun's large-scale magnetic field since the Maunder minimum, *Nature*, 408, 445–447
- Solanki, S. K., Schüssler, M., Fligge, M., 2002, Secular variation of the Sun's magnetic flux, *A&A*, 383, 706–712

- Solanki, S. K., Usoskin, I. G., Kromer, B., Schüssler, M., Beer, J., 2004, Unusual activity of the Sun during recent decades compared to the previous 11,000 years, *Nature*, 431, 1084–1087
- Solanki, S. K., Krivova, N. A., Wenzler, T., 2005, Irradiance models, *Advances in Space Research*, 35, 376–383
- Spruit, H. C., 1982, Effect of spots on a star's radius and luminosity, *A&A*, 108, 348–355
- Stott, P. A., Jones, G. S., Mitchell, J. F. B., 2003, Do Models Underestimate the Solar Contribution to Recent Climate Change?, *Journal of Climate*, 16, 4079–4093
- Stuiver, M., Braziunas, T. F., 1989, Atmospheric C-14 and century-scale solar oscillations, *Nature*, 338, 405–408
- Stuiver, M., Braziunas, T. F., 1998, Anthropogenic and solar components of hemispheric <sup>14</sup>C, *Geophys. Res. Lett.*, 25, 329–332
- Taylor, R. J., 1997, *The Sun as a star*, Cambridge ; New York, NY, USA : Cambridge University Press, 1997.
- Unruh, Y. C., Solanki, S. K., Fligge, M., 1999, The spectral dependence of facular contrast and solar irradiance variations, *A&A*, 345, 635–642
- Unruh, Y. C., Solanki, S. K., Fligge, M., 2000, Modelling solar irradiance variations: Comparison with observations, including line-ratio variations, *Space Science Reviews*, 94, 145–152
- Usoskin, I. G., Alanko, K., Mursula, K., Kovaltsov, G. A., 2002a, Heliospheric modulation strength during the neutron monitor era, *Sol. Phys.*, 207, 389–399
- Usoskin, I. G., Mursula, K., Solanki, S. K., Schüssler, M., Kovaltsov, G. A., 2002b, A physical reconstruction of cosmic ray intensity since 1610, *Journal of Geophysical Research (Space Physics)*, 107, 13–1
- Usoskin, I. G., Solanki, S. K., Schüssler, M., Mursula, K., Alanko, K., 2003, Millennium-Scale Sunspot Number Reconstruction: Evidence for an Unusually Active Sun since the 1940s, *Physical Review Letters*, 91, 211 101 (1–4), astro-ph/0310823
- Usoskin, I. G., Mursula, K., Solanki, S., Schüssler, M., Alanko, K., 2004, Reconstruction of solar activity for the last millennium using <sup>10</sup>Be data, *A&A*, 413, 745–751, astro-ph/0309556
- Usoskin, I. G., Schüssler, M., Solanki, S. K., Mursula, K., 2005, Solar activity, cosmic rays, and Earth's temperature: A millennium-scale comparison, *Journal of Geophysical Research (Space Physics)*, 110, 10 102 (1–10)
- Usoskin, I. G., Solanki, S. K., Korte, M., 2006, Solar activity reconstructed over the last 7000 years: The influence of geomagnetic field changes, *Geophys. Res. Lett.*, 33, 8103 (1–4)

- van Loon, H., Labitzke, K., 2000, The Influence of the 11-year Solar Cycle on the Stratosphere Below 30km: a Review, *Space Science Reviews*, 94, 259–278
- Vaquero, J. M., Gallego, M. C., Sánchez-Bajo, F., 2004, Reconstruction of a Monthly Homogeneous Sunspot Area Series Since 1832, *Sol. Phys.*, 221, 179–189
- Wagner, G., Laj, C., Beer, J., Kissel, C., Muscheler, R., Masarik, J., Synal, H.-A., 2001, Reconstruction of the paleoaccumulation rate of central Greenland during the last 75 kyr using the cosmogenic radionuclides  $^{36}\text{Cl}$  and  $^{10}\text{Be}$  and geomagnetic field intensity data, *Earth and Planetary Science Letters*, 193, 515–521
- Waldmeier, M., 1961, The sunspot-activity in the years 1610-1960, Zurich : Schulthess, 1961.
- Wang, Y.-M., Sheeley, Jr., N. R., 1995, Solar Implications of ULYSSES Interplanetary Field Measurements, *ApJ*, 447, L143–L146
- Wang, Y.-M., Lean, J., Sheeley, Jr., N. R., 2000a, The long-term variation of the Sun's open magnetic flux, *Geophys. Res. Lett.*, 27, 505–508
- Wang, Y.-M., Sheeley, Jr., N. R., Lean, J., 2000b, Understanding the evolution of the Sun's open magnetic flux, *Geophys. Res. Lett.*, 27, 621–624
- Wang, Y.-M., Lean, J. L., Sheeley, Jr., N. R., 2005, Modeling the Sun's Magnetic Field and Irradiance since 1713, *ApJ*, 625, 522–538
- Weiss, N. O., 1994, Solar and Stellar Dynamos, in *Lectures on Solar and Planetary Dynamos*, (Eds.) M. R. E. Proctor, A. D. Gilbert, pp. 59–96
- Wenzler, T., Solanki, S. K., Krivova, N. A., Fluri, D. M., 2004, Comparison between KPVT/SPM and SoHO/MDI magnetograms with an application to solar irradiance reconstructions, *A&A*, 427, 1031–1043
- Wenzler, T., Solanki, S. K., Krivova, N. A., 2005, Can surface magnetic fields reproduce solar irradiance variations in cycles 22 and 23?, *A&A*, 432, 1057–1061
- Wenzler, T., Solanki, S. K., Krivova, N. A., Fröhlich, C., 2006, Reconstruction of solar irradiance variations in cycles 21-23 based on surface magnetic fields, *A&A*, 460, 583–595
- White, O. R., Skumanich, A., Lean, J., Livingston, W. C., Keil, S. L., 1992, The sun in a noncycling state, *PASP*, 104, 1139–1143
- White, W. B., Lean, J., Cayan, D. R., Dettinger, M. D., 1997, Response of global upper ocean temperature to changing solar irradiance, *J. Geophys. Res.*, 102, 3255–3266
- Willson, R. C., 1997, Climate variability and the influence of the sun, *Science*, 277, 1963–1965
- Willson, R. C., Hudson, H. S., 1988, Solar luminosity variations in solar cycle 21, *Nature*, 332, 810–812

- Willson, R. C., Hudson, H. S., 1991, The sun's luminosity over a complete solar cycle, *Nature*, 351, 42–44
- Willson, R. C., Mordvinov, A. V., 2003, Secular total solar irradiance trend during solar cycles 21–23, *Geophys. Res. Lett.*, 30, 3–1
- Willson, R. C., Duncan, C. H., Geist, J., 1980, Direct measurement of solar luminosity variation, *Science*, 207, 177–179
- Wolff, C. L., Hickey, J. R., 1987, Solar irradiance change and special longitudes due to r-modes, *Science*, 235, 1631–1633
- Woods, T. N., Prinz, D. K., Rottman, G. J., London, J., Crane, P. C., Cebula, R. P., Hilsenrath, E., Brueckner, G. E., Andrews, M. D., White, O. R., VanHoosier, M. E., Floyd, L. E., Herring, L. C., Knapp, B. G., Pankratz, C. K., Reiser, P. A., 1996, Validation of the UARS solar ultraviolet irradiances: Comparison with the ATLAS 1 and 2 measurements, *J. Geophys. Res.*, 101, 9541–9570
- Worden, J. R., White, O. R., Woods, T. N., 1998, Evolution of Chromospheric Structures Derived from Ca II K Spectroheliograms: Implications for Solar Ultraviolet Irradiance Variability, *ApJ*, 496, 998–1014
- Wright, J. T., Marcy, G. W., Butler, R. P., Vogt, S. S., 2004, Chromospheric Ca II Emission in Nearby F, G, K, and M Stars, *ApJS*, 152, 261–295, [astro-ph/0402582](#)
- Zhang, Q., Soon, W. H., Baliunas, S. L., Lockwood, G. W., Skiff, B. A., Radick, R. R., 1994, A method of determining possible brightness variations of the Sun in past centuries from observations of solar-type stars, *ApJ*, 427, L111–L114
- Zwaan, C., Harvey, K. L., 1994, Patterns in the solar magnetic field (Invited Review), in *Solar Magnetic Fields*, (Eds.) M. Schüssler, W. Schmidt, pp. 27–48

# Acknowledgements

I would like to deeply thank the various people who, during the three years in which this endeavor lasted, helped me with useful and helpful assistance. Without their care and consideration, this work would likely not have matured.

Big thanks, above all, to my supervisor, Prof. Dr. Sami Solanki. To outline just a few reasons for my gratitude towards him; my sincere thanks for having accepted me as his student and showing confidence in my ability to carry out my project work. Secondly, for all his patience and understanding during those frustrating times in ones' PhD, when progress is stalled and things look very difficult. Finally, for the time he devoted, in between his busy schedules, not only to monitor progress in my work but also advising me on my career and problems of various nature that I faced on the way. His constant support, encouragement and motivation in this early phase of my career has gone a long way in moulding me in my scientific research. I am glad I had this great opportunity to work with him.

Special thanks to Natasha for her unconditional help during these years of my PhD. Without her constructive feedback much of this work would not have been completed. On occasions when I found myself in the dark, her words of advice were invaluable.

Friends and colleagues are an essential part of ones' career. This could not have been more true in my experience. My apologies to all whom I have forgotten to mention. I would like to start by thanking Thomas Wenzler, who was always ready to answer my questions and send me all the materials I needed, especially at the beginning of my PhD. Secondly, Rajat Thomas, who always had time for my sometimes silly queries. I would like to thank him for showing me the fun-side of doing science, for his constant care and support. I am deeply thankful to Luis Eduardo Vieira and happy that we could work together again during the last phase of my thesis. All our brainstorming sessions and coffee breaks, with his questions but also his suggestions were always the source of numerous interesting ideas.

Sincere thanks to Dr. Dieter Schmitt for his kind invitation to take part in the IMPRS and for all his efforts in getting me adjusted to the Max Planck research environment. Lots of thanks also to Prof. Dr. Glassmeier, Prof. Dr. Blum and Prof. Dr. Motschmann for their help and predisposition to answer our questions and organize seminars at Braunschweig University.

A big and special "thank you" to my dear Prof. Dr. Rainer Schwenn, without whose help I would not be here. Also to my first supervisor Dr. Guillermo Stenborg, who help me in my first steps in my career and showed me the way. Both were my role-models and my inspiration.

Severely incomplete will be my already short acknowledgement, without mentioning my close friends who were always present when I needed them. Thanks very much to

Dr. Marilena, Dr. Durgesh, Dr. Roopali and Rajat, the ones who made my first year easier with their company and support. To my dear friends Lupe and Marian for so many moments of happiness and for being always there when I needed the most. To my cheerful officemate Cleme, who saw me cry so many times behind the monitor after a bad day and comforted me with soothing words. To Ceci, Hebe and Sanja for listening patiently to me and being close to me in days of "porca miseria". To Martin, for being always so friendly and supportive from the very first day we met till present and also for his tutorials in German language. To Elias, for his useful tips and help in moments of 'panic'. To Jean, and all my friends from Brazil who visited me here and also the ones who stayed on the other side of the Atlantic, just for being my friends no matter the distance or time. To the ones in Argentina, also always present.

Of course, I cannot finish my acknowledgements without thanking once more to my family. This thesis is dedicated to them, who taught me that life is full of adventures and that there is plenty of mysteries waiting for us to be unraveled. I thank them from my heart for giving me the tools to do it, for encouraging me and supporting me over all these years in all my crazy decisions.

# Lebenslauf

## Persönliche Daten

Name: Laura Antonia Balmaceda  
Geboren: 13.12.1977 in Rosario, Argentinien  
Nationalität: Argentinisch

## Schulbindung

1983 – 1990 Primary School  
Colegio "El Tránsito de Nuestra Señora"  
San Juan – Argentinien

1991 – 1995 Secondary School  
Colegio "El Tránsito de Nuestra Señora"  
San Juan – Argentinien

## Studium

1996 – 2001 Universidad Nacional de San Juan - Argentinien  
Facultad de Ciencias Exactas, Físicas y Naturales  
Licenciatura in Astronomy  
Thesis: "Morphological analysis of transient events in the lower solar corona"

2001 – 2003 Instituto Nacional de Pesquisas Espaciais - Brasilien  
Master in Space Geophysics  
Thesis: "Possible solar causes of geomagnetic storms"

## Promotion

2004 – 2007 Stipendiat am Max-Planck-Institut für Sonnensystemforschung

### Veröffentlichungen

- **Balmaceda, L.**; Dal Lago, A.; Stenborg, G.; Francile, C.; Gonzalez, W. D.; Schwenn, R. Continuous tracking of CMEs using MICA, and LASCO C2 and C3 coronagraphs, *Adv. Space Res.*, 32, 12, 2625-2630, 2003.
- **Balmaceda, L. A.**; Gonzalez, W. D.; Echer, E.; Santos, J. C.; Vieira, L. E. A.; Dal Lago, A.; Guarnieri, F. L.; Gonzalez, A. L. C. The Solar Origins of the Sun-Earth Connection Events on April 1999 and February 2000, *Brazilian Journal of Physics*, 34, 4B, 1745-1747, 2004.
- Dal Lago, A.; Vieira, L. E. A.; Echer, E.; Gonzalez, W. D.; Clúa de Gonzalez, A. L.; Guarnieri, F. L.; **Balmaceda, L.**; Santos, J.; da Silva, M. R.; de Lucas, A.; Schuch, N. J. Great Geomagnetic Storms in the Rise and Maximum of Solar Cycle 23, *Brazilian Journal of Physics*, 34, 4B, 1542-1546, 2004.
- Dal Lago, A.; Gonzalez, W. D.; **Balmaceda, L. A.**; et al. The 17-22 October (1999) solar-interplanetary-geomagnetic event: Very intense geomagnetic storm associated with a pressure balance between interplanetary coronal mass ejection and a high-speed stream, *J. Geophys. Res.*, 111, A7, 2006.